ANALYSIS OF CRYSTAL GROWTH OF HIGH TEMPERATURE MATERIALS IN A PLASMA FURNACE

By

WILLIAM AUSTIN SMITH

A DISSERTATION PRESENTED TO THE GRADUATE COUNCIL OF
THE UNIVERSITY OF FLORIDA
IN PARTIAL FULFILLMENT OF THE REQUIREMENTS FOR THE
DEGREE OF DOCTOR OF PHILOSOPHY

UNIVERSITY OF FLORIDA

August, 1966


University of
1853

ACKNOWLEDGEMENTS

I would like to express my deepest gratitude to Dr. D. T. Williams, chairman of my supervisory committee, for his considerable help, criticism and encouragement during the course of this research. I would also like to express my appreciation to Dr. E. A. Farber, for introducing me to the problem of the growth of refractory crystals, and to Drs. M. H. Clarkson, K. T. Millsaps, O. E. Myers and W. O. Smith for their suggestions and efforts in my behalf.

Thanks are due in large measure to Harry Stroud, for his expert advice and physical aid in constructing the furnace, to Hector Millan, for his machining and photographic help, to Dr. B. E. Mathews, Professor C. A. Langston and Walter Powers of the Induction Heating Laboratory for their help in establishing and maintaining the rf generating unit, and to Dr. L. L. Hench and the Metallurgy Department for their help in cutting, mounting and photographing the crystal specimens.

Finally, I would like to thank the National Aeronautics and Space Administration and the members of the University of Florida's N.A.S.A. Steering Committee for their generous financial support, over the past two years, that has made this effort possible.

TABLE OF CONTENTS

LIST OF TABLES

LIST OF FIGURES

Page

KEY TO SYMBOLS

a,b	constants of integration
A,B, ...	constants of integration
A	area
A_i	constant of the ith term of a series
C	constant of proportionality
C_p	specific heat
d	distance of spacing between crystalline planes
D	a characteristic dimension
e	Naperian base of logarithms
$g_{(r)}$	a function dependent on r
h	coefficient of convection heat transfer
h_b	ditto above, at the base of the boule
$\bar{h}_b$	ditto above, average value for various boule lengths
h_p	ditto above, for the plasma to the boule tip
h_s	ditto above, at the side of the boule
$\bar{h}_s$	ditto above, average value for the entire side
$h_{1,2}$	dimensionless heat transfer coefficients defined by equations 7 and 8, page 26
i	an index number
J_n	Bessel function of order n
k	thermal conductivity
k	Boltzman's constant
L	length
$\dot{m}$	mass flow rate of powder impinging on the boule
n	an integer
q_e	charge on an electron
Q_b	heat flow from the base
Q_p	heat flow from the plasma to the boule tip

$Q_{p(net)}$	net heat flow to the boule, from the plasma, defined by equation 10, page 26
Q_S	heat flow from the side of the boule
r	radial distance
r_o	radius of the boule
r_1	dimensionless radial parameter, r/r_o
$R_{(r)}$	a function depending on r alone
T	temperature
T_A	ambient temperature
T_C	colder temperature
T_H	hotter temperature
T_L	temperature at the top of the liquid layer of the boule
$\bar{T}_L$	average temperature of the liquid layer on the boule
T_M	temperature of the powder grains impinging on the boule
T_S	temperature at the solid-liquid interface
T_P	plasma temperature
$T_{(x,r)}$	temperature at a given position in the boule
∇T	thermal gradient
V_i	equivalent voltage associated with an electron so that its energy can be expressed in electron-volts
x	axial distance
x_1	dimensionless axial parameter, x/L
$X_{(x)}$	a function depending on x alone
α	degree of ionization of the plasma, given by equation 13, page 51
α	a dimensionless parameter, L/r_o
α	an experimental exponent, given by equation 2, page 15
β	an experimental exponent, given by equation 2, page 15
β	a constant parameter of the system, given by equation B-6 and B-7, page 107

ϵ	average emissivity of the boule in the temperature range under consideration
$\ominus$	angle of incidence of an incoming wave
$\Theta(x,r)$	a dimensionless, temperature-dependent parameter defined by equation B-9, page 108
λ	wavelength
λ	an arbitrary constant given by equation B-17, page
λ_i	the eigenvalues of equation B-46, page 112
μ	viscosity
ρ	density
σ	Stefan-Boltzman constant

Abstract of Dissertation Presented to the Graduate Council in Partial Fulfillment of the Requirements for the Degree of Doctor of Philosophy

ANALYSIS OF CRYSTAL GROWTH OF HIGH TEMPERATURE MATERIALS IN A PLASMA FURNACE

by

William Austin Smith

August, 1966

Chairman: Dr. D. T. Williams
Major Department: Aerospace Engineering

The increased understanding of electron behavior in solids has stimulated research into developing ways of growing specialized crystals having electrical properties particularly suited to a given application. One special field of interest is in crystals of refractory materials for use in applications where high temperatures are either encountered or desired. One such case is that of the thermoelements located directly in the core of a nuclear reactor.

This dissertation contains an analysis of the crystal growth mechanism of refractory materials taking place in the fireball of a plasma-heated Verneuil-type furnace. The fireball temperature is estimated at well over 9,000 K. On the basis of this analysis predictions can be made for properly adjusting the furnace environment to one that is conducive to the growth of high quality, single crystals of various refractory materials. Such parameters as the powder feed rate, thermal gradient at the liquid-solid interface, rf power level, powder grain size, geometry of the boule tip with respect to the powder probe and fireball, powder-gas flow rate and the presence of a diatomic gas are investigated and their effects on crystal growth and quality are determined.

It was found that the large radiation heat loss from the side of the boule dominates the thermal conditions during crystal growth. When the rf power is low, the boule is cool and the thermal gradients are large. As the boule increases in length, the rf power must be boosted in order to maintain a molten cap. If the power were not boosted the molten cap would eventually vanish as the boule grew longer, at which point all growth would stop.

The large radiant heat losses from the side of the boule are not always as important as was found in the case of growing aluminum oxide crystals. If materials of a lower melting point are involved, radiation losses become less important. If materials of higher melting points are involved, clearly the importance of the radiation losses becomes much more critical.

The importance of a diatomic gas as a means of heat transfer to the boule was an interesting observation. The use of such gases is not, of course, original with this work. On the other hand, the dramatic increase in the heat transfer rate from the plasma when diatomic gases are used constitutes an important improvement in this application.

The effect of loss of heat due to the introduction of fine powder grains into the plasma is another observation not originally anticipated. The study here clarifies and rationalizes the observations.

It was further found that the parameters important to crystal quality are the ratio of the thermal gradient at the liquid-solid interface to the powder feed rate and the average temperature of the molten cap. Crystal quality was generally better at the periphery than at the core of a boule.

It is concluded that the work reported on contributes to a more effective use of the plasma-Verneuil furnace in growing crystals of refractory materials.

CHAPTER I. BACKGROUND

A. Introduction and Purpose of this Investigation

The increased understanding of electron behavior in solids has stimulated research into developing ways of growing specialized crystals having electrical properties particularly suited to a given application. One special field of interest is in crystals having high melting temperatures (above 2000 C). One use for these crystals would be in thermoelectric energy conversion, where high temperature is advantageous to high energy conversion efficiency. It has been suggested that a major advancement in nuclear thermoelectric energy conversion might be made by the development of a high temperature solid state thermoelement that is resistant to deterioration from neutron bombardment.

Progress in high temperature, solid state research requires progress in the growth of high temperature crystals. High temperature metal oxide crystals have been grown for over 60 years by the Verneuil method, which uses an oxygen-hydrogen flame to melt powder falling on a boule. The crystal then grows as a controlled stalagmite. The method has been highly developed commercially for the growth of gem-alumina (rubies, sapphires) for use as bearings in watches and instruments, and, more recently, for lasers.

This classical method, however, is limited to growing crystals in an oxidizing atmosphere and to a melting temperature of approximately 2500 C. An extension of the method to inert or reducing atmospheres, and at considerably

higher temperatures, can be made by utilizing a plasma heat source in place of the oxy-hydrogen flame. Such a device increases enormously the range of materials that can be crystallized.

The usefulness of the plasma furnace in growing high temperature crystals is dependent upon an understanding of the heat transfer-crystallization mechanism that takes place in the plasma fireball. The purpose of the present research is to investigate this mechanism.

B. The Plasma-Heated Verneuil Furnace

A picture of the plasma-heated Verneuil furnace, shown while being used to grow an aluminum oxide crystal, is seen in Figure 1. A schematic drawing of the furnace is shown in Figure 2. A vibrating hopper (a) feeds powder at a controlled rate to a powder probe (b). The powder probe (water-cooled) extends into the plasma fireball (c) and terminates a few centimeters above the crystal boule (d). Powder, accompanied by a "powder-gas" flow (e), impinges on the boule and is melted. The term "powder-gas" refers to gas injected into the plasma fireball from the powder probe; it is usually a mixture of argon and a diatomic gas. Crystallization occurs at the liquid-solid interface, causing the crystal to grow as a stalagmite. The boule is lowered at the same rate as the vertical growth rate of the crystal so that the boule tip always remains at one location in the plasma.

The heart of the apparatus is the plasma torch assembly (f), of Figure 2, and also shown in greater detail in Figure 3. Argon is introduced tangentially into two concentric quartz tubes (g) of Figure 3, the outer tube being longer than the inner one. The plasma fireball is established at the base of the outer quartz tube by an rf

Figure 1 The Plasma-Verneuil Furnace being Used to Grow an Aluminum Oxide Crystal

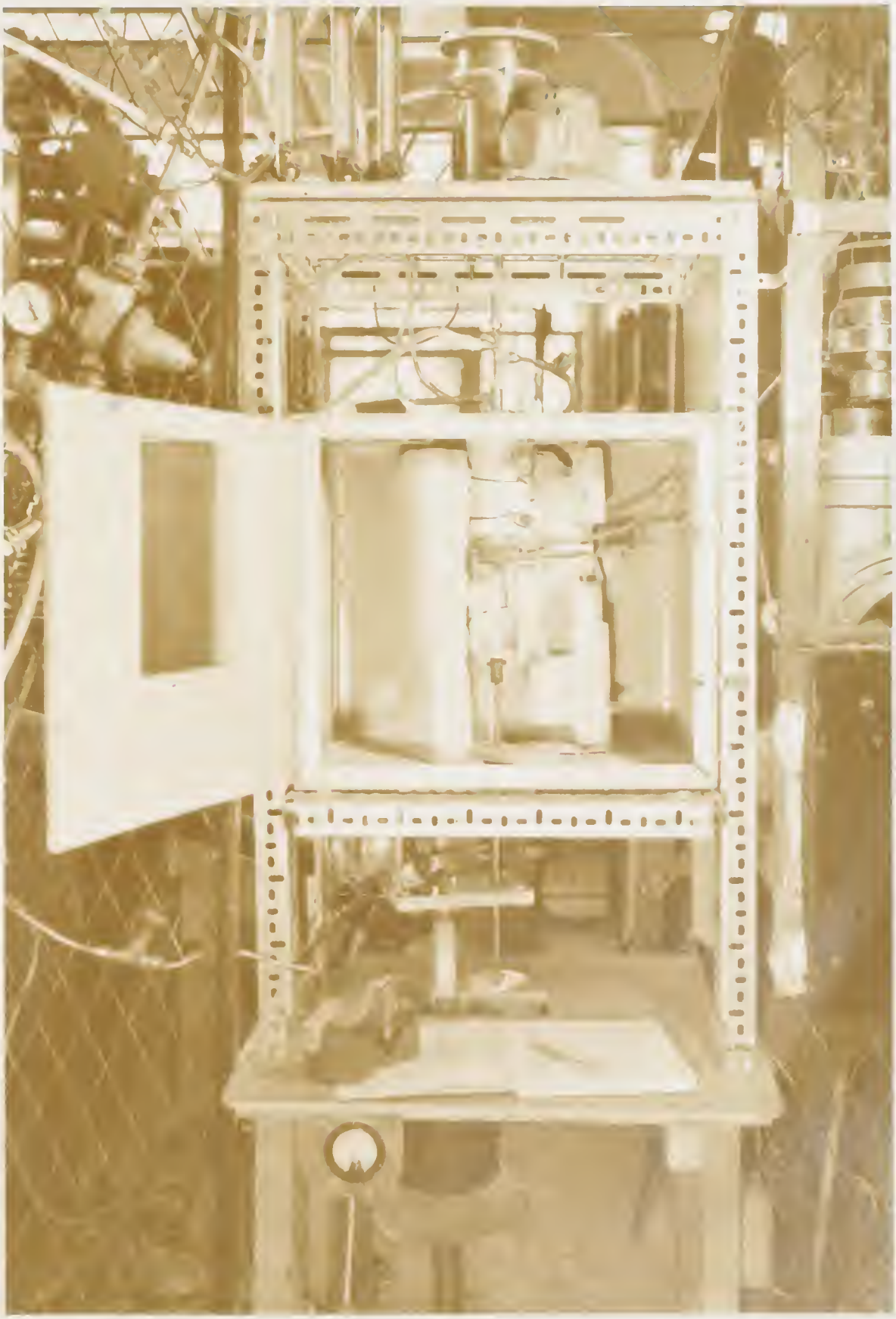

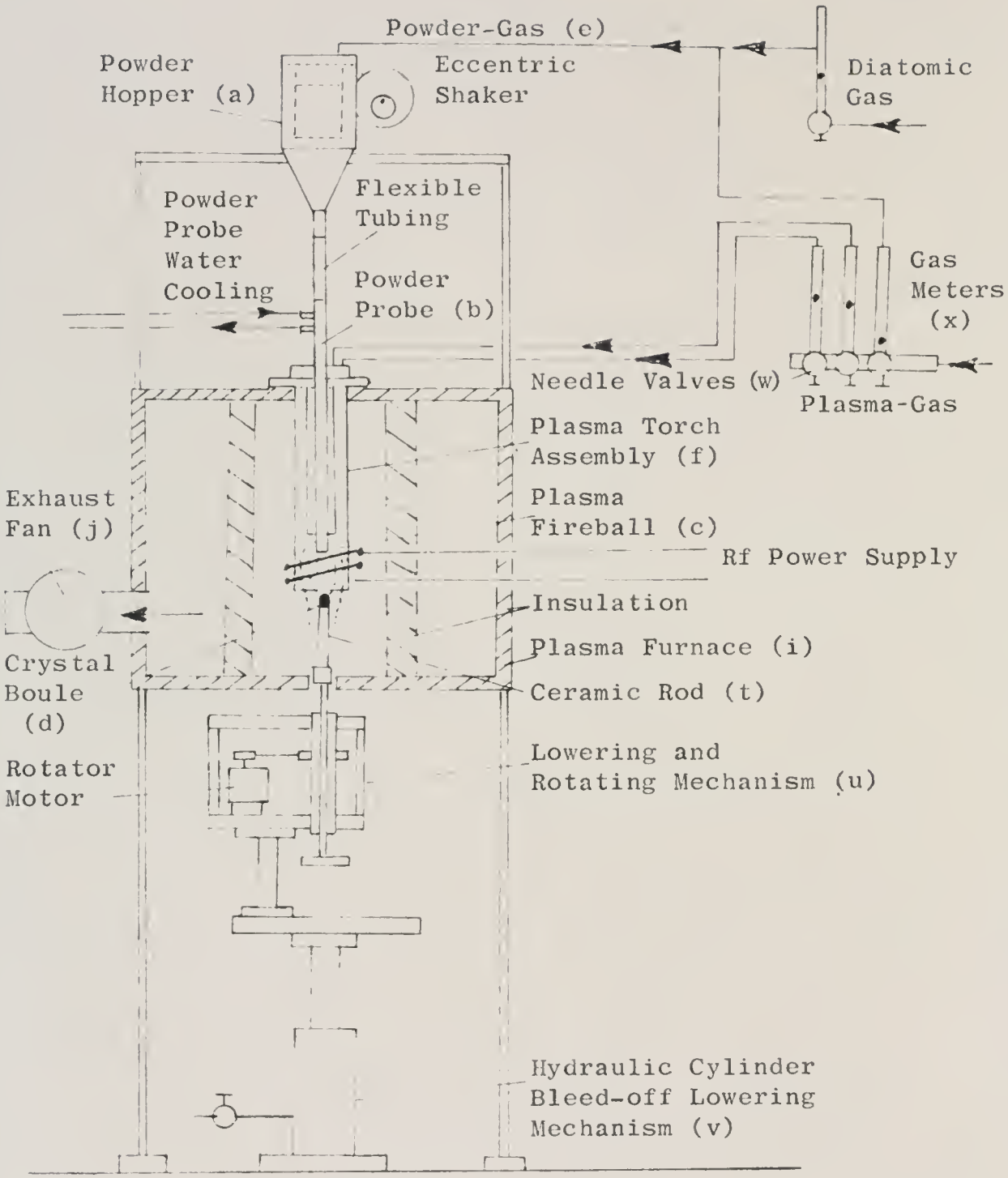

Figure 2 Plasma-Verneuil Furnace Assembly

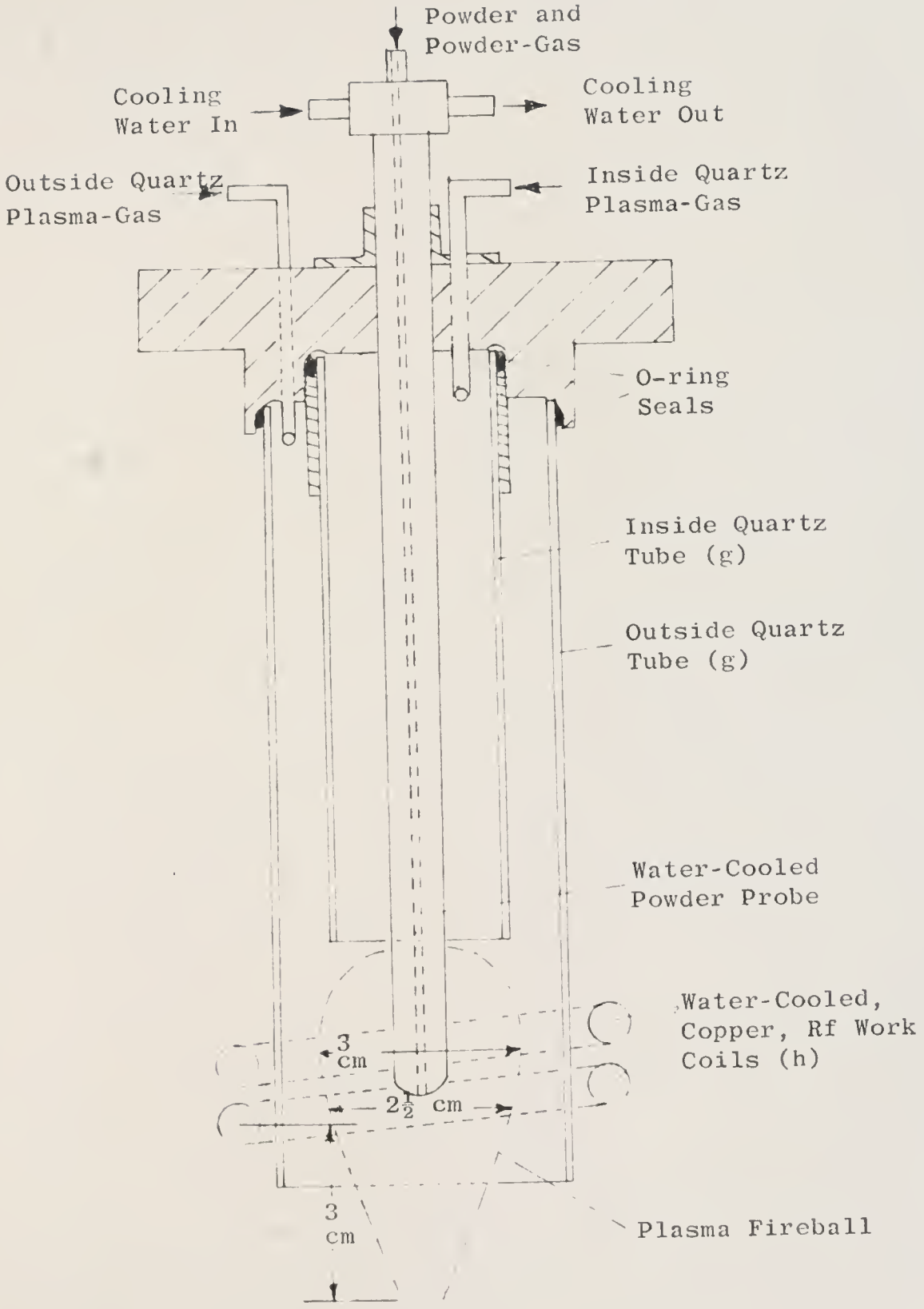

Figure 3 Plasma Torch Assembly

power supply coupled to the ionized argon by means of copper work coils (h). Initiation of the discharge is accomplished by a d.c. arc momentarily placed between the rf work coils. The powder probe is located along the axis of the torch assembly.

The entire torch and boule assembly is insulated against heat loss by a transite box (i) of Figure 2, called the "furnace". An exhaust system (j) is attached to the furnace to remove hot gases and any toxic fumes produced by the powder. A sight glass (not shown) permits observation of the crystallization process.

The powder feed apparatus, shown in Figure 4, is of critical importance. This unit must supply a steady, controlled flow of powder over time intervals of several hours. The feed method used here is that of a vibrating hopper (k) of Figure 4. Control is accomplished by proper matching of the powder grain size, size of hole in the bottom of the hopper (ℓ), and the vibrating frequency. For any given strong shaking of the unit the parameter that governs the flow rate is the ratio of the hole size to the powder grain size. When this ratio was 10 or more it was found that the powder flowed freely even when the unit was stationary. When this ratio was 3 or less it was found that the flow rate was erratic, presumably due to blockage of the hole. The ratio that gave the best flow control was found to be dependent on the powder grain size; a ratio of 8 or 9 was good for very fine powder (less than #250 mesh, or 0.0024" diameter). A quantitative study of the powder feed mechanism is described in Appendix A.

The powder hopper is enclosed in a gas-tight container (m) in such a way that powder gas (n) can be utilized to aid the flow of powder to the boule. The hopper is mounted in the container in a manner that permits it to bang against the container wall as it shakes.

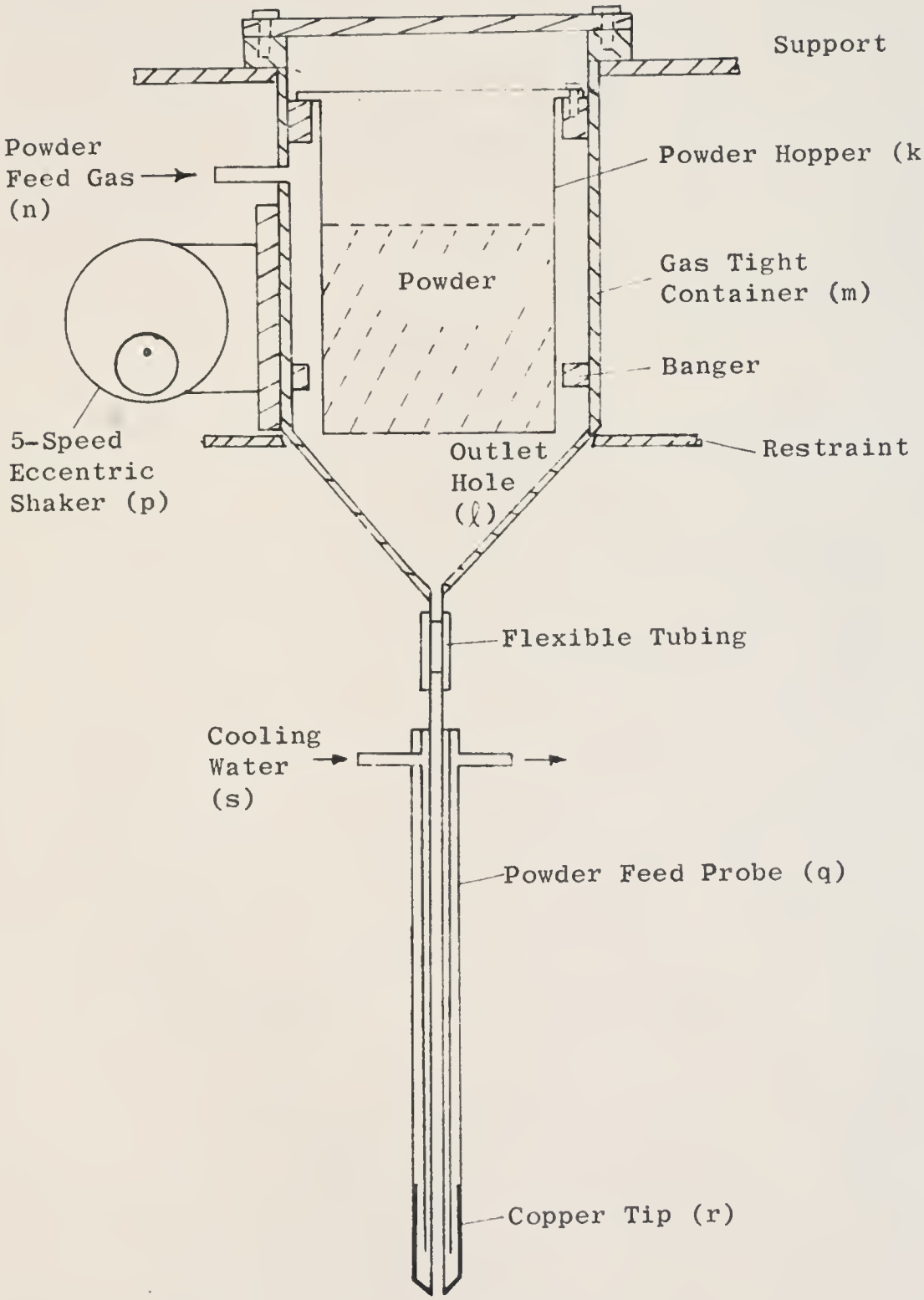

Figure 4 Powder Feed Apparatus

A five-speed eccentric shaker (p) is attached to the hopper assembly. It was found that one of the speeds produced a frequency that closely matched one of the natural frequencies of the assembly, producing a strong shaking response and excellent uniformity of powder flow rate.

The powder probe (q) of Figure 4 consists of three concentric, small diameter brass tubes having a 2.5 cm long, pure copper tip (r). Powder flows down the innermost tube. The outer tubes are for water cooling (s). The water-cooled tip permits the probe to be inserted directly into the plasma fireball. Materials of zero resistivity and infinite resistivity cannot be inductively heated. Copper has such a low resistivity that it is only poorly heated by the rf fields. In addition, the high thermal conductivity of copper helps to prevent it from burning out in the plasma.

The crystal boule (d) of Figure 2 is grown on the tip of a ceramic rod (t). This rod is held by a mechanism (u) that permits rotation of the boule (4 rpm) and withdrawal either manually, by a screw mechanism, or automatically, by a controlled bleed-off from an hydraulic system (v).

Flows of plasma, powder and diatomic gases are controlled by needle valves (w) and are measured by variable-area, floating-ball-type gas meters (x).

C. Previous Investigation and Scope of this Investigation

Irving Langmuir of the General Electric Research Laboratory is credited with first using the word "plasma" to describe an ionized gas (1928). Since then, use of low pressure plasmas has been commonplace, as in fluorescent lights. Somewhat higher pressure plasmas (to 500 mm Hg.), created by induction coupled power supplies, were reported in 1941 by G. I. Babat of the USSR.[1] In 1961, T. B. Reed of the Massachusetts Institute of Technology reported coupling a

radiofrequency power supply to an argon plasma at atmospheric pressure.[2] Later that year Dr. Reed reported using the plasma torch to grow refractory crystals.[3]

A subsequent article by Dr. Reed in 1962[4] again mentions using a plasma torch for growing crystals. But neither article includes an analysis of the heat transfer-crystallization mechanism taking place in the plasma fireball.

The Verneuil method of crystal growth was first reported in 1902.[5] Descriptions of the apparatus and general method appear in numerous publications; and commercial apparatus is described in German and Russian publications.[6] But again, details of the heat transfer-crystallization mechanism are not considered.

The purpose of this investigation is to analyze the crystallization mechanism within a plasma fireball. The scope of the investigation will be:

1. the experimental determination of the heat transfer capabilities of a plasma flame, including the effects of diatomic gases, rf power levels, geometry of boule and powder probe, powder-gas flow rates, and powder sizes;

2. the construction of a theoretical model for the heat transfer-crystallization mechanism;

3. the experimental correlation of temperatures and thermal gradients to the temperature dependence of the model; and

4. an analysis of the quality of the crystal as a function of its growth rate and the thermal gradient at the liquid-solid interface.

CHAPTER II. THEORY

A. Rf Coupled Plasma

The mechanism of the coupling of an rf power supply to a plasma is essentially the same as the mechanism of induction heating. An induction coil of a tuned circuit is placed around the material to be heated - the plasma. A time-varying magnetic field, produced in the rf work coil, and oriented essentially along its axis, causes "eddy currents" to be set up in the plasma, provided the plasma has sufficient conductivity. The direction of the eddy currents in the plasma is such as to produce a magnetic field that opposes any change in the applied field, in accordance with Lenz's law. Thus the plasma current must flow in a plane perpendicular to the coil axis, i.e., in the same plane as the rf current that produces the original magnetic field.

A perturbation of the plasma current is caused by the electric field in the induction coil. Potentials of 3000 - 4000 volts are common across the work coil terminals. The field caused by this voltage causes motion of the charged particles in accordance with the laws of Coulomb and Newton. The actual trajectory of the charged particles is not easily analyzed, however, since the geometry of the electric field within the rf work coil is not a simple one.

A further perturbation on the plasma current derives from the fact that materials, in general, exhibit capacitance when placed in a high frequency field. The effect of this capacitance is to alter the distribution of the time-varying electric and magnetic field intensities within the material.

The amount of the alteration, for any given rf frequency, is a function of the material's capacitance, conductance, permeability and geometry. For a good conductor, of small capacitance and large enough radius for the effect to take place, the high frequency eddy currents, produced by a time-varying magnetic field, tend to crowd to the periphery of the material. This phenomenon is known as the skin effect. The solution of the magnetic field equations for the simple case of a cylinder enclosed by a coil yields a magnetic field intensity that is a function of the radius of the cylinder, plus a grouping of physical constants called the "skin thickness". If the ratio of the cylinder's radius to its skin thickness is less than 1, then the field is almost uniformly intense within the material. However, if this ratio exceeds 1, the magnetic field becomes more intense at the periphery, and produces a larger current there than on the axis.

Assuming that the plasma has the permeability of a vacuum and a conductance of 100 $(\text{ohm-cm})^{-1}$,[2] then at 4 mc rf supply the skin thickness is 0.25 cm. The plasma fireball used in this work had a radius of approximately 1.25 cm; thus the effects of skin thickness are probably present.

The net motion of the charged particles in the plasma, i.e., the current, is determined by the net strengths and directions of the electric and magnetic fields produced in and by the rf work coil, including, if present, the influence of skin thickness. Resistance to the motion of these charged particles is provided by a collision mechanism in which part of the energy gained by the charged particles, due to their acceleration in the force fields, is distributed to the other species of particles present. This mechanism increases the energy content, or temperature, of the non-ionized species of the plasma. If the mean free path between collisions is small, then the energy distribution among all

species present tends to approach "equilibrium". By "equilibrium" it is meant that steady state conditions exist and that the energy distribution among all particles present can be expressed by the Maxwellian distribution function.

Steady state is the easier of the above conditions to meet, only requiring that the total energy and mass content of the fireball be constant with time. This requirement is satisfied when the gas flow rate and rf power are held constant.

The second condition, involving the specific manner in which the total energy must be distributed amongst the particles present, is not easily met. This condition requires that the temperature of the fireball be uniform throughout, i.e., that no thermal gradients exist within the fireball. On a microscopic scale this implies that for every mechanism involving a transfer of energy between particles there be an inverse mechanism, of exactly the same nature, occurring elsewhere, so that the distribution of energy amongst particles remains constant. Since the plasma is optically thin, and a net radiant emission is always present, this condition could only be satisfied, physically, by enclosing the fireball in an isothermal container, i.e., by creating a black body of it.

The fact that the fireball is not contained in an isothermal enclosure, and that thermal gradients do exist in it,[2] precludes any possibility that the entire fireball mass is in thermal equilibrium. However, it can be argued that, under certain physical conditions of pressure and size, small volumes within the fireball may exist in a state that is very close to equilibrium. Under these conditions the assumption of "local thermodynamic equilibrium", abbreviated LTE, is often made for analytical purposes. LTE is defined as the existance of near-equilibrium in the immediate neighborhood

of a given point at a given time. The physical conditions leading to LTE are a high number density of all species present, a high collision frequency amongst particles, a low radiant emission, and a negligible thermal gradient. Griem, 1963,[7] discusses these conditions for atmospheric plasmas, such as used in this experiment, and concludes that the assumption of LTE appears justified.

B. Plasma Heat Transfer

Thermal, rf coupled plasmas are a relatively new laboratory phenomenon (1961). The diagnostics of their properties has not yet reached the stage where final conclusions can be made about their behavior and properties. No theory has yet been advanced that reliably predicts and explains their heat transfer capabilities.

There is a growing amount of literature, however, giving experimental heat transfer data. The bulk of the evidence indicates that the primary mechanism of heat transfer is that of convection. The radiation component apparently only becomes significant at very high power levels, where the degree of ionization is more than just a few percent.

T. B. Reed[8] has compared the net heat transfer rates of a 4 kw argon plasma to that of an oxy-hydrogen flame and found them to be almost equal. The result is surprising, considering the large temperature difference that presumably exists between the two flames, i.e., approximately 8000 K average for the plasma and 3000 K average for the oxy-hydrogen flame. No satisfactory explanation of this seeming anomaly is yet available. The reasons for it must be sought in the better understanding of the plasma's transport properties of diffusion, viscosity, thermal conductivity, and specific heat.

Even for non-ionized gases, whose transport properties are fairly well established, the theoretical determination of the convection heat transfer is still not an easy matter. Traditionally, this component of heat transfer has been described in terms of a simple, empirical equation:

$$Q = h(T_H - T_C) \tag{1}$$

where h, the coefficient of heat transfer, is either determined experimentally for each application or estimated from other empirical equations. The most common of the latter is that for the Nusselt number:

$$\left(\frac{hD}{k}\right) = C\left(\frac{DV\rho}{\mu}\right)^{\alpha}\left(\frac{C_p\,\mu}{k}\right)^{\beta} \tag{2}$$

where the groupings in parenthesis are recognized as the Nusselt number, the Reynolds number, and the Prandtl number respectively. The exponents and coefficient of (2) must be determined from experiment.

The empiricism of (1) and (2) obscures any real insight into the true mechanism of convection heat transfer. There have been efforts to correct this deficiency by describing convection heat transfer in terms of the more basic concepts of boundary layer and kinetic theory. One of the earliest publications of this nature is by E. Pohlhausen, 1921,[9] who presented a solution of the Navier-Stokes equations for a laminar stream parallel to a plane plate, thus obtaining the temperature profile in the boundary layer, from which the gradients could be determined. The gradients can then be related to the heat flow from the Fourier equation, which is considered fundamental. One of the more recent papers of this nature, concerned with plasma heat transfer, is by Fay and Riddell, 1958.[10] These authors derive an expression for the convective heat transfer in

terms of the Fourier heat flow across the boundary layer plus the diffusion through the boundary, and the recombination on the surface, of dissociated ions. The thermal profile in the boundary layer is calculated from a solution of the conservation equations. Another solution to convective heat transfer, using a similar approach, is that by J. P. Reilly, 1964.[11] In this paper the radiation component from the ionized gas is also considered and found to be less than 10% of the total heat transfer.

The radiant heat transfer from any gas is, in general, either small or negligible when compared to its convection heat transfer. The reason for this lies in the mechanism of radiant emission. The radiant spectrum from an ionized gas consists of a line spectrum, due to electron transitions in bound states between allowed energy levels, and a continuum spectrum, caused by the sudden stopping of free electrons as they collide with other particles present (bremsstrahlung) and by the acceleration of free electrons in the rf magnetic and electric fields. The radiant intensity of a line spectrum is very small. The radiant intensity of a continuum spectrum is a function of the degree of ionization of the gas, and thus is small at low ionization levels, but can become significant at large ionization levels.

The emissive power from any hot gas can be considerably increased by the introduction of a fine powder. The fine powder is heated in the flame, becomes luminous, and emits a strong radiation continuum spectrum. Wohlenberg and Morrow, 1925,[12] investigated the radiative power from coal-powder flames and found that the emissivity of the flame increases substantially as the number density of the particles increases and as the particle size decreases. The application of this mechanism to the present research relates to the situation when powder is fed through the plasma fireball to be

crystallized on the boule. When the powder grains are small and numerous they will become luminous and emit a strong radiation continuum spectrum that will tend to cool the plasma and, therefore, cause a reduction in the boule temperature.

C. Crystal Growth

There are many methods by which large, single crystals can be grown. These methods are often catagorized by the phase from which the crystal is grown, i.e., growth from a vapor, solution, melt, or by a disorder-order solid phase transformation. The mechanism of the lattice formation is not necessarily the same for all methods. The movement and deposition of an atom, or groups of atoms, from a vapor phase to the lattice is, in general, influenced by different factors than is the deposition of atoms from a viscous melt.

Although the microscopic mechanism of deposition may vary between the methods, the laws of thermodynamics must apply in all cases. The thermodynamic laws governing phase transitions and phase equilibrium were first proposed by Willard Gibbs, 1906. He postulated that the driving force causing phase transitions, i.e., crystallization in this case, is the difference in free energies between the phases; that for equilibrium to exist in any single phase the phase must be at a minima of free energy; and that for two phases to be in equilibrium, the free energies, temperatures and partial pressures of the components comprising the phases must be equal.

Gibbs considered the phenomena of crystallization and developed an expression for the free energy of a crystalline nucleus that included a term to account for surface tension. As a nucleus grows it must expand against its own surface tension. The work done in this expansion adds to the

the free energy of the nucleus, and is most pronounced for small radii, when the ratio of surface area to volume is largest. Counteracting the rise in free energy due to surface tension is the decrease in free energy due to the loss of the latent heat of solidification. This loss of free energy is directly proportional to the volume increase. Thus for materials of large surface tension it is possible for the net free energy of a nucleus to rise as it first starts to grow. The increase in free energy continues until at some critical ratio of surface area to volume the free energy starts to decrease due to the overriding effects of the loss of latent heat of solidification. If the free energy of the nucleus should ever rise to a level where it is above the free energy of the phase from which it is growing, the driving force reverses and the nucleus starts to dissolve. This effect emphasizes the importance of having large differences in free energy between phases whenever self-nucleation is desired, so as to assure that the free energy of the nucleus never exceeds that of the phase from which it is growing. However, once the critical size has been exceeded, further growth can proceed at smaller driving forces, since volume effects override. If only small driving forces are available, then seed crystals can be used to initiate the growth process.

Another interesting result from an analysis of Gibbs' postulates is that, due to entropy, it is impossible to form a perfect crystal at temperatures above absolute zero. The reason is that a crystal seeks its equilibrium state at a minimum of its free energy. Assuming a solid aggregate originally in a state of relative disorder (perhaps having been cooled rapidly from a high temperature) then any increase in the degree of order (annealing) reduces its internal energy and its enthalpy. However, the increase

in order causes a decrease in the entropy; and the combined effects are such as to cause a minimum of free energy at some intermediate point between order and disorder. It can also be shown that this equilibrium point of disorder can be shifted by a change in the annealing temperature. Only if annealed at absolute zero could the crystal become perfectly ordered. Thus, for all practical purposes, perfect lattices can be considered an impossible achievement.

The thermodynamic arguments deal with macroscopic, equilibrium states. Although powerful as diagnostic tools, they do not give insight into the microscopic behavior nor the rates of the process. W. Kossel and I. N. Stranski (1927, 1928) are regarded as the first to publish theories of crystal growth based on the microscopic nature of the chemical bond.[13] Although published separately, their theories are so similar that they are referred to as the Kossel-Stranski theory. One of their basic assumptions is that atoms or molecules are deposited one at a time on the growing lattice. They assume that the latent heat of solidification is given up in steps as an atom or molecule adheres to the lattice and is gradually covered over. The total latent heat is taken as the sum of all the bond energies holding the particle to the completed lattice. The strengths of the bonds vary with orientation, and may be different for the various faces of a lattice. Thus the fraction of the total latent heat given up by a particle attaching to the center of one flat face may be different from that attaching to the center of another, differently oriented, face; and both will be different from that attaching to a site alongside a previously deposited particle, where more than one bond is involved in the mechanism.

The authors calculated the bond energies (based on Coulomb forces) for 27 possible sites on an ionic, cubic

lattice. They postulated that the most favored sites are those having the largest attractive forces, or the largest possible decrease in latent heat. That these sites are the most favored can also be postulated from a consideration of probability theory. By assuming that the equilibrium phase is that of the completed crystal, then the atoms in the vapor state have energy levels farthest removed from their equilibrium value and are, thus, least probable. The atoms most strongly attached to the lattice are nearest in energy level to those of the completed lattice and are, therefore, most probable. Probability theory also predicts that at very high temperatures the difference in preference between the sites will vanish. Thus the mechanism of deposition, and the final form of the crystal, for crystals grown from a melt at high temperature can be expected to be different from those grown from a vapor or from a solution. In general, the Kossel-Stranski assumption of deposition of particles one at a time makes it applicable mainly to crystallization from the vapor state, where the chances of finding single atoms or molecules is greatest.

Another limitation of the Kossel-Stranski theory lies in their concept of a basically flat surface at the interface between the phases. Atoms then deposit on the surface one layer at a time. Burton and Cabrera, 1949,[14] employed statistical concepts to show that a surface must be very rough, on a microscopic level, and that, therefore, an interfacial surface must continually present a great many of the kinds of sites proposed by Kossel-Stranski. Burton and Cabrera further postulate that the probability of nucleation taking place on a perfectly flat surface, at low driving forces, is small and that a rough surface is required to explain the observed growth rates at low driving forces.

F. C. Frank, 1949,[15] further considered surface effects on crystal growth and proposed a growth mechanism in the form of a screw dislocation (or spiral staircase growth pattern). Such a dislocation would preclude any need for deposition of a single particle on a flat surface, since no new flat faces are ever formed in this pattern of growth. Frank cites figures that predict supersaturations of 10% or more are required for self-nucleation from a vapor, 5% for self-nucleation from a solution, and 1.5% for single particle deposition upon a perfectly flat surface. He notes that observed growth rates on seemingly flat surfaces can occur at 0.8% supersaturation, and postulates that the mechanism allowing this growth must be that of the screw dislocation. Since his paper was published there have been numerous X-ray photos appearing in the literature showing this type of growth pattern. However, not all crystals show it. It does occur most often in crystals grown from a vapor, and thus does give some confirmation to the basic premise that some mechanism other than deposition layer by layer is required for growth from the vapor phase at low driving forces.

The most recent published theories of crystal growth seem to be based on the Kossell-Stranski, Burton and Cabrera and Frank theories, and are thus most suited to models of growth from a vapor phase. Their common assumption that particles deposit individually on a surface appears to be a simplification, however, since it is estimated[16] that even in a supercooled vapor there can exist aggregates of as many as 1000 molecules or more. Their theories are less applicable to growth from solutions or melts where it has been established that a definite degree of order exists in the liquid state.[17] X-ray diffraction patterns of liquid metals reveal a substantial ordering of atoms, suggesting a conglomeration of aggregates that can be considered partially

solidified, although still fluid. Thus any theory of growth from a liquid phase must consider the degree of order already existing in this phase. Deposition would seem to occur by groups of atoms rather than by single atoms.

Unfortunately a kinetic theory of the liquid state is not yet available. Temperature, motion (perhaps ultrasonic), pH, impurities, and the transport properties of a melt or solution are all known to affect the crystal growth mechanism.[16] A classic example of this, often cited, is that sodium chloride crystals are cubic when grown in an aqueous solution but are octahedral when grown in a 15% aqueous-urea solution.[13] The phenomenon is not completely understood. Such difficulties in understanding the liquid state prompted the following statement from N. N. Sheftal, after the 1956 Conference of Crystal Growth, USSR: "...the gulf between theory and practice is so wide that not even a roughly approximate theory of crystal growth could be proposed."

In spite of the uncertainty concerning the microscopic mechanism of crystal growth, the thermodynamic laws governing the process must still hold. And from these laws, and from certain experimental observations, apparatus for the growing of crystals can be designed. The following are some of the more important observations on crystal growth.

1. Certain crystalline faces, of some materials, grow more rapidly than do other faces. Generally, the faster growing faces are those of high surface energy, and low reticular density. However, this rule is not always adhered to.[18]

2. Equivalent interfacial angles between crystals of the same material are always the same.

3. The final form of a crystal can be changed by altering the environment in which it is grown.

4. The rate of growth of a crystal varies as the degree of supercooling or supersaturation varies.

5. The most perfect crystals are grown slowly.

6. Imperfections in crystals are the rule, not the exception.

D. Heat Transfer-Crystallization Model

A hypothetical model describing the growth of a boule in a plasma furnace can be postulated from the laws of thermodynamics and heat transfer. The boule, Figure 5, is covered by a liquid layer of varying thickness, having a temperature T_L at the top and T_S at the bottom. T_S is slightly below the melting point of the liquid so that the liquid at the solid-liquid interface is slightly subcooled. The degree of subcooling is primarily governed by the thermal gradient at the interface, other factors such as plasma heat transfer and powder feed rate being held constant.

The driving force for the crystallization mechanism is the degree of subcooling. Presumably, if the degree of subcooling is large, self-nucleation is possible and a polycrystalline boule may result. Also, if the subcooling is very large, the average temperature of the molten layer will not be much greater than the melting temperature of the material. Under these conditions any powder falling on the boule will not be completely liquefied before solidification takes place. The result will be a boule composed of an agglomeration of incompletely melted powder particles.

Another disadvantage of too high a degree of subcooling is that high driving forces imply fast deposition rates, which may not allow sufficient time for impurities to diffuse out of the growing lattice. In general, therefore, excessive subcooling, due to high thermal gradients, can be equated with poor crystal quality. Very low degrees of

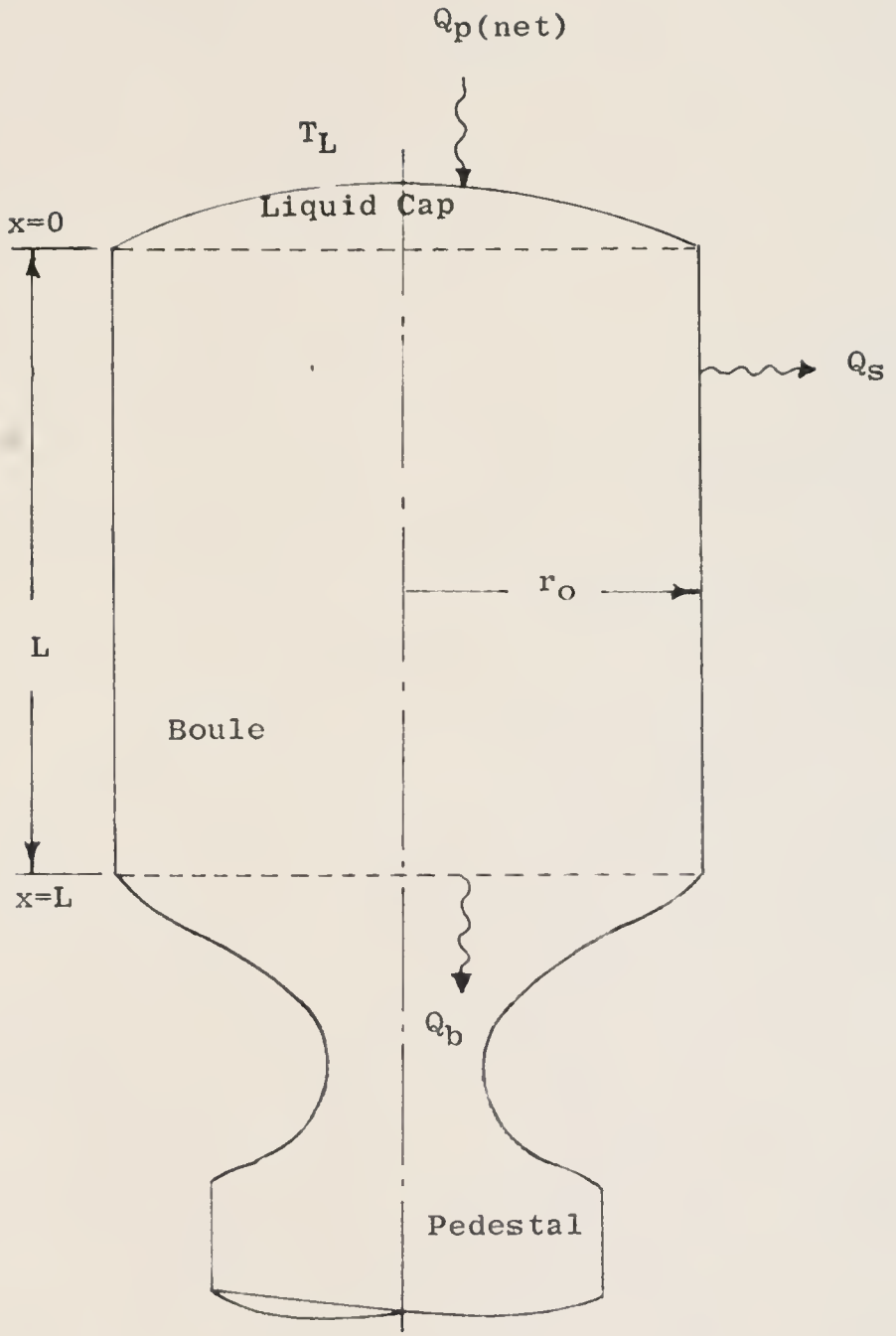

Figure 5 Simplified Boule Geometry on which the Mathematical Model for the Heat Transfer-Crystallization Mechanism is Based

subcooling, caused by small thermal gradients, imply slow rates of deposition, and possibly a defective growth mechanism such as the screw dislocation. Thus it appears that the axial thermal gradient is an important parameter in the determination of crystal quality.

Since the axial thermal gradient is one of the key parameters in the analysis of the growth process, a method has been developed (Appendices B and C) to obtain the profile of the thermal gradient across any given cross sectional sample of a boule. The method is based both on theory and experiment. Essentially, the method employs the use of an observed axial thermal gradient at the periphery of a boule as the boundary condition for a theoretical determination of the axial thermal gradient within the boule. Any differences in crystal quality found as a function of the radial distance from the center of the boule might be explained in part by the thermal gradient profile across the slice, that existed at the time the crystal was formed.

Although the theoretical equation is based on a simplified geometrical model, and on certain linearization approximations, still, the imposition of the known peripheral condition should hold the approximation errors to a minimum.

The following equation (3) for the thermal profile at the solid-liquid interface is similar to that given by Carslaw and Jaeger.[19] The derivation, giving the necessary assumptions, is presented in Appendix B.

$$\left.\frac{dT}{dx}\right)_{\substack{x=0\\r=r}} = -T_A \sum_{i=1}^{\infty} A_i \alpha \lambda_i \left[\frac{\alpha \lambda_i \sinh \alpha \lambda_i + h_2 \cosh \alpha \lambda_i}{\alpha \lambda_i \cosh \alpha \lambda_i + h_2 \sinh \alpha \lambda_i}\right] J_o(\lambda_i r) \qquad (3)$$

where:

$$A_i = \frac{2\lambda_i^2}{J_o^2(\lambda_i)\left[\lambda_i^2 + h_1^2\right]} \int_0^1 rg(r) J_o(\lambda_i r)\, dr \qquad (4)$$

$$g(r) = \frac{T_{mp}}{T_A} - 1 \qquad (5)$$

$$h_1 = \frac{\lambda_i J_1(\lambda_i)}{J_o(\lambda_i)} \text{ , eigenvalue equation for the } \lambda_i \qquad (6)$$

$$h_1 = \frac{r_o \bar{h}_s}{k} \qquad (7)$$

$$h_2 = \frac{L\, \bar{h}_b}{k} \qquad (8)$$

$$\alpha = \frac{L}{r_o} \qquad (9)$$

The thermal gradient given by equation (3) has been plotted in Figures 6, 7, 8, 9 and 10 for various assumed values of boule radius, length and side coefficient of heat transfer. The figures show how the thermal gradient increases as the boule grows, for $\bar{h}_s$ above $(0.075)(10^{-3})$ cal/sec cm^2 ^oC, and decreases for lower values of $\bar{h}_s$, for constant boule radius. Figure 10 shows, for a constant side coefficient of heat transfer of $(0.15)(10^{-3})$ cal/sec cm^2 ^oC, how the thermal gradient decreases as the boule radius increases.

Further understanding of the growth behavior can be obtained by comparing the results of the above figures with a heat balance on the molten cap, given in equation (10):

$$\bar{T}_L = T_M + \frac{Q_{p\ net} - KA\nabla T\big)_{\substack{x=0 \\ r=r}}}{\dot{m}\, C_p} \qquad (10)$$

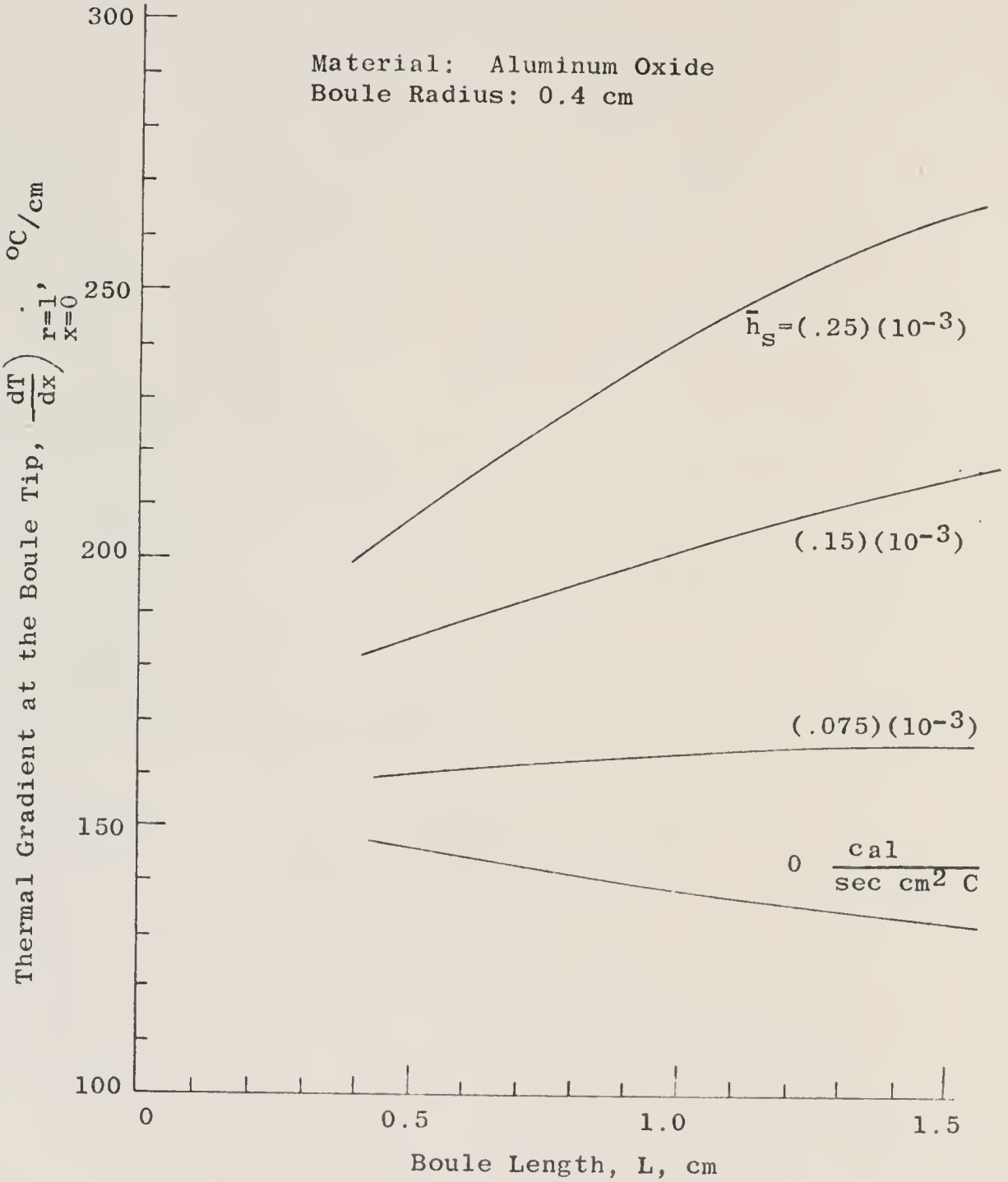

Figure 6 Thermal Gradient at the Boule Tip as a Function of the Boule Length and Average Coefficient of Heat Transfer Along the Side, for a Boule of 0.4 cm Radius

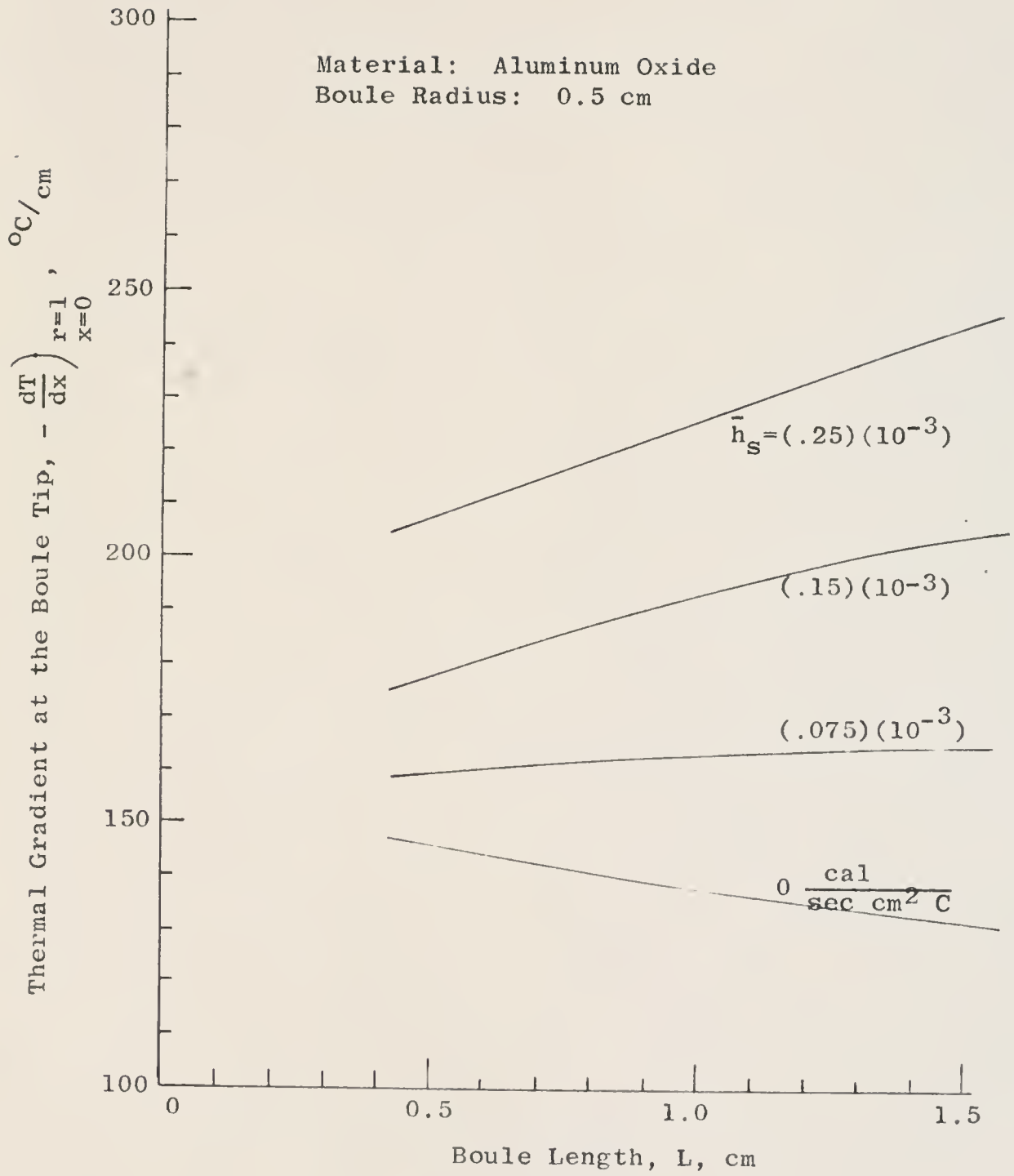

Figure 7 Thermal Gradient at the Boule Tip as a Function of the Boule Length and Average Coefficient of Heat Transfer Along the Side, for a Boule of 0.5 cm Radius

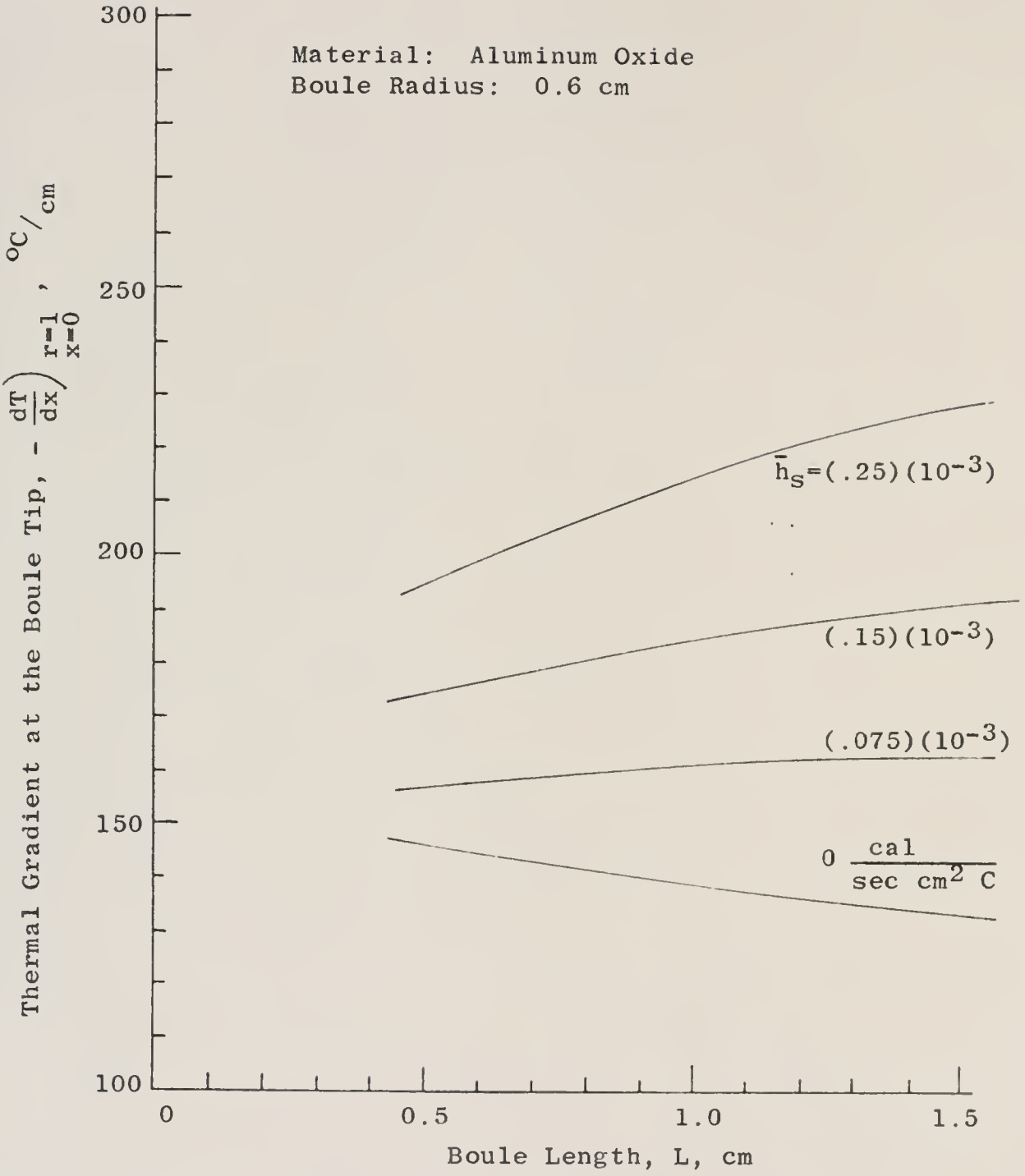

Figure 8 Thermal Gradient at the Boule Tip as a Function of the Boule Length and Average Coefficient of Heat Transfer Along the Side, for a Boule of 0.6 cm Radius

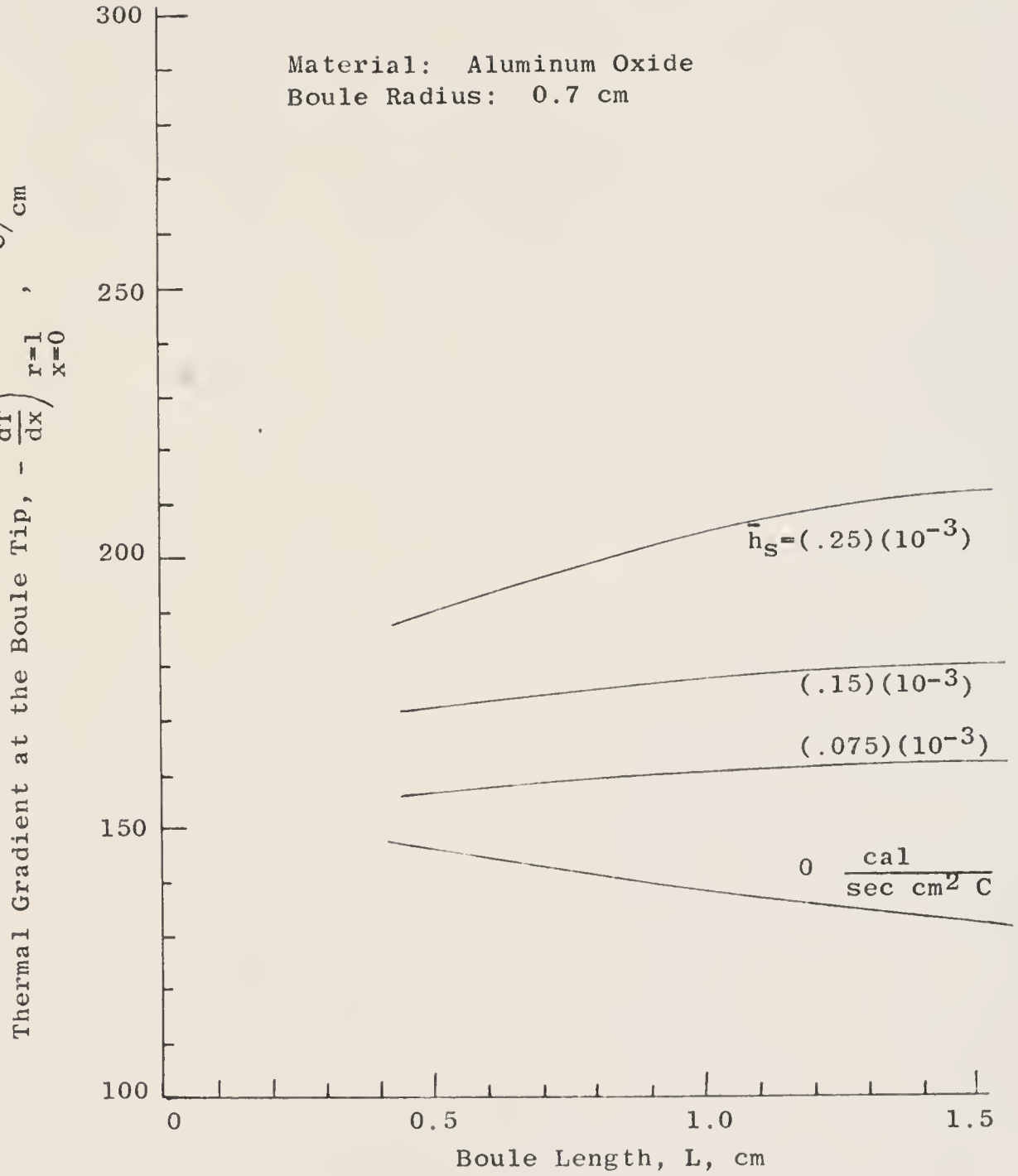

Figure 9 Thermal Gradient at the Boule Tip as a Function of the Boule Length and the Average Coefficient of Heat Transfer Along the Side, for a Boule of 0.7 cm Radius

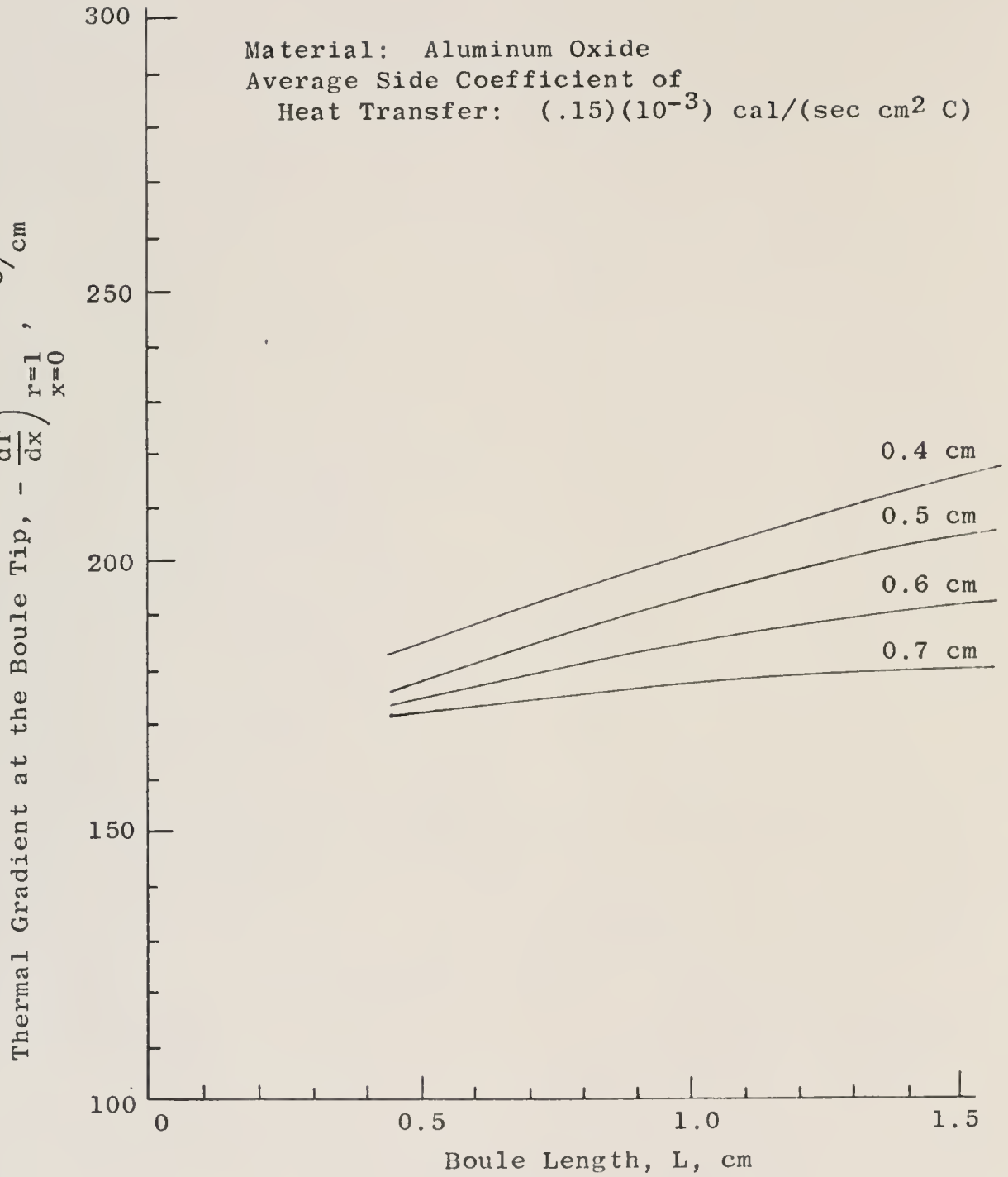

Figure 10 Thermal Gradient at the Boule Tip as a Function of the Boule Length and Radius, for a Constant Average Side Coefficient of Heat Transfer of (.15)(10-3) cal/(sec cm^2 C)

For the condition where the thermal gradient increases as the boule grows longer, and from equation (10), it can be reasoned that if $Q_{p\ net}$ and $\dot{m}$ are held constant, then $\bar{T}_L$ must decrease as the boule grows. The decrease in $\bar{T}_L$ will continue, as the boule gets longer, until a point is reached where the conduction heat loss from the tip is large enough to cause the molten layer to vanish. At this point, crystal growth ceases.

Thus if long boules are required, and the $\bar{h}_s$ is greater than $(.075)(10^{-3})$ cal/sec cm^2 ^oC, then either $Q_{p\ net}$ must be increased or $\dot{m}$ decreased as the boule grows, in order to maintain a molten cap. In other words, long boules can be grown only when $\bar{h}_s$ is less than the above given value. Also, it can be postulated that the crystal quality will be poorest at the segment to solidify last, since this segment was grown under conditions of highest thermal gradient and lowest $\bar{T}_L$.

Consideration of equation (10) also leads to the conclusion that, for a given thermal gradient and $Q_{p\ net}$, $\bar{T}_L$ is reduced by excessive powder feed, $\dot{m}$. And if $\bar{T}_L$ is low, and $\dot{m}$ high, then, regardless of the gradient, the crystal quality will be poor since solidification will take place before the powder has completely melted, thus resulting in an agglomeration of powder particles instead of a single crystal. It appears, therefore, that for any given input power $Q_{p\ net}$, there is a certain relationship between the thermal gradient and the powder feed rate that produces the best quality crystals.

Another deduction that can be made from an analysis of Figures 6, 7, 8 and 9 and equation (10) is that if $Q_{p\ net}$ is initially quite high, causing $\bar{T}_L$ to be high, then the liquid cap may become limpid and extend over the sides,

causing the boule to increase in diameter as it grows. This tendency to a large radius will be aggrevated by the fact that the thermal gradient decreases with increasing radius (Figure 10) for $\bar{h}_s$ greater than $(.075)(10^{-3})$ cal/sec cm^2 ^oC, thus tending to keep $\bar{T}_L$ high. The result of this condition will be the growth of a boule in the form of an inverted cone.

From an analysis of the variables in equation (3) it is seen that the boule tip thermal gradient is a function of:

a) thermal conductivity of the material, k
b) average coefficient of heat transfer from the sides of the boule, $\bar{h}_s$
c) radius and length of the boule, r_o and L
d) temperature at the liquid-solid interface, T_{mp}
e) ambient temperature, T_A
f) average coefficient of heat transfer from the base of the boule, $\bar{h}_b$.

These variables cannot be controlled by the equipment operator. The variables affecting the plasma heat transfer to the boule, Q_p, however, are capable of control by the operator. These are the:

a) rf power level
b) flow rate of the powder-gas
c) presence of a diatomic gas in the plasma
d) quantity and grain size of the powder being fed.

Thus the maintenance of a proper value of $\bar{T}_L$ for good crystal quality must be sought in variations of Q_p and $\dot{m}$. And within the limits of the available power supply it is presumably possible to match the rise in thermal gradient as the boule grows longer with an increase in Q_p so as to maintain $\bar{T}_L$ constant. If $\bar{T}_L$ is maintained at a value that does not cause a limpid liquid layer, then proper matching of the above parameters can conceivably result in the growth of a boule of constant radius.

It should be mentioned that crystal quality might also be improved by the use of a proper flux, or catalyst, which would have greater solubility in the liquid phase than in the solid phase, and which might aid in the removal of absorbed gases from the molten cap. The discovery of such a flux is generally the result of trial and error experimentation.

In summary, the heat transfer-crystallization model predicts the following:

1. $\bar{T}_L$ should be kept high enough to adequately melt all the powder impinging of the molten layer,

2. $\bar{T}_L$ should not be allowed to become too low, or else an agglomeration of partially melted powder grains will result,

3. $\bar{T}_L$ can be controlled easiest by variations of Q_p and $\dot{m}$,

4. Q_p should be steadily increased to compensate for the increasing thermal gradient as the boule grows longer,

5. $\dot{m}$ should be kept small to maintain an adequate $\bar{T}_L$ with a minimum of rf power,

6. crystal quality is dependent upon the maintenance of a proper matching of $\bar{T}_L$, thermal gradient, $\dot{m}$, and possibly appropriate flux or catalyst,

7. crystal quality can be expected to vary with linear growth due to the variations in thermal gradient with length, and also due to the tendency of impurities to diffuse towards the molten end, and

8. crystal quality may vary radially if there are large variations in the thermal gradient between the center core and the periphery of a cross sectional slice.

E. Crystal Quality

The key parameter describing the effectiveness of any crystal growth process is that of crystal quality. Although "quality" means different things to different people, depending on their particular use of the crystal in question, still there is one absolute standard against which any crystal can be judged. This standard is that of a perfectly ordered array of atoms, each species present occupying a given and periodic site on a uniformly geometrical and stationary lattice. Then any deviation from this standard can be considered an imperfection.

Imperfections in crystals are, of course, the rule, not the exception. They run through a full spectrum in degree, from the gross imperfections existing in a rough foundary casting, to the carefully controlled amount of dopant in a transistor. For any given process of crystal growth, however, the source of the crystalline imperfection can sometimes be traced as coming from the method of growth, or impurity of the materials used.

The major gross defects attributable to the method of growth are the following:

a) polycrystalline boule -- caused by too rapid cooling, or too large a thermal gradient within the crystallizing material,

b) bubbles -- caused both by gases used in the crystallization process and also by the partial pressures of the vapors of the materials being crystallized. This latter defect can be considered a process defect since if large partial pressures are to be expected, then a method of growth should be used in which the partial pressures are kept small, i.e., vapor deposition, or growth from solution,

c) cracks -- caused by thermal stresses in an anisotropic crystal, due to rapid cooling, and

d) agglomerate -- due to insufficient melting of powder, caused by a low temperature of the liquid layer.

Macroscopic defects traceable to the purity of the materials used are as follows:

a) gross inclusions -- caused by large foreign particles (dirt), and

b) cloudiness -- occuring in otherwise translucent crystals due to large quantities of uniformly distributed impurities.

Defects that cannot be easily traced to any specific source are as follows (all are too small to see except for dislocations, which can be viewed under an optical microscope):

a) Frenkel defects -- the diffusion of atoms from their normal lattice sites to interstitial positions,

b) Shottky defects -- vacancies on normally occupied lattice sites,

c) dislocations -- distortions of the basic lattice geometry,

d) impurities -- both intentional, as the dopant in a transistor, and unintentional, due to the impossibility of refining any material to 100% purity,

e) non-stoichiometry -- occuring whenever the ratio of atoms present in a compound crystal is different from the ratio of atoms in the "normal" molecule of the material comprising the crystal, and

f) phonons -- a term referring to the (quantized) vibrations of the lattice, due to thermal energy. The effect of vibrations is a periodic alteration of the lattice geometry. Phonons are considered as defects in solid state technology due to their scattering of charge carriers.

The macroscopic defects can be detected with an optical microscope. A flat specimen is first prepared by polishing and etching, which makes grain boundaries, bubbles,

cracks and stressed regions show up more clearly (since they are preferentially attacked by the etch). Then the speciman is viewed under the microscope. A recent publication describing this procedure for an aluminum oxide crystal is by Gliki and Urusovskaya.[20] The authors describe the sample as etched by phosphoric acid at 320 C for 5 minutes, and polished with borax at 1000 C for 40 minutes. They report a dislocation density of $6x10^4$ per cm^2.

Another optical method of detecting dislocations involves the use of a polarization microscope.[21] If the specimen is of a single crystal, and its optic axis is straight (undistorted), then no light should pass through the combination of crossed Nicols and the crystal (along its optic axis). This method can also be used to determine the orientation of a particular crystal.

Other methods of measuring gross defects include the determination of a crystal's specific gravity and its hardness (to measure voids and compactness).[22] The hardness scale normally used is that of the mineralogist in which diamonds, the hardest known substance, is given the rating of 10 on the Moh scale, and corundum is rated at 9 on the Moh scale. Talc is the softest material at 1 on the Moh scale. Steel files are about 7 on the Moh scale. This indicates that corundum (rubies, sapphires) cannot be cut with steel, but requires diamond tools to be worked. Gemologists, in addition to the above, also judge crystal quality on the basis of its color and hue, pleochroism (hue vs. orientation in a light beam), dispersion (difference in refractive index from one end of the visible spectrum to the other), translucency, and asterism (starlike effect in a light beam). Many of these gem properties are, however, dependent on the cut and polish of a crystal, and not upon the crystal itself.

One of the more sensitive techniques of determining crystal quality is that of X-ray diffraction.[23] X-rays, of about 1 Angstrom wavelength λ, are diffracted at an angle Θ from the crystalline planes (separated by d of about 3 Angstroms) in accordance with the Bragg Law:

$$2 d \sin\Theta = n\lambda \qquad (11)$$

The Laue method of diffraction utilizes white X-rays (of mixed wavelengths) impinging on a fixed crystal. The reflected rays strike a photographic plate, where they produce spots providing information on the orientation and spacing of the reflecting planes. The broadness and intensity of the reflected beams are a measure of the crystal perfection. If the Laue spots are smeared out, then the reflecting planes in the crystal are distorted, indicating dislocation defects.

The field ion microscope is perhaps the most powerful tool that can be used in determining crystal quality.[24] The waves associated with its gas ions are of the order of 0.1 Angstrom in wavelength, or less, and thus pass easily through a crystal without being diffracted. The pictures taken with this instrument reveal vacancies, interstitials, and impurity atoms as individuals. It actually allows one to see single atoms. Unfortunately, the device is limited in its application, at present, to high melting materials of peculiar shapes (to fit into the instrument), and its use is beset by experimental difficulties. At present there are only about 20 of these instruments in the United States, one of which is being set up in the Metallurgy Department of the University of Florida.[25] The electron microscope is also used to view crystal defects,[26] but its resolution is such (about 20 Angstroms) that nothing much smaller than dislocations can be seen in it.

Since the purpose of this research is to analyze a method of crystal growth, the imperfections caused by the method of growth will be stressed as the criteria of crystalline quality. In general, these are macroscopic and so can be viewed with an optical microscope.

CHAPTER III. EXPERIMENTAL PROCEDURE

The following experiments can be divided into two categories, the first having to do with plasma heat transfer capabilities, and the second concerned with the crystallization mechanism in the plasma fireball. The purpose of the first set of experiments is to determine where in the plasma fireball the maximum heat transfer rates occur, the kind of thermal gradients that can be expected, the effect on heat transfer of certain geometries of boule and powder feed probe, the effect of powder feed gas rates on heat transfer, the effect of diatomic gases and rf power levels on the heat transfer rates, and the effect on the plasma and the boule due to the introduction of powder grains into the fireball. The second set of experiments will correlate these heat transfer data to the thermal dependence of the heat transfer-crystallization model just proposed and to the quality of the crystal grown.

Part 1. Plasma Heat-Transfer Capabilities

A. Plasma Heat Transfer Profile

The purpose of this experiment was to establish optimum crystallization sites in the plasma fireball. The boule tip temperature, thermal gradient and plasma heat transfer rate were determined at various positions in the fireball (see Figure 11). A 3/8th inch diameter aluminum oxide rod was used as a test probe. Holes of 1/16th inch diameter were drilled halfway into the rod (radially) at

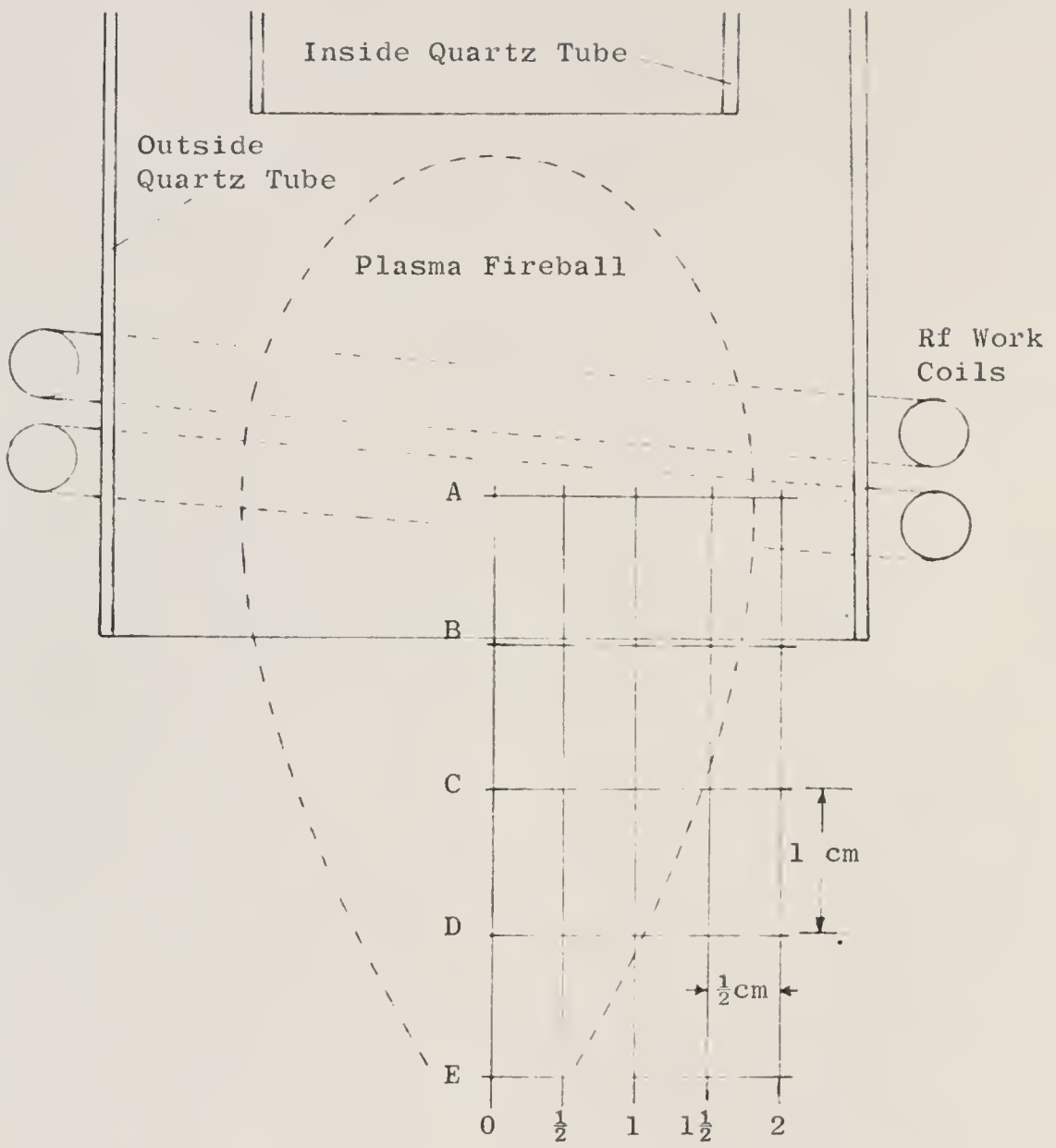

Figure 11 Grid Showing the Positions in the Plasma Fireball at which Temperature and Thermal Gradient Data Were Taken

half centimeter intervals from the top; these holes served as black bodies for optical pyrometer measurement of the boule temperature at the respective axial distances from the top. The data were plotted and the curves extrapolated to the boule tip to give tip temperatures. Thermal gradients were established from the data, and the local heat transfer rate was calculated from the following equation:

$$Q_p = \sigma \epsilon A \, T_L^4 + k \, A \left(\frac{dT}{dx} \right)_{x=0} \qquad (12)$$

The results are tabulated in Table 1. For test rod positions off the center line of the plasma torch the temperature profile along the rod differed depending upon which side of the rod faced the bulk of the fireball. Temperatures were higher and thermal gradients lower on the side exposed to the flame. Data for the off-center positions show that a radial thermal gradient is set up in the test rod (from the cold side to the hot side) that varied from a value of 32 C per cm at position A-1 (see Figure 11) to as much as 67 C per cm at position B-1.

It is also seen from the results of Table 1 that the most rapid temperature changes occur radially through the plasma. At level "A" the change in the average boule temperature, as the test rod was moved radially through the plasma, was 26 C per cm. At level "B" this radial change was 15 C per cm. The changes in boule temperature along axial positions in the plasma are not as pronounced. There was a 21 C change over a two-centimeter distance, from position A-0 to D-0. Axial thermal gradients in the rod increased as the rod was lowered from its top position as an example, at A-0 the thermal gradient was 183 C per cm at the boule tip, but this gradient increased, as the rod was lowered, to a value of 343 C per cm at position E-0.

Table 1

Temperature, Thermal Gradient, and Heat Transfer Profiles in a Plasma Fireball

	Boule Tip → Location	0	1/2 Hot Side	1/2 Cold Side	1 Hot Side	1 Cold Side
	T, °C	1696	1692	1672	1720	1690
A	$\frac{dT}{dx}$, °C/cm	-183	-173	-188	-180	-177
	Q_p, $\frac{\text{watts}}{(\text{cm})^2}$	32.5	32.2	32.2	31.1	31.1
	T	1683	1705	1683	1710	1646
B	dT/dx	-202	-260	-282	-287	-285
	Q_p	33.7	42.8	42.8	38.9	38.9
	T	1675	1686	1633		
C	dT/dx	-289	-305	-317		
	Q_p	38.9	40.0	40.0		
	T	1675	1679	1640		
D	dT/dx	-321	-357	-340		
	Q_p	41.2	42.6	42.6		
	T	1589				
E	dT/dx	-343				
	Q_p	39.6				

Plasma Condition	
Gas	45 SCFH Argon
Rf power	4.7 kw
Length of probe rod	9 cm
Distance of powder probe to position B-0	5.0 cm

An interesting point to note is that the maximum tip temperatures occur at positions off the center line of the plasma. This phenomena is currently being investigated as part of the general diagnostics of an rf plasma, with respect to temperature profiles in the plasma itself.[27] One postulate of the mechanism causing this is that of the skin effect, whereby maximum induced currents occur at the periphery of the plasma, and thus create higher temperatures there. Another model proposed to explain the phenomenon is that the electric field within the plasma, created by the rf work coil, has an axis that is tilted with respect to the plasma torch axis. This also would account for higher intensity currents, degree of ionization, temperature and heat transfer rates off-center.[28]

The theoretical model for the crystallization mechanism is simpler if the boule tip has a constant temperature. For the present purpose, the off-center positions, with their large radial thermal gradients (in the boule), appear unattractive. On the other hand, positions B-0 and C-0 offer about the same boule tip temperatures while having different values of axial thermal gradient in the plasma. Since the model for the crystallization is dependent on the axial thermal gradient, these positions appear most attractive for further investigation as boule-tip locations.

B. Boule Temperature as a Function of Its Distance from the Powder Probe Tip

The purpose of the next experiment was to determine the optimum distance of the powder probe from the boule tip. This distance is important since if it is too large the powder fed from the probe disperses to such an extent in the fireball that only a fraction actually impinges on the boule. On the other hand, if the powder probe is too close to the boule, the boule temperature is reduced.

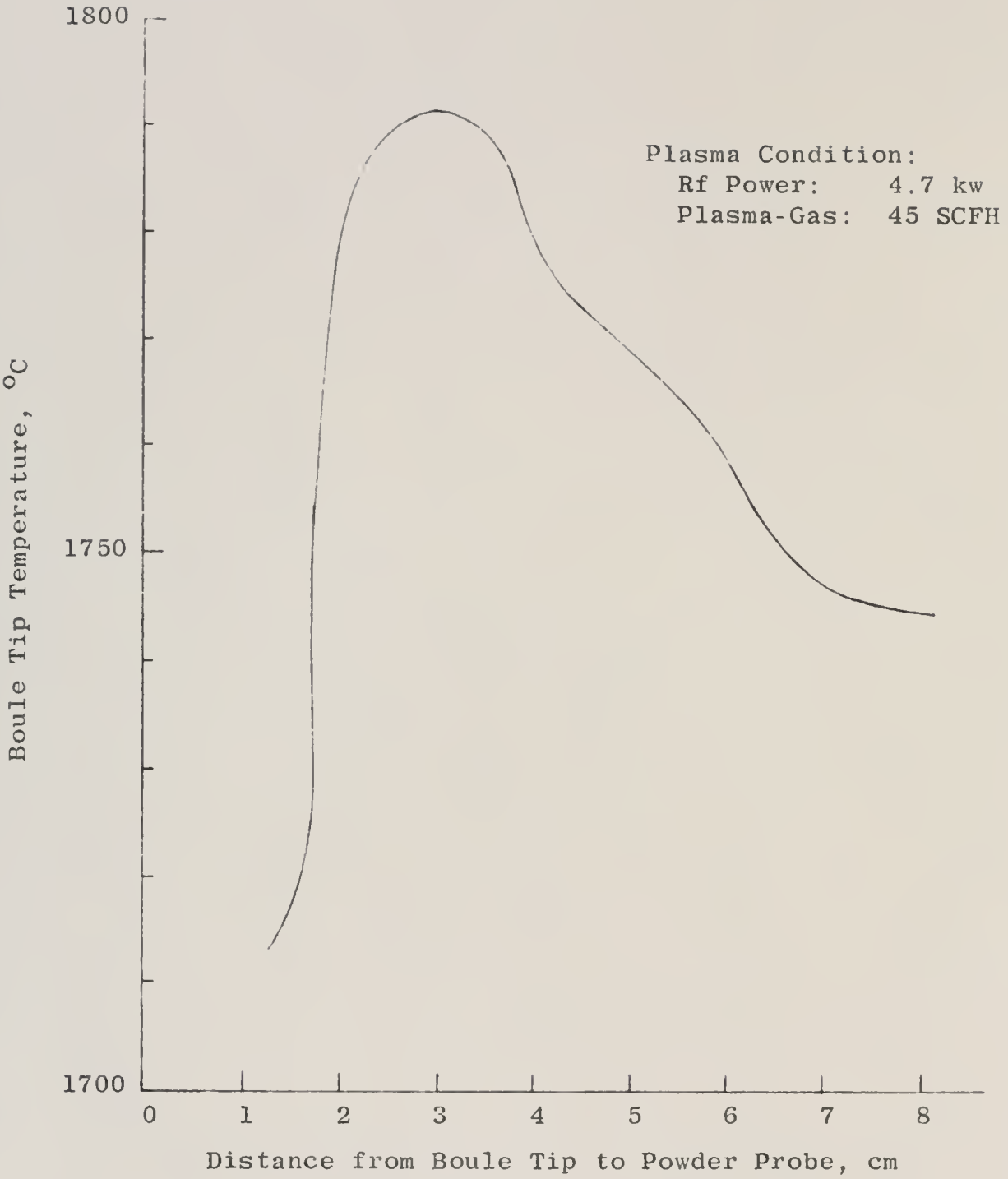

Figure 12 Boule Tip Temperature as a Function of the Distance of the Boule Tip from the Powder Probe, with the Boule Tip at Position B-0 (see Figure 11)

To determine the optimum boule-probe distance, the test rod was set in one location, under constant plasma conditions, and its temperature profile measured as a function of the probe-boule distance. The results of this experiment are presented in Figure 12.

An interesting result is that the boule temperature rose as the copper probe was brought closer, up to a certain critical point (approximately 3 cm) beyond which the boule temperature dropped. Based on these results, probe-boule distances of 2 or 3 centimeters appear to be the minimum practical, from the point of view of heat transfer. These distances were investigated further (in later experiments) as to their effect on the powder heating and dispersion during transit through the fireball.

C. Boule Temperature as a Function of the Powder-Gas Flow Rate

The purpose of this experiment was to determine the amount of powder-gas that should be used. Some powder-gas is necessary since free falling powder tends to flow erratically and to be dispersed more rapidly than powder fed with gas. On the other hand, too large a powder-gas flow rate tends either to cause ablation of the boule (if the boule tip is molten) or substantial cooling, due to a jet action of the gas flow from the powder feed probe.

To determine the optimum powder-gas flow rate, based on heat transfer considerations (not powder flow considerations), the test-rod-to-powder-probe distance was set at either 2 or 3 centimeters, and the test-rod temperature profile (axial) measured as a function of the powder-gas flow rate. From these measurements the boule tip temperature and thermal gradient were determined.

The results are presented in Figure 13. It is evident that for the 3 cm probe-boule distance, no more than

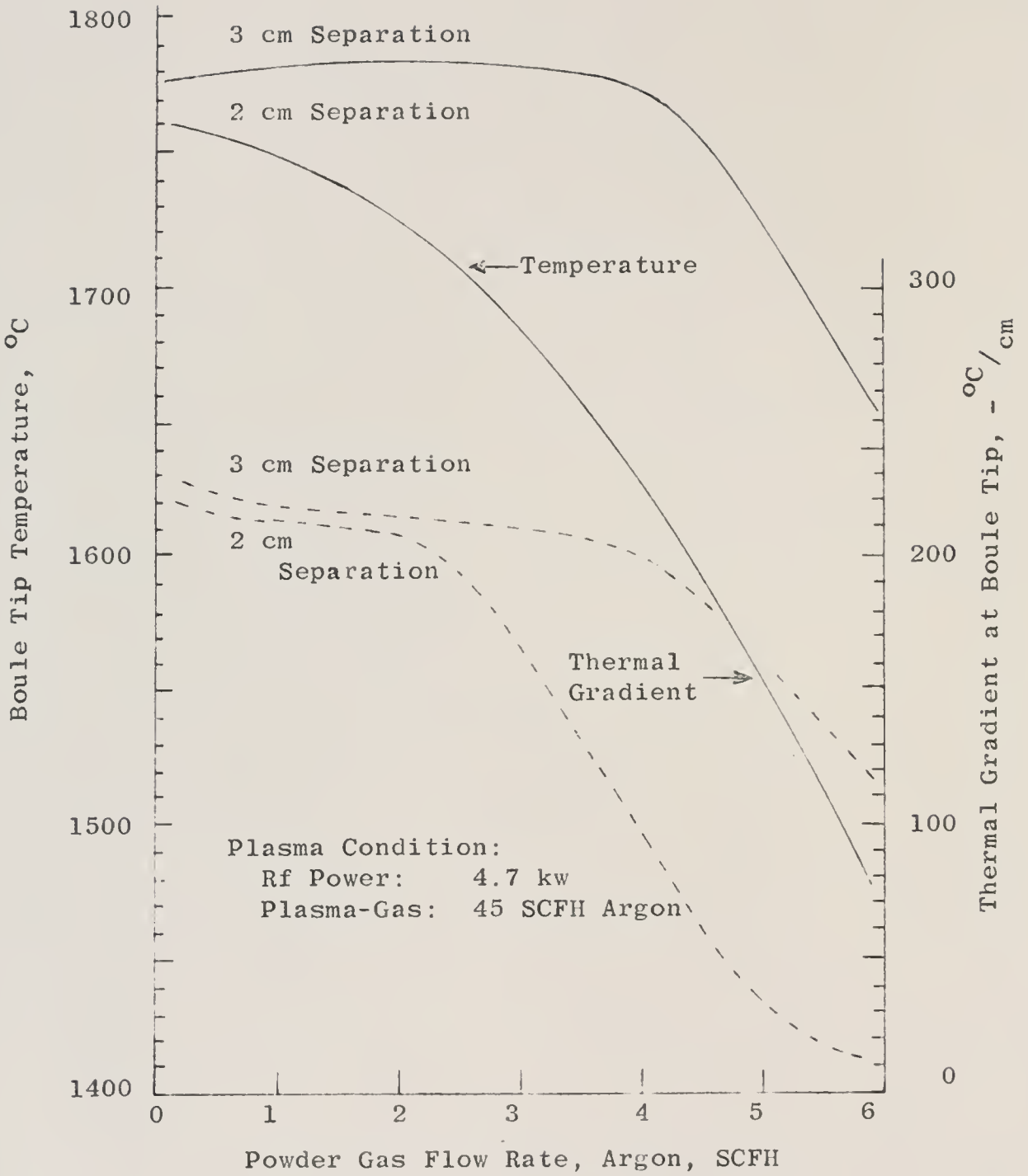

Figure 13 Boule Temperature and Thermal Gradient as a Function of the Powder-Gas Flow Rate, at Position B-0, for 2 and 3 cm Boule-Probe Separation

4 SCFH powder gas can be tolerated. For the 2 cm distance, 2 SCFH is the most that can be permitted before an excessive temperature drop occurs. These figures are for the test rod at position B-0. The data obtained for position C-0 (not presented) show similar results, but with lower boule temperatures and larger thermal gradients.

D. Boule Temperature as a Function of the Presence of Diatomic Gases

The purpose of this experiment was to determine the effects of diatomic gases introduced into the argon plasma. The test rod was set at either position B-0 or C-0; probe-boule distances were either 2 or 3 centimeters; powder-gas flow rate was either 2 or 4 SCFH; and the boule temperature profile (axial) was measured as a function of the amount of either oxygen or nitrogen introduced into the total plasma-gas. The boule tip temperature was then determined from these measurements.

The results, for position B-0, are presented in Figure 14. The effect on the boule temperature due to even small quantities of either diatomic gas is seen to be very pronounced. As little as 0.5 SCFH of oxygen in 45 SCFH argon caused the boule temperature to rise 25 C for the 3 cm-2 SCFH probe and powder-gas condition, and 90 C for the 2 cm-2 SCFH condition. Approximately the same temperature rises could be produced with nitrogen using only 0.17 SCFH. The apparent mechanism causing the phenomenom is dissociation of the diatomic molecules in the plasma and then their recombination on the boule surface. The reason less nitrogen produced the same effect as more oxygen can be rationalized by the differences in their dissociation energies, 118.9 Kcal/mole for oxygen and 225.9 Kcal/mole for nitrogen.

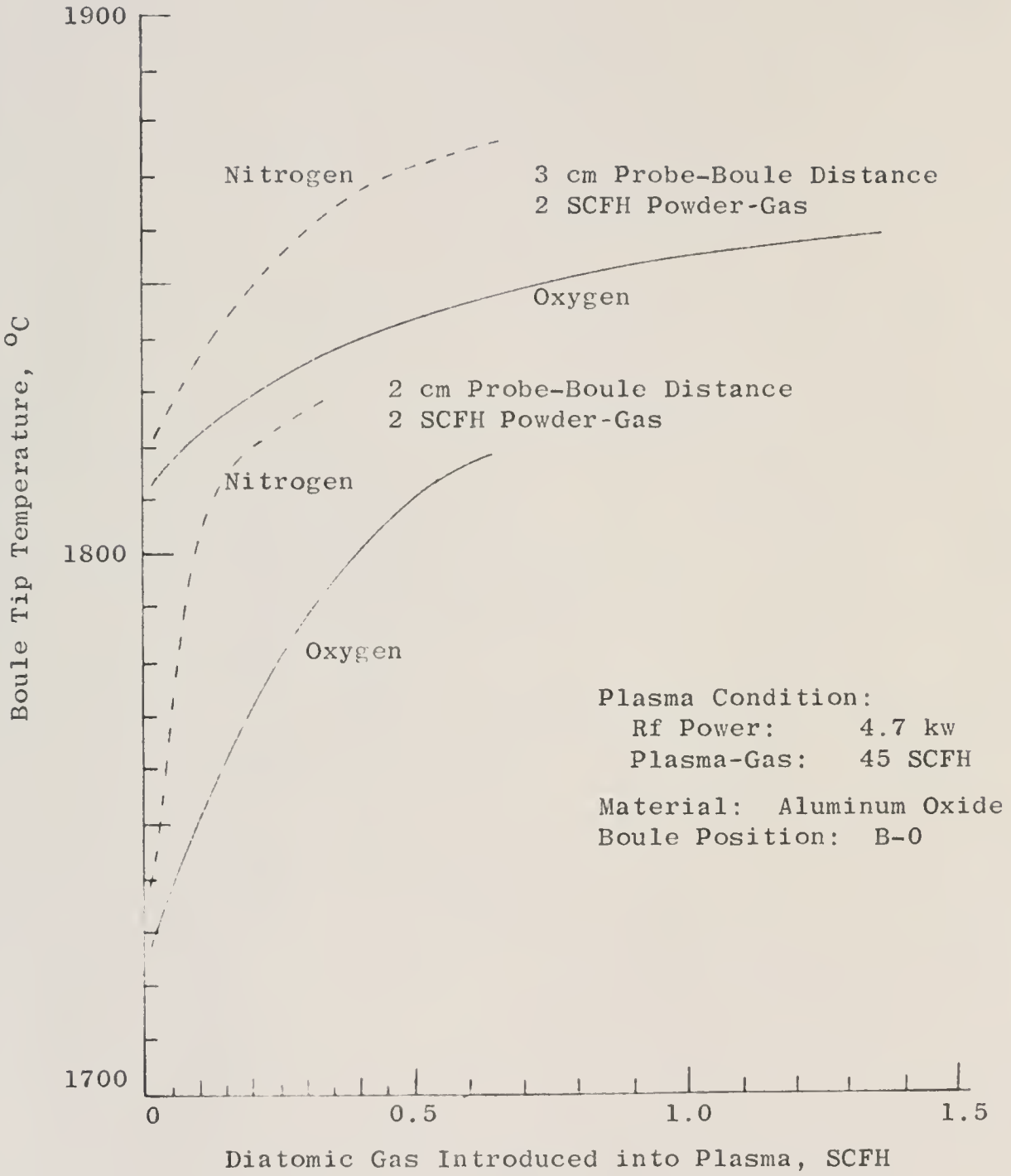

Figure 14 Boule Tip Temperature as a Function of the Amount of Diatomic Gas in the Plasma

This appears to be a very efficient, highly localized mechanism of heat transfer. One disadvantage, however, is that the diatomic molecules, due to their dissociation and higher specific heat, absorb considerable energy from the plasma. The effect is to cool the plasma, thus reducing its degree of ionization. If too much diatomic gas is introduced, the plasma becomes spatially unstable and is extinguished. This disadvantage was encountered with only small quantities of diatomic gas at the power level (4.7 kw) of the experiment. At higher power levels it is found that more diatomic gas can be tolerated.

In an effort to enhance the heat transfer effects, while minimizing plasma instability, the diatomic gases were introduced only in the powder feed gas, instead of into the entire plasma-gas. Negligible differences in heat transfer and stability were noticed, however, compared to the diatomic gases being introduced into the entire plasma-gas. One possible explanation is that the diffusion rate of gas molecules in a plasma is so large that location of entry is unimportant to the mixing mechanism.

Although the plasma furnace already had insulation to reduce heat loses, a second shield was placed around the boule in an attempt to raise the temperature further. This muffle was a 5.0 cm I.D. ceramic oxide tube. A section of the top was cut away to allow observation and measurement of temperature profiles. The result was that the boule tip temperature remained almost constant while the rod's axial thermal gradient was reduced slightly (from 300 to 272 C/cm). An adverse effect was that the plasma became slightly unstable outside the quartz tubes of the torch, and tended to jump to the work coil, thus short-circuiting the coil and extinguishing the plasma. It can be concluded that this method of increasing the boule temperature is not as effective as others being tried (diatomic gas, rf power level, etc.).

E. Boule Temperature as a Function of the Rf Power Level

The purpose of the following experiment was to determine the effect on the boule tip temperature caused by variations in the rf power level. In all previous experiments the rf power level had been kept at 4.7 kw, a value that was low enough to avoid melting the test rod. In this experiment the test rod was set at the B-0 position (see Figure 11), with 3 centimeter probe-boule distance and 2 SCFH powder-gas flow rate. The temperature profile (axial) in the test rod was measured as the rf power level was raised from 4.7 kw to 9.7 kw. The high power level was maintained only long enough to obtain steady state temperatures and observe them, in order not to melt away too much of the test rod. Boule tip temperatures were then calculated from the data.

The results are presented in Figure 15. The temperature is seen to rise sharply beyond about 7.3 kw rf power, and begin to level off at 9.7 kw rf power. The temperature rise was only 25 C for a power increase from 4.7 to 7.3 kw, but was 225 C for the power rise from 7.3 to 9.7 kw.

One possible explanation of this behavior of boule temperature with input power can be made by postulating that the key mechanism of heat transfer at the boule tip is that due to recombination of the ionized gas atoms. That is, the boule tip temperature is a function of the degree of ionization of the plasma-gas. It has been established that a reasonable approximation of the degree of ionization of a gas can be made by using the one-level Saha equation:[29]

$$\alpha \simeq C\, T^{5/4}\, e^{\frac{-q_e V_i}{2kT}}, \text{ for } \alpha << 1 \qquad (13)$$

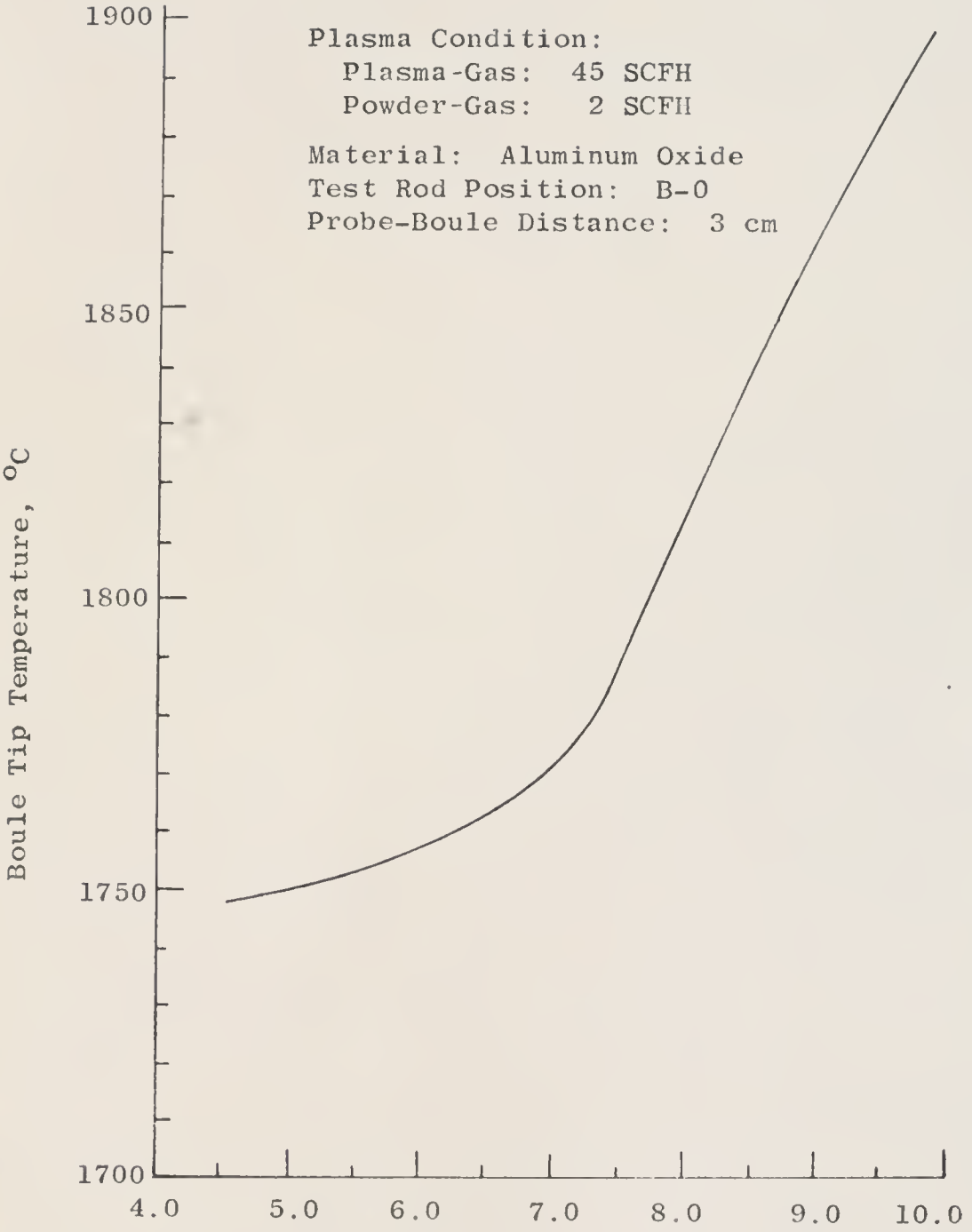

Figure 15 Boule Tip Temperature as a Function of the Rf Power Level

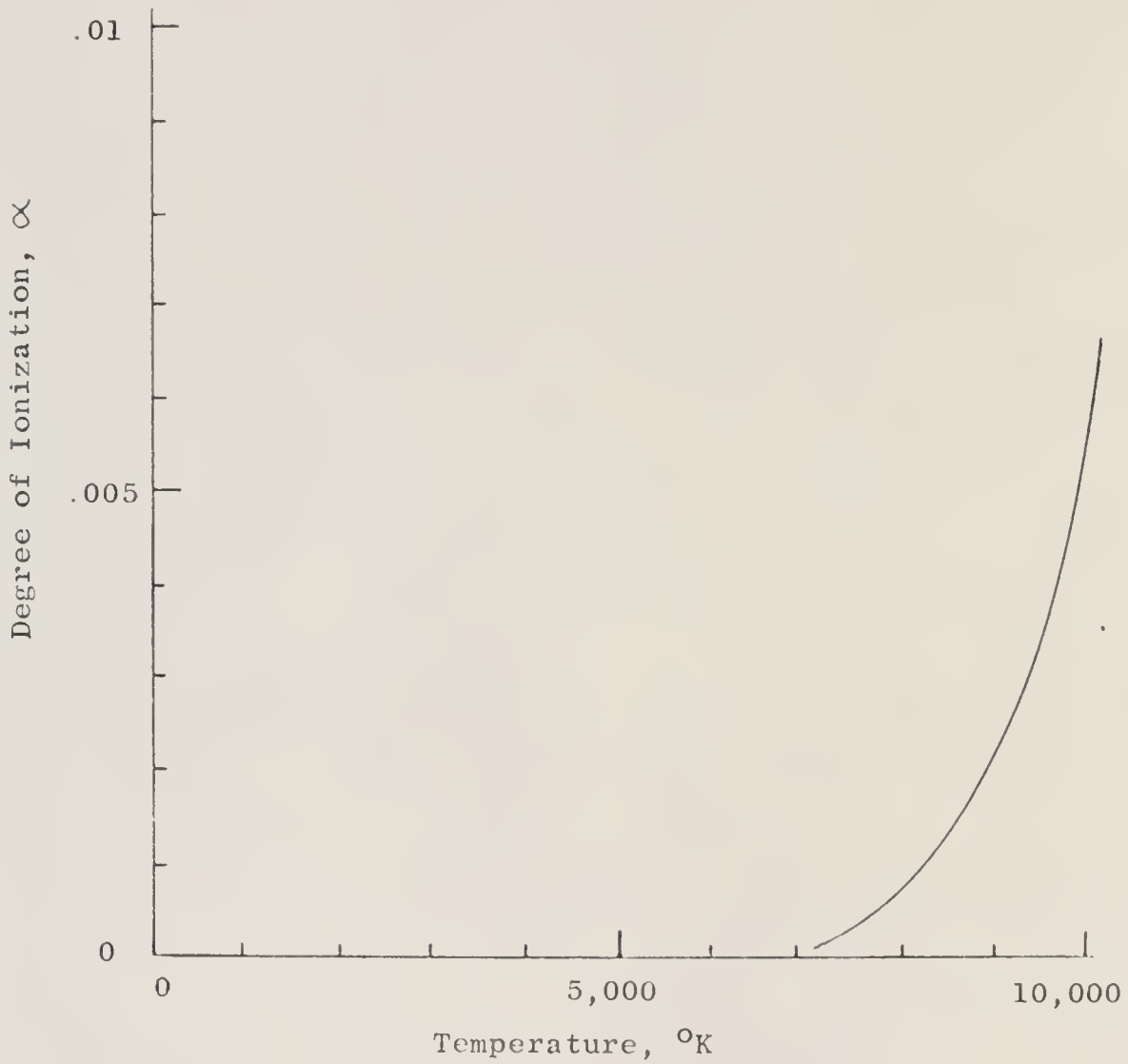

Figure 16 Degree of Ionization of Argon, at One Atmosphere Pressure, as a Function of the Temperature, Based on the One-Level Saha Equation; Reproduced from Reference 30

A plot of this equation as a function of temperature appears in Figure 16 (for argon at atmospheric pressure).[30] The degree of ionization is seen to rise very sharply for temperatures above 7,000 K.

Assuming that the specific heat of the plasma is nearly constant with temperature, and provided that the radiation loss from the plasma is small, then the plasma temperature should vary almost linearly with power input, in accordance with the First Law of Thermodynamics. Assuming these conditions apply, then the degree of ionization will rise sharply with power input. And, by the postulate above, the heat transfer to the boule, and the boule temperature, will also rise sharply with power input.

A possible factor contributing to the start of a leveling off of the boule temperature beyond 9.7 kw power input could be that of an increasing radiation component of heat transfer from the plasma fireball. As the degree of ionization of the plasma increases, the amount of continuum radiation from the fireball should increase. This larger radiation loss would limit the plasma temperature rise as the power level is increased, and thus limit the rise in the degree of ionization. Since it is postulated that the heat transfer rate is dependent on the degree of ionization, this limiting mechanism of radiation loss also limits the rise in the boule temperature as the power levels become very high.

The above analysis indicates that equipment efficiency could be improved with an effective radiation shield around the plasma torch assembly.

F. Boule Temperature and Powder Feed Rate

The boule temperature is significantly affected by both the rate of powder feed and the size of the powder grains. The following experiments were performed to determine the

relationship between the boule temperature, distance of the boule to the powder probe, powder-gas flow rate, powder feed rate and grain size. The powder feed mechanism was calibrated (Appendix A) using a mixed powder of aluminum oxide and 2% chromium metal. This particular refractory oxide was used for the initial crystallization experiments since it is inexpensive, readily available, and melts in the required temperature range (2100 C). Also, the crystal formed from it (ruby) is well known and presents a standard against which the plasma - Verneuil crystallization method can be gauged.

The boule temperature was measured at the B-0 position for settings of 3 cm-2 SCFH, 3 cm-4 SCFH and 2 cm-2 SCFH boule-probe distance and powder-gas flow rate. At each setting the boule temperature was measured as a function of the varying flow rates of five different powder sizes.

The results of this experiment, presented in Figures 17, 18, 19 and 20, must be considered somewhat qualitative. Difficulty was encountered in measuring temperatures due to the presence of the powder jet. Also, the powder striking the boule tended to accumulate and thus alter the position of the top during the time of the measurements. The experimental method used was to obtain a zero-powder temperature measurement just before introducing the powder. The effect on the boule temperature due to the powder was thus made most apparent as the simple difference between a before-and-after condition, where the time difference between the before-and-after measurements was kept to a minimum.

Figure 17 shows the change in the boule temperature caused by the introduction of fine-grained powder, for various settings of probe-boule distance and powder-gas flow rate. Figures 18, 19 and 20 are presented to emphasize the drop in temperature caused by the powder alone. There is scatter in the data, presumably due to the difficulties of measurement.

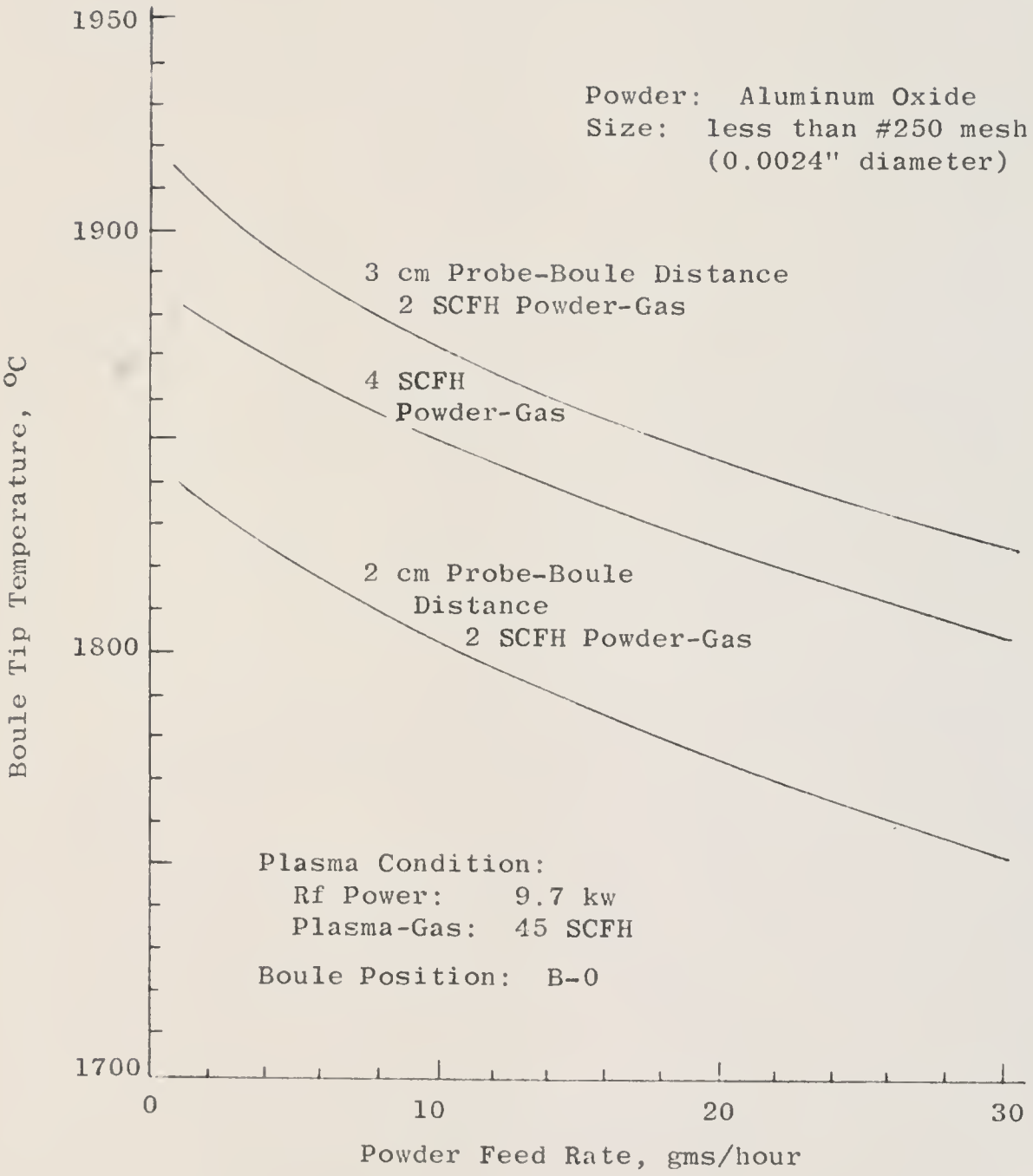

Figure 17 Boule Tip Temperature as a Function of the Powder Feed Rate

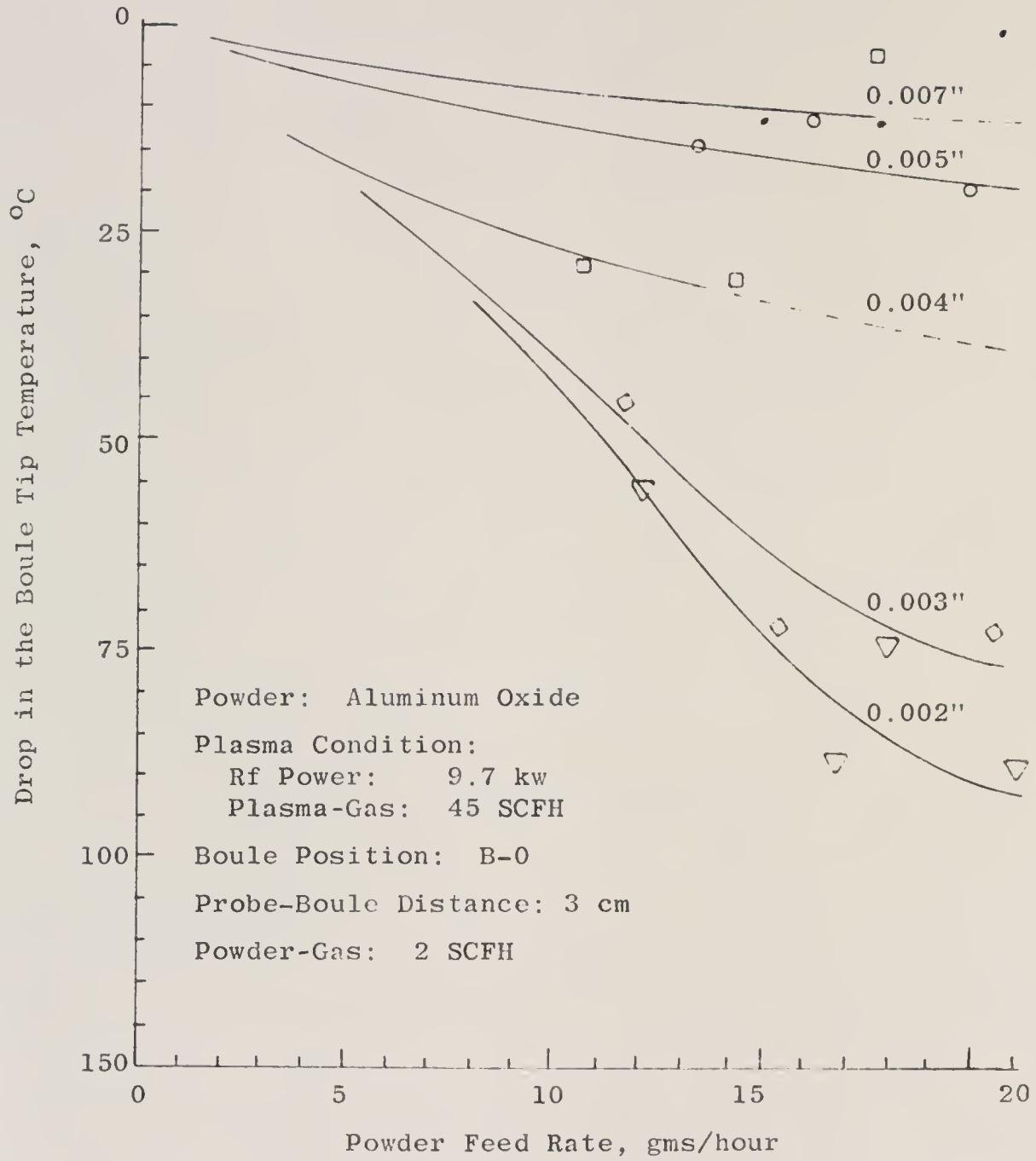

Figure 18 Drop in the Boule Tip Temperature as a Function of the Powder Feed Rate, for Various Sizes of Powder Grains, for a Probe-Boule Distance of 3 cm, and a Powder-Gas Flow Rate of 2 SCFH

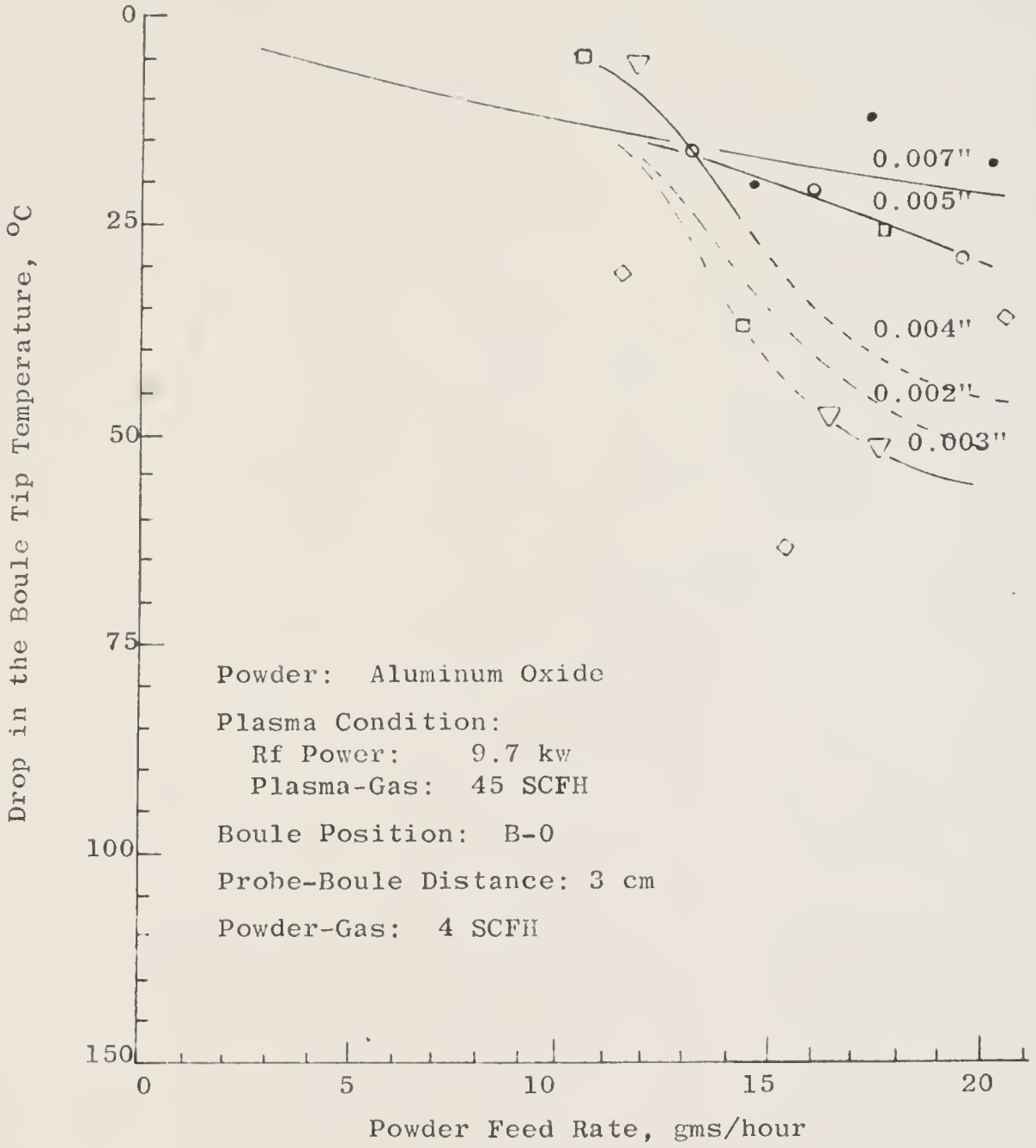

Figure 19 Drop in the Boule Tip Temperature as a Function of the Powder Feed Rate, for Various Sizes of Powder Grains, for a Probe-Boule Distance of 3 cm and a Powder-Gas Flow Rate of 4 SCFH

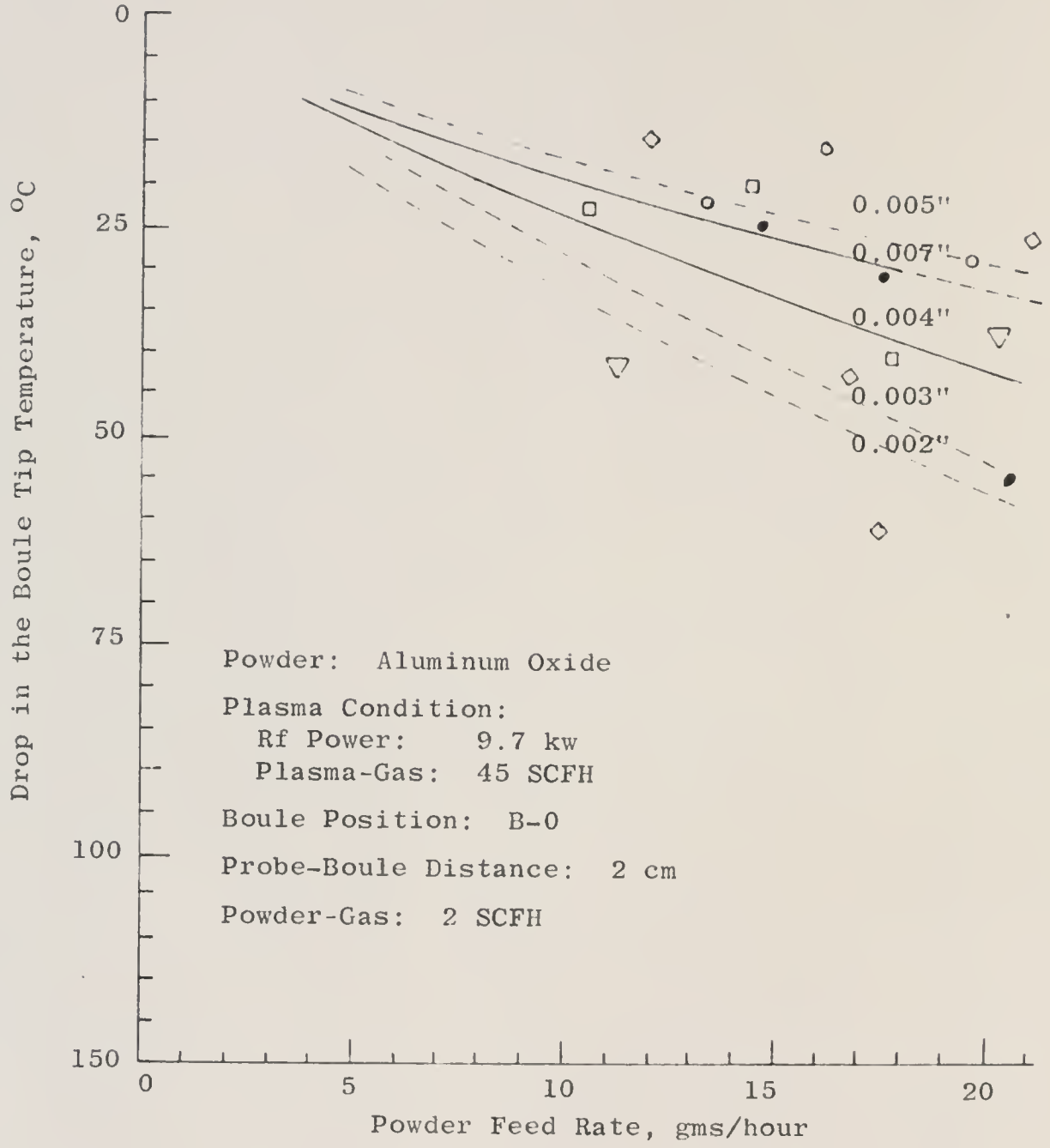

Figure 20 Drop in the Boule Tip Temperature as a Function of the Powder Feed Rate, for Various Sizes of Powder Grains, for a Probe-Boule Distance of 2 cm and a Powder-Gas Flow Rate of 2 SCFH

The overall trend, however, is that the smaller-grained powder cooled the boule more than did the larger-grained powder for the same powder flow rate. This is most noticeable in Figure 18 where the probe-boule distance was 3 cm and the powder-gas flow rate was 2 SCFH. At this setting the comparatively large travel distance through the fireball coupled with only a small powder-gas flow rate presumably allowed maximum dispersion of the fine-grained powder throughout the plasma. Visual observation showed a broadening of the fireball, a diminution of its intensity at the center, and a change of its "color" from a bright white to a dull blue-green. Thus the powder dispersion apparently does cause cooling of the plasma in accordance with the theory outlined on page 16 (whereby the radiation heat loss from the luminous grains causes a heat loss from the plasma). Cooling of the plasma then causes cooling of the boule.

The amount of dispersion of the fine-grained powder was reduced either by increasing the powder-gas flow rate or by lowering the powder probe closer to the boule. These results are seen in Figures 19 and 20. Visual observation for these settings shows that the plasma fireball does not become broadened by the powder but remains concentrated with an intense "white flame". The tail flame, however, did turn to the characteristic blue-green color caused, presumably, by excitation of the powder atoms. Dispersion of the larger-grained powders was not observed, regardless of the probe-boule distance or the powder-gas flow rate.

G. Powder Grains in the Plasma Fireball

The purpose of this experiment was to determine the degree of melting of the powder grains during their transit through the fireball. Powder of various grain size was fed at approximately 15 gms/hour, under varying conditions of

probe-boule distance and powder-gas flow rate. Samples of the grains, after passing through the fireball, were obtained by briefly inserting a copper strip into the fireball and allowing the grains to impinge on it. In most cases the grains stuck to the strip, due to a partially molten periphery of both grains and strip.

The results of this experiment are presented in Table 2. In no case was the melting so complete as to cause wholly molten droplets to impinge on the test strips. At best the powder grains melted only enough to form a liquidus region at their periphery, as evidenced by their sticking to the plates by a small part of their surface area. Also, tracks were sometimes seen indicating where a grain skidded over the test strip. For the smaller grains there was sufficient heating to allow them to form clear, crystalline spheroids. The larger grains did not form as many spheroids as did the smaller ones and, when they did, the spheroids were generally not clear but were a dull, cloudy color, indicating incomplete melting. Figure 21 is a photograph showing four observed degrees of grain melting.

The setting of 3 cm probe-boule distance and 2 SCFH powder-gas flow rate resulted in the most complete melting of the grains of the three settings used, as might be expected since this setting provided maximum exposure time for the grains in the fireball.

The results of this experiment indicate that if small-grained powder is to be used, then small probe-boule distances, or large powder-gas flow rates, are required. However, the least boule temperature drop occurs when the larger-grained powders are used, and thus these would appear better suited for use in the plasma-Verneuil method of crystallization.

Table 2

Condition of Aluminum Oxide Powder Grains Impinging on Copper Test Strips, at Position B-0, and for 9.7 kw Power Input

Powder Size	Present Spheroids	Clarity of Spheroids	Indication of Molten Condition
Setting 1. 3 cm Probe-Boule Distance; 2 SCFH Powder-Gas Flow Rate.			
.007	20	Most dull white; a few partially clear	No; very few spheroids stuck to surface
.005	60	Most dull; a few clear	Some; several spheroids stuck to surface
.004	80	Many clear; a few dull	Some; more spheroids stuck to surface
.003	90	Most all clear	Partially; many marks appear where a partially molten grain hit the surface but did not stick
.002	100	All clear	Yes; streak marks appear where grains skidded over surface; other marks show slattering of grains on surface
Setting 2. 3 cm Probe-Boule Distance; 4 SCFH Powder-Gas Flow Rate			
.007	20	Most dull white	No; very few stuck to surface
.005	40	Most dull white	No; few stuck to surface
.004	60	A few clear; most dull white	Some; a few marks and streaks appear where partially molten grains struck surface
.003	80	Most clear; a few dull white	Partially; many marks appear where partially molten grain struck surface but did not stick
.002	100	Most clear; a few cloudy or dull	Yes; many marks similar to above condition for .003
Setting 3. 2 cm Probe-Boule Distance; 2 SCFH Powder-Gas Flow Rate			
.007	5	Dull white	No; very few stuck to surface
.005	10	Dull white	No; few stuck to surface
.004	50	Most dull white; a few clear	Some; a few stuck to surface; a few marks and streaks where partially molten grains struck
.003	70	Most clear; a few cloudy	Some; several grains stuck to surface; more marks and streaks
.002	100	Most clear	Partially; many marks and streaks

Figure 21 Photograph Showing the Degree of Melting of the Powder Grains After Traveling Through the Plasma Fireball

(a) 0.007" powder grains, 3 cm probe-boule distance, 2 SCFH powder-gas flow rate. Note only little indication of molten grains.

(b) 0.005" powder grains, 3 cm probe-boule distance, 2 SCFH powder-gas flow rate. Note roundness of grains, but no indication of complete melting.

(c) 0.003" powder grains, 3 cm probe-boule distance, 2 SCFH powder-gas flow rate. Note several grains appear clear and round, indicating higher degree of melting than in either (a) or (b).

(d) 0.002" powder grains, 2 cm probe-boule distance, 2 SCFH powder-gas flow rate. Note all grains appear round and clear. Also note skid marks on surface, indicating high degree of melting.

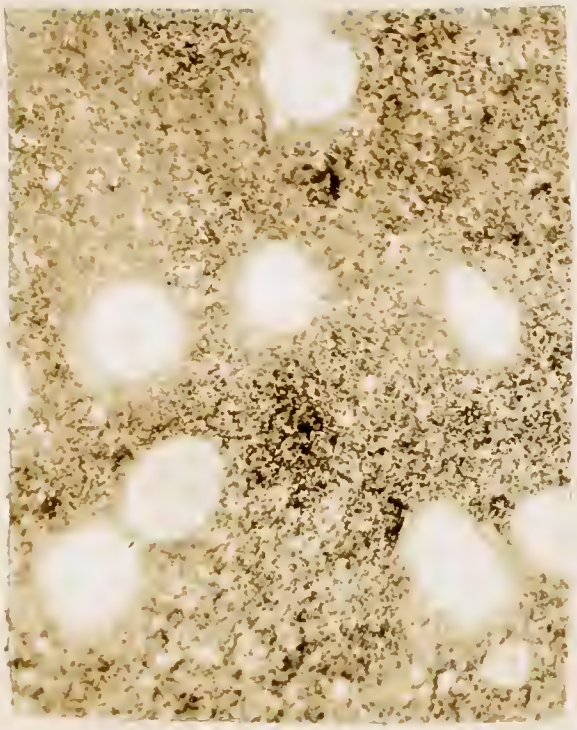

(a)

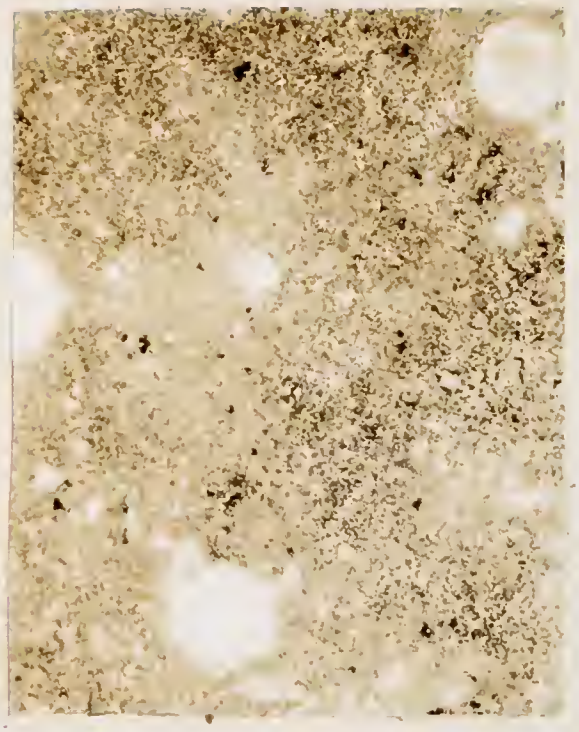

(b)

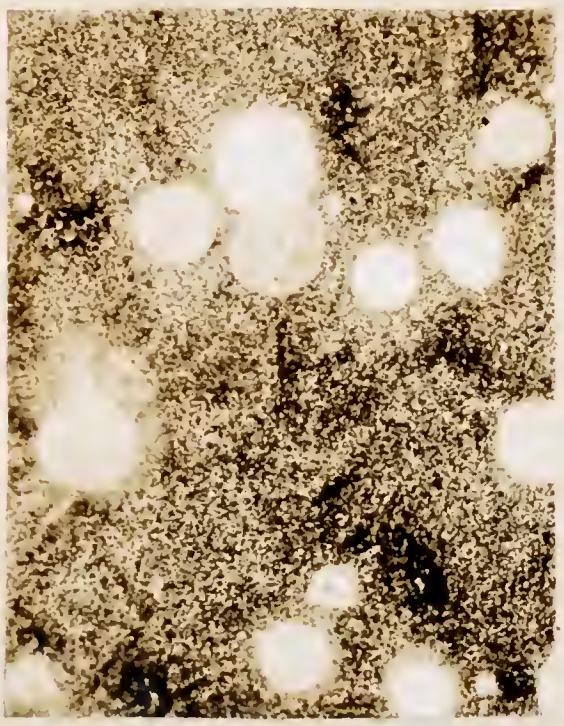

(c)

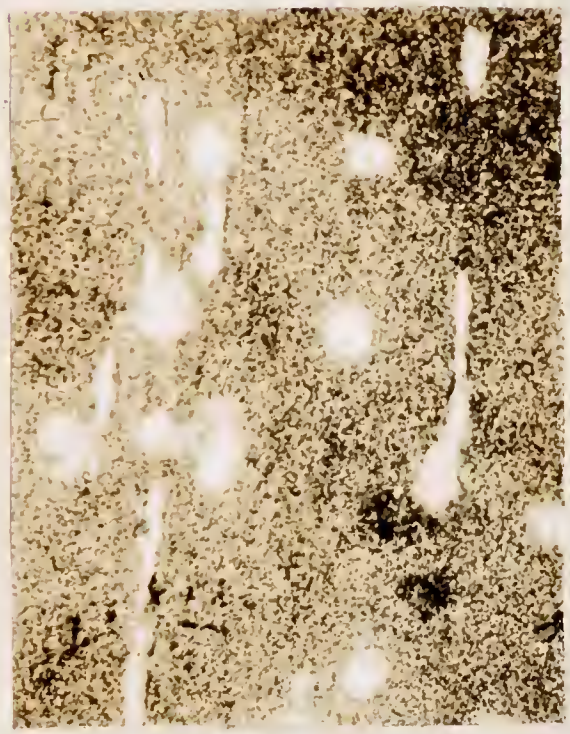

(d)

H. Summary of Plasma Heat Transfer Capabilities

The preceding experiments were performed to find the condition and geometry for optimum plasma heat transfer to the boule. From the results of these experiments, the following conclusions can be drawn.

1. The optimum sites in the plasma are nearest the fireball center, where boule temperatures are highest, and thermal gradients lowest. These are positions A-0 and B-0 of Figure 11.

2. At position B-0, maximum boule temperatures occur for the combination of 3 cm probe-boule distance and 2 SCFH powder-gas flow rate.

3. The introduction of as little as 0.5 SCFH of diatomic gas raises the boule temperature significantly. Additional quantities do not show proportionately higher boule temperatures.

4. Boule temperatures increase rapidly when the rf power level is increased above 7.3 kw. The rate of increase diminishes at very high power levels.

5. The optimum size of aluminum oxide powder (2015 C melting point) to use is in the range of 0.004"-0.005" diameter. This size is large enough to prevent dispersion in the fireball, but small enough to permit the grains to be significantly heated during transit through the fireball.

6. Powder feed rates should be kept below 15 gm/hour.

Thus the conditions for crystal growth are:

a) boule at position A-0 or B-0,
b) powder probe 3 cm from boule tip,
c) powder feed gas at about 3 SCFH, with 0.5 SCFH diatomic gas,
d) powder at about 0.005" diameter, fed at less than 15 gm/hour, and
e) rf power level high enough to maintain molten cap on boule.

Part 2. Crystallization in the Plasma Fireball

A. Outline of Procedure

The following series of experiments were designed to establish the conditions under which high quality crystals can be grown. The heat transfer-crystallization theory leads to the prediction that there is an optimum range of thermal gradient, liquid-layer temperature and rate of growth, or combination of these parameters, that produces the best quality crystals. The equipment variables that affect these key parameters are the rf power, the flow rate of the powder gas, and the quantity and grain size of the powder being fed. A more detailed discussion of this theory and the influence of these variables was given in Chapter II.

Other factors that can conceivably affect quality are whether or not the crystal was initiated from a seed, and whether or not a flux or catalyst was used in the powder to aid in maintaining the limpidity of the molten layer and in removing entrained gases. The first factor, seeding, is the easier to determine by experimentation. The latter factor, flux, involves considerable trial-and-error type experimentation since little theory is available to aid in flux or catalyst selection. Although it is realized that this factor could be an important one in the growing of high quality crystals, it is felt that its examination lies somewhat beyond the scope of the present research. Consequently only those factors touching on the heat transfer-crystallization mechanism in the fireball will be considered.

The method of experimentation used to determine the conditions for the growth of high quality crystals was to grow several boules in a number of different ways such that the range of possible variations of the quality parameters

were covered. A general outline of the experiments is as follows:

A. Standard conditions for all experiments:
   1. powder probe set 3 cm from the boule tip
   2. 2 SCFH powder-gas:
      a. 0.7 SCFH argon
      b. 1.3 SCFH oxygen
   3. sufficient plasma-gas to maintain a stable plasma flame; approximate flow rates are:
      a. low rf power levels (to 11 kw)
         1. 19 SCFH argon, outside quartz tube
         2. 19 SCFH argon, inside quartz tube
      b. high rf power levels (11 kw to 13.5 kw)
         1. 19 SCFH argon, outside quartz tube
         2. 32 SCFH argon, inside quartz tube
   4. aluminum oxide powder with 2% (weight) chromium powder (40 micron)

B. Variable conditions:
   1. boule tip at B-0 or C-0 positions
   2. pedestal seeded or unseeded
   3. 0.004" or 0.005" diameter powder grains
   4. powder feed rates from 8.5 gms/hour to 16.1 gms/hour
   5. rf power levels from 9.0 kw to 13.5 kw, either constant throughout run, or increasing during run as the boule grew longer

Data taken during the growth of the boules are given in Appendix E. A photograph showing how a boule appears while growing in the furnace is presented in Figure 22. The pedestal (vertical) is supporting the glowing boule that is barely seen within the highly luminous plasma fireball near the top of the picture. The background is insulation in a somewhat

Figure 22 Photograph Showing a Boule (Within the Bright Plasma at Top) Growing on an Aluminum Oxide Pedestal in the Plasma-Verneuil Furnace

deteriorated state. A photograph of the boules immediately after removal from the furnace is presented in Figure 23. This figure also shows one boule (#8) still attached to the pedestal. Boules #1 and #5 had already been cut, and are shown mounted in plastic holders awaiting polishing, preparatory to examination of internal structure.

A few general observations on boule growth in the plasma fireball are in order before presenting the results relating to boule and crystal quality.

B. Plasma Stability at High Power Levels

There is a pronounced tendency towards plasma instability at high power levels. The instability is spatial, appearing as an oscillation of the fireball within the rf work coils. The periodicity of the oscillation is large enough to be observed with the naked eye and is presumably caused by a coupling of the charged particles in the fireball to the applied, 4 mc frequency of the work coils.

There appear to be several modes of oscillation possible, since changes in the vibrating frequency can be observed to occur spontaneously. At low power levels it appears that all possible modes are stable; at high power levels, the fireball has been observed to go into such a severe oscillating condition that it extinguishes itself. Apparently some modes are more highly resonant than others.

It was found that the stability of the fireball could be improved at high power levels by increasing the flow of plasma-gas to the inside quartz tube. It was also observed that the stability improved after the furnace was heated to its steady state temperature. This led to the establishment of a warm-up period at low power levels before the full power was applied.

Figure 23 Photograph showing the Appearance of the Boules Immediately after Removal from the Plasma-Verneuil Furnace

1
2
3
4
5
6
7
8
9
10
11
12

A final observation on stability is that, at the peak power level (13.5 kw), and when the furnace is fully heated, there are two predominant modes of vibration of the fireball. The first, of higher frequency, is the most stable. The second, of a lower frequency, causes a more promounced spatial distortion of the fireball, but is not severe enough to extinguish the "flame". It does not last for long periods of time.

C. Initiation of a Crystal

Initiation of a crystal from the pedestal can be achieved in two ways. The first method is to direct a stream of powder onto the pedestal, allowing the powder to build up until, by chance, a crystal stalagmite juts forth. This stalagmite is then encouraged to grow into a completed boule. For this method, initiation is best accomplished at low power levels, since, at high levels, the powder tends to melt and combine with the material of the pedestal, resulting in a very impure base on which to start a crystalline boule.

The second method is to place a small seed crystal, taken from a previous boule, on the pedestal, and then to encourage its growth into a completed boule. One difficulty of using the seed lies in providing enough heat to obtain a molten cap on the seed while not giving it so much heat as to cause the seed to melt and merge into a molten pedestal (thus contaminating the seed). When seeding is done, it should be with a large enough crystal so that its cap can be molten while its base is still solid.

Both methods were tried. In general, boules were grown faster from a seeded pedestal than from an unseeded one, due to the length of time needed to create an initial stalagmite in the latter case. Also, seeded boules seemed to

result in better quality crystals, especially at the core, as is discussed more fully later on. Consequently, it appears that boule initiation from a seed is the more satisfactory method.

One point that should be considered when attaching the seed to the pedestal is that it is important to taper the pedestal up to the seed to prevent a powder build-up alongside the seed. Such a powder build-up could result in the initiation of an unseeded boule that would compete with, and contaminate, the seeded part.

D. Size, Shape and Growth Rate of the Boule

It is obvious from looking at Figure 23 that there was little uniformity in either the size or shape of the boules grown. The only definite point of similarity was that all the boules increased in radius as they grew longer, in spite of some efforts to grow boules of constant radius by varying the rf power as the boule grew longer.

If the boule cap is kept molten during growth, the mass growth rate of the boule is directly proportional to the quantity of powder intercepted per unit time. Therefore boules of large radius should grow more rapidly in mass than those of small radius, since they intercept more powder. However, not all boules start out with the same radius of stalagmite. Thus it can be expected that boules of otherwise identical environmental growth conditions will still have different mass growth rates whenever conditions of the formation of the initial stalagmite were different.

From considerations of limpidity discussed in the heat transfer-crystallization theory, it might be expected that boules grown at high power levels, especially at the start, should expand in radius more rapidly than those grown at low power levels, and in turn, these boules should show a larger rate of mass growth.

Figure 24 is presented to show, qualitatively, how the mass growth rate varied with both powder feed rate and the initial power level. The mass growth rate of the boule is seen to increase with the powder feed rate, for constant rf power, and to increase with the rf power for a constant powder feed rate. The scatter in the data can presumably be attributed to the differences in the initial radius of the stalagmite or seed, and to variations in the power level as the boules were grown. The criterion for the "initial power level" was taken arbitrarily as the average power applied during the first 30 or so minutes of growth. The division between high and low power at 11.5 kw resulted from an analysis of the data.

In one case (boule #6) it was observed that the stalagmite coming from the seeded pedestal grew at an angle of about 10° from the vertical. This permitted powder to fall on the side of the stalagmite, which initiated the growth of a twin crystal alongside the first at an angle of about -10° from the vertical. Thus the total mass of boule #6 is really that of two boules; and this factor has been considered in the plotting of the data for boule #6.

In general, the results conform to the theory just discussed. The boules that were initiated at high power levels had a larger mass growth rate than did those initiated at low power levels. In general, boules grew faster for the higher rates of powder feed than for the lower rates of powder feed.

E. Thermal Gradient as a Function of the Rf Power Level

One of the key parameters affecting crystal quality is the thermal gradient at the liquid-solid interface existing at the time of growth. As was discussed in the heat transfer-crystallization theory, this thermal gradient varies with the

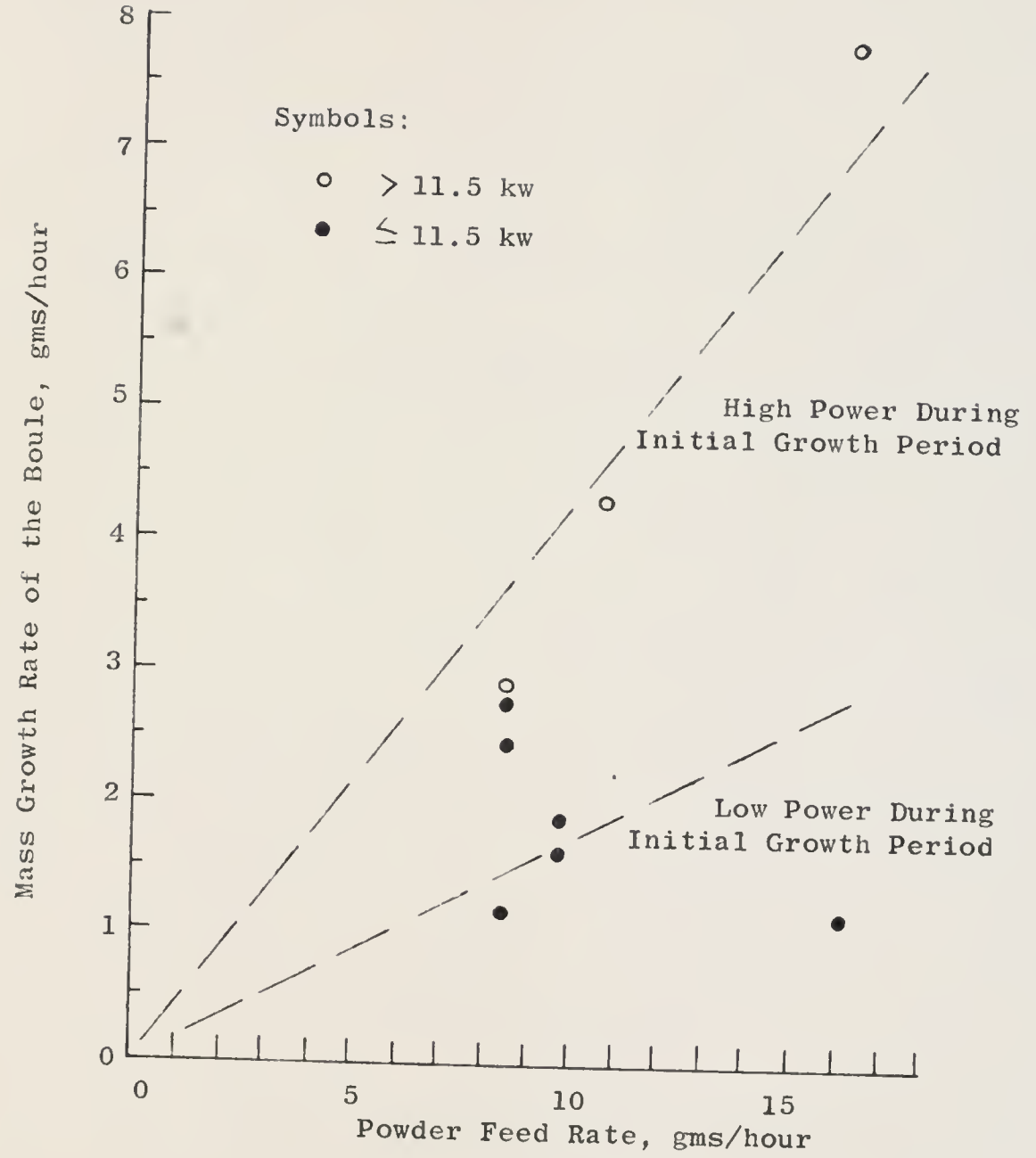

Figure 24 Mass Growth Rate as a Function of the Powder Feed Rate, for both High and Low Rf Power During the Initial Growth Period of an Aluminum Oxide Boule

boule radius, length, and the average side coefficient of heat transfer, $\bar{h}_s$. Since plasma heat transfer is a function of the rf power level, it is to be expected that the side coefficient of heat transfer will vary with the rf power.

Figure 25 is presented to show the experimental variation of $\bar{h}_s$ with rf power. It is seen that the curve of $\bar{h}_s$ as a function of rf power is approximately a straight line with a negative slope of about 0.032 cal/sec cm^2 C per kw. The curve of Figure 25 was plotted from the thermal gradient and size data obtained at the time of growth of the boule (Appendix E) and from the theoretical curves involving $\bar{h}_s$ of Figures 6, 7, 8 and 9. Data is for the case where the boule length is 1.0 cm. It is assumed that $\bar{h}_s$ is independent of boule radius, for the range of radii encountered. The expected trend does exist; as the plasma gets hotter, due to increasing the rf power, the heat loss from the sides is reduced, and $\bar{h}_s$ decreases.

Figure 26 is presented to show how the thermal gradient varies with rf power. It is seen that the curve of thermal gradient as a function of rf power is also approximately a straight line, having a negative slope of about 10 cal/sec cm^2 C per kw. This curve was plotted from the data of Appendix E after correcting the thermal gradient so that it conformed to that of a boule having a standardized radius of 0.6 cm. This standardization of the data was done by assuming that $\bar{h}_s$ is constant for any given rf power (and independent of boule radius). The important conclusion to be drawn from these curves is that, for a given size of boule, low power can be equated with high thermal gradients, and vice versa. There is an interdependency of these two quality parameters, thermal gradient and rf power, related by the variations of $\bar{h}_s$ with the rf power.

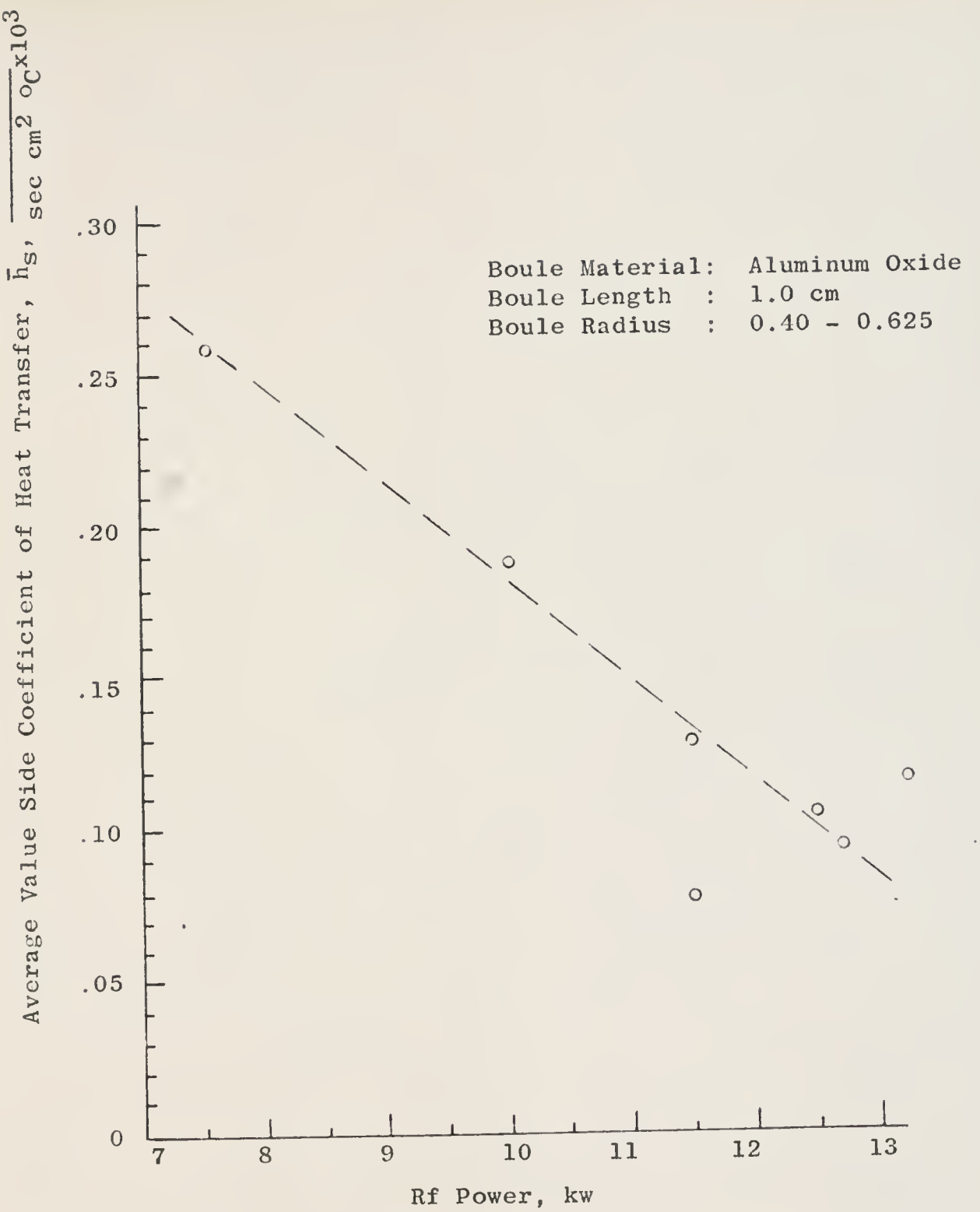

Figure 25 Average Value of the Side Coefficient of Heat Transfer as a Function of the Rf Power

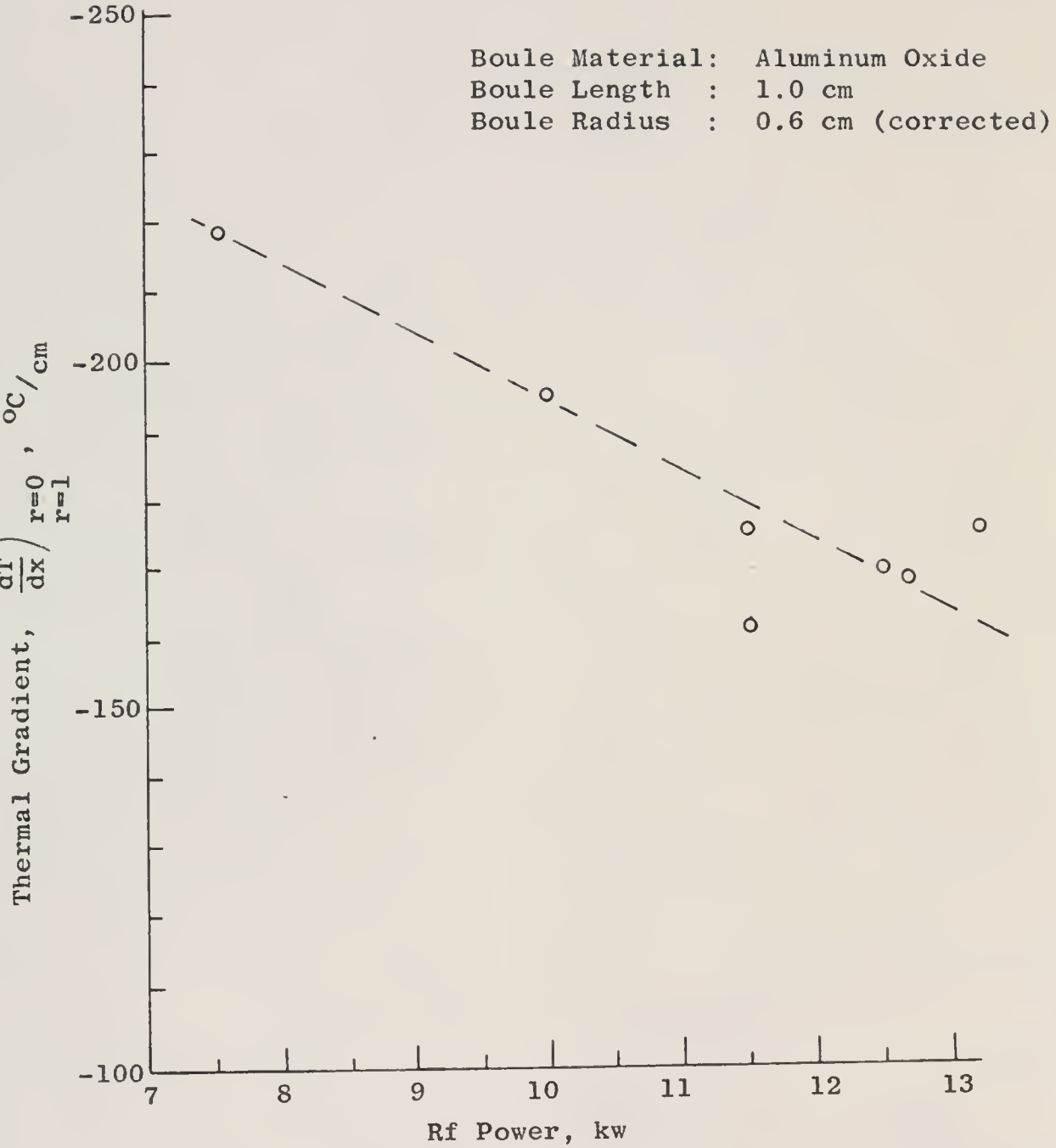

Figure 26 Thermal Gradient as a Function of the Rf Power for Aluminum Oxide Boules of Standardized Length and Radius

F. Crystal Quality Parameters and Quality Level Scale

The heat transfer-crystallization theory suggests that the parameters affecting crystal quality are the thermal gradient ∇T at the solid-liquid interface at the time of growth, the average temperature $\bar{T}_L$ of the liquid layer and the growth rate of the crystal. However, a good deal of interdependence between these parameters has been established. For instance, the thermal gradient has been found to increase as the boule grows, for constant power; it decreases as power is increased for constant boule size (see Figure 26). The growth rate of the crystal has been found to increase as the powder feed rate increases at constant power; and if power is increased at constant feed rate, growth rate increases (see Figure 24). The average temperature of the liquid layer, from equation 10, has been found to increase with the rf power, but to decrease as the thermal gradient and the powder feed rate increase. In short, the parameters controlling quality are the thermal gradient, the rf power and the powder feed rate. It should be noted that seeding and introduction of a flux can affect crystal quality, and may be of primary importance in growing perfect crystals.

The correlation of these factors to crystal quality is facilitated by defining an arbitrary scale against which the quality of the various boules can be measured. This scale, presented in Table 3, and using letter grades for quality levels, is based on the degree to which the boule achieves being an optically clear, single crystal. The microscopic imperfections within the crystal lattice will be ignored for the present. Also, cracking of the boule, due to thermal stresses on cooling, will be ignored since it is believed that this difficulty could be overcome by additional annealing equipment.

Table 3

Definition of an Arbitrary Quality Scale With Which to Judge the Quality of the Boules Grown in This Experiment

Quality Scale Rating	Boule Description
A	Major part of boule optically clear and single crystal
B	Large sections of the boule optically clear and single crystal
C	Either large part of the boule single crystal but optically cloudy, or small part of the boule single crystal but optically clear
D	Polycrystalline boule, optically clear or cloudy
E	Polycrystalline boule with gross imperfections of incompletely melted powder, optically cloudy

The pertinent quality parameter data on the boules grown in this experiment is presented in Table 4. Core quality is taken to be the interior quality extending to approximately one-half the boule radius. Peripheral quality refers to the quality extending from mid-radius to the outer edge of the boule.

G. Crystal Quality as a Function of Seeding

If initial growth is started from a seed, and if the procedure is successfully executed to prevent contamination, then there appears to be a pronounced difference in the quality of the boule, especially noticeable at the core. Referring to Table 4, it is seen that no boule initiated without a seed had a core quality better than D (Table 3). Of those started from seeds, it is believed that only three were successfully started (#7, #9 and #11). These had core qualities of B. The remainder of those started from seeds apparently were contaminated since their core quality was not much better, in general, than those started unseeded.

The effect of the seed apparently diminishes as the boule grows in radius and length. It seems that even a polycrystalline core can result in a high quality periphery if the boule is allowed to grow large enough under proper conditions for quality growth. The small crystals at the core appear to expand as they grow outward. This result is most striking in boules #5 and #10, grown unseeded, where the core quality was D but the peripheral quality was B. However, if the environmental conditions of thermal gradient, rf power and powder feed rate are not proper for quality growth, then the small core crystals do not expand as growth proceeds, and the boule becomes polycrystalline throughout. This result is noticed in boule #7, started with a seed, that

Table 4

Pertinent Quality Data on the Boules Grown in this Experiment

Boule No.	Seed	Dimensions r_o (cm)	Dimensions L (cm)	Growth Rate (av) (gms/hr)	$\bar{h}_s$ (1)	Rf Power (kw)	Thermal Gradient (°C/cm) *	Thermal Gradient (°C/cm) **	T Powder Feed Rate (2) *	T Powder Feed Rate (2) **	Quality Level (Table 3) Core	Quality Level (Table 3) Periphery
1	No	0.60	1.0	1.13	0.080	11.5	-155	-162	9.6	10.0	D	D
2	No	0.55	0.5	7.75	0.125	13.2	-149	-165	9.3	6.5	E	D
		0.65	1.0		0.125	13.2	-152	-175	9.4	10.9	D	C
3	No	0.50	1.0	2.75	0.130	11.5	-164	-178	19.3	20.9	D	C
4	Yes	0.60	0.5	2.47	0.180	11.8	-166	-180	19.5	21.2	E	D
5	Yes	0.60	1.0	1.22	0.105	12.5	-147	-170	17.3	20.0	D	B
6	Yes	0.30	0.5		0.190	9.4	-221	-240	21.0	22.8	C	B
		0.40	1.0	3.65	0.188	10.0	-199	-210	18.9	21.6	C	C
7	Yes	0.25	0.5		0.260	7.4	-216	-246	20.5	25.4	B	C
		0.40	1.0	1.62	0.260	7.5	-216	-246	20.5	25.4	D	D
8	Yes	0.40	0.5	4.35	0.260	10.8	-175	-216	16.7	24.4	D	C
9	Yes	0.45	1.0	2.88	0.094	12.7	-160	-168	18.8	19.6	B	B
10	No	0.60	1.0	3.32	-.002	13.4	-132	-132	15.6	15.6	D	C
11	Yes	0.50	0.5	2.44	-.002	13.5	-137	-137	16.2	16.2	C	C

(1) $\frac{\text{cal/sec cm}^2\ ^\circ\text{C}}{}$ (2) $\frac{^\circ\text{C/cm}}{\text{gms/hr}}$ * at r=0 ** at r=1

had an initial core quality of B but which grew so poorly that it ended as a D quality crystal at the periphery.

Thus it appears that seeding, as well as environmental conditions, is important to crystal quality.

H. Crystal Quality as a Function of Thermal Gradient, Rf Power and Powder Feed Rate

It has been pointed out that if proper environmental conditions are provided, and if the boule is allowed to grow large enough, then the quality level of the periphery of the boule should be high, regardless of whether or not growth had been initiated from a seed. Utilizing this fact, an evaluation of the heat transfer-thermodynamic quality parameters can be made by comparing them to the peripheral boule quality, for large size boules. Such a comparison should show the approximate values of the quality parameters that are adequate for the growth of high quality boules.

Examination of Table 4 leads to the conclusion that it is not the thermal gradient alone that establishes quality. For instance, boules #1 and #9 were grown with almost identical thermal gradients (-162 and -168 respectively) yet their peripheral quality levels are D and B respectively. Clearly, these differences in quality must be related somehow to the remaining parameters involved, i.e., powder feed rate and rf power.

The thermodynamic crystallization theory leads to the prediction that, for small thermal gradients, and constant $\bar{T}_L$ and $\dot{m}$, crystal quality increases with an increase in thermal gradient. The theory further predicts that at large thermal gradients, and for a constant $\bar{T}_L$ and $\dot{m}$, crystal quality decreases as the thermal gradient increases. In the former case, a defect growth mechanism is involved. In the latter case, self-nucleation occurs. For the range of thermal

gradients encountered in these experiments it might be expected that the first case would apply, i.e., that crystal quality will increase as the thermal gradient increases. The reason being that the thermal gradients observed are quite small.

Observations of crystal growth have also shown that crystal quality improves as the rate of growth decreases. Combining these statements, one is led to predict that the ratio of $\nabla T/\dot{m}$ might constitute a quality parameter by itself.

Plotting this ratio of thermal gradient to powder feed rate, $\nabla T/\dot{m}$, against the third parameter, rf power, produces a quality chart that appears to fit the data of Table 4. This chart is presented in Figure 27. It is seen that crystal quality improves with an increasing $\nabla T/\dot{m}$ ratio, for constant rf power, and improves for increasing rf power, for a constant $\nabla T/\dot{m}$ ratio. Figure 27 omits consideration of boules #4 and #8 which are less than 1.0 cm in length. Admittedly, a larger number of samples would be desirable to confirm this relationship. However, granting that the quality level grades of Table 3 are arbitrary, and therefore subject to interpretation by different observers, then it becomes somewhat doubtful that a refinement in the chart, obtained by data from many more boules, could ever convert it into a perfect representation of a cause-and-effect relationship. Figure 27 does describe the trends and observed requirements for producing quality crystals, and therefore does constitute a valuable aid in interpreting and presenting the results of this research.

In the actual growing of crystals, the most easily controlled of the quality parameters are the powder feed rate and the rf power. The third parameter, thermal gradient, can only be varied, within restricted limits, by changing the

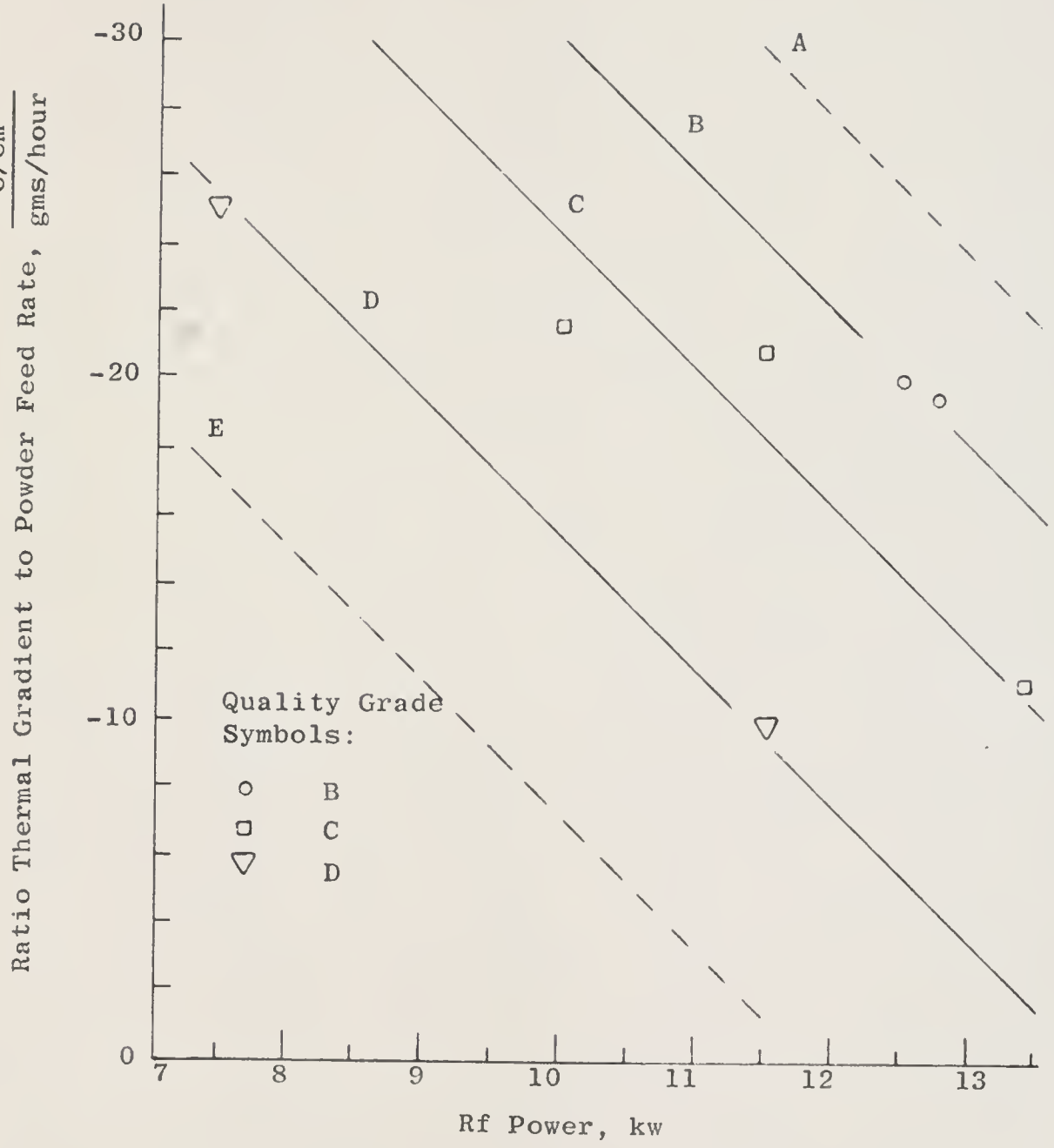

Figure 27 Ratio of Thermal Gradient to Powder Feed Rate as a Function of the Rf Power for the Growth of Boules of Quality Levels A to E (see Table 3), When the Boule Tip Is Located at Position B-0. The Material is Aluminum Oxide with 2% Chromium.

location of the boule tip in the plasma fireball. As is seen in Table 1, the thermal gradient rises as the boule tip is lowered. However, as is also seen in Table 1, the boule tip temperature, and therefore $\bar{T}_L$, decreases as the boule tip is lowered. This combination of changes in ∇T and $\bar{T}_L$, as the boule tip is lowered, creates an opportunity for determining which of the two quality parameters, $\nabla T/\dot{m}$ or $\bar{T}_L$, has the greater effect on crystal quality. For example, a boule grown at position B-0 will have a higher value of $\bar{T}_L$ than one grown at C-0, but both could conceivably have (or be made to have) the same value of $\nabla T/\dot{m}$. If two crystals are grown under the above conditions, and their qualities compared and found to be the same, then it can be argued that the parameter $\nabla T/\dot{m}$, which was the same for both boules, has a greater influence on crystal quality than does $\bar{T}_L$. However, if the boule grown at the position C-0 is of lesser quality than the one grown at B-0, under identical conditions of $\nabla T/\dot{m}$, then it would appear that the parameter $\bar{T}_L$ is the more important to crystal quality.

With these ideas in mind, boules #10 and #11 were grown at position C-0. Both were grown under peak rf power and to a size adequate for comparison with those grown at B-0. The results are given in Table 4 and Appendix E. The thermal gradient to powder feed rate ratios were 15.6 and 16.2 respectively, which, at 13.5 kw, should have produced boules of B level quality, by Figure 27. The actual quality was less than B, indicating that the lower $\bar{T}_L$ at C-0 had a more pronounced effect on quality than did the thermal gradient to powder feed ratio.

Thus it can be concluded that the maintenance of a highly molten liquid layer is essential to the growth of optically clear, single crystalline boules, in addition to the requirement of a high thermal gradient to powder feed rate ratio.

I. Crystal Quality as a Function of the Radius and Length of the Boule

As was shown in the mathematical analysis of Chapter II, the axial thermal gradient at the liquid-solid interface varies with boule radius and length. If these variations in thermal gradient are large enough they could conceivably affect the quality of the boule, through changes in $\bar{T}_L$ and the thermal gradient to powder feed ratio.

Examination of Table 4 shows that the general trend in quality is to either remain the same or to improve as the radial distance from the core increases. There is one boule that goes counter to this trend, namely #7; but its contrary behavior can be understood by realizing that this boule was successfully initiated from a large seed, and that the core quality results from this seed, not from the method of growth. The environmental conditions for growth were actually so poor that, even from this excellent beginning, the crystal quality became progressively worse as the boule grew larger. The normal case appears to be where the core quality is inferior to the peripheral quality.

For a few of the boules grown the improvement of quality with radial distance from the core can be explained on the basis of the analysis leading to Figure 27, since the quality parameter of thermal gradient to powder feed rate ratio, $\nabla T/\dot{m}$, generally increases with radial distance from the center, i.e., since the thermal gradient generally increases with radial distance from the center. In most cases, however, the quality difference between the center and periphery cannot be entirely explained in this manner. For instance, in boule #5, the observed quality difference is between grade D at the core and B at the periphery, whereas the small difference in the quality parameter of thermal gradient to powder feed rate (2.7) is not large enough to account for this wide spread of quality.

Two possible explanations can be offered. The first is that there appears to be a natural tendency for the small core crystals to enlarge as they grow outwards, assuming that an adequate growth environment is provided. The second is that the powder grain density at the boule might also be a function of the radius. For instance, it can be expected that the density of powder grains impinging on the boule will be greater at the center than at the edge due to some dispersion of the grains during transit through the fireball. And the larger the boule radius, the larger will be this dispersion-related difference in powder grain density between core and periphery of the boule. When this powder grain density difference is large enough it means that the thermal gradient to powder feed rate ratio is lower at the core than would be predicted by assuming a constant, average powder grain density as a function of radius; and this lower-than-expected ratio could account for the large observed difference in crystal quality, by Figure 27.

It is probable that both these factors apply to crystal growth, in varying degrees depending on the radius of the boule and the adequacy of the environmental parameters. The analysis leads to the conclusion that proper seeding and low powder feed rates are required for production of high crystal quality at the core.

The change in boule quality with length appears totally dependent on the adequacy of the environment. If successfully initiated from a seed, a boule appears to maintain or improve the quality of the seed as it grows longer, providing the growth environment is adequate. For an inadequate environment, the quality worsens with growth. In practically every case the quality of the tip, the last part to solidify, was poorest. This could be attributed to the tendency of impurities to migrate towards the liquid end

(since they are generally more soluble in the liquid than in the solid phase) and also to the tendency of $\bar{T}_L$ to become lower as the boule grows longer. The peak capacity of the rf power supply used in this work appears to be only marginally adequate to maintain a high enough $\bar{T}_L$ for good crystal quality. Any factor tending to reduce $\bar{T}_L$, such as growth of long boules or growing the boule at a lower position in the fireball, had a pronounced adverse effect on crystal quality.

Figures 28, 29 and 30 are presented as illustrations of the arguments just presented. Figure 28 is of boule #5. Superimposed on it are the thermal gradient profile and quality parameter profile (thermal gradient to powder feed ratio, assuming constant powder grain density with boule radius). The boule was initiated without a seed. The core is seen to be rough, due to entrained gas bubbles, cloudy, due to impurities, and polycrystalline. The periphery contains large, single, optically clear crystals, indicating an adequate environment for growth.

Figure 29 is of boule #9, also shown with thermal gradient and quality parameter profiles superimposed. This boule was successfully initiated from a seed, and was provided with an adequate growth environment. The tendency of the core crystal to enlarge as it grows outwards is seen, along with the generally superior quality of the periphery. Figure 30 is of boule #7, successfully initiated from a seed as is seen in (a), a photograph of the core just above the seed. The boule then grew progressively worse, as is seen in (b), due to a completely inadequate growth environment (low rf power of 7.5 kw, and, therefore, low $\bar{T}_L$).

J. Crystal Quality as a Function of the Powder Grain Size

Boule #8 was grown using 0.004" diameter powder grains instead of 0.005" grains as was used for the rest of

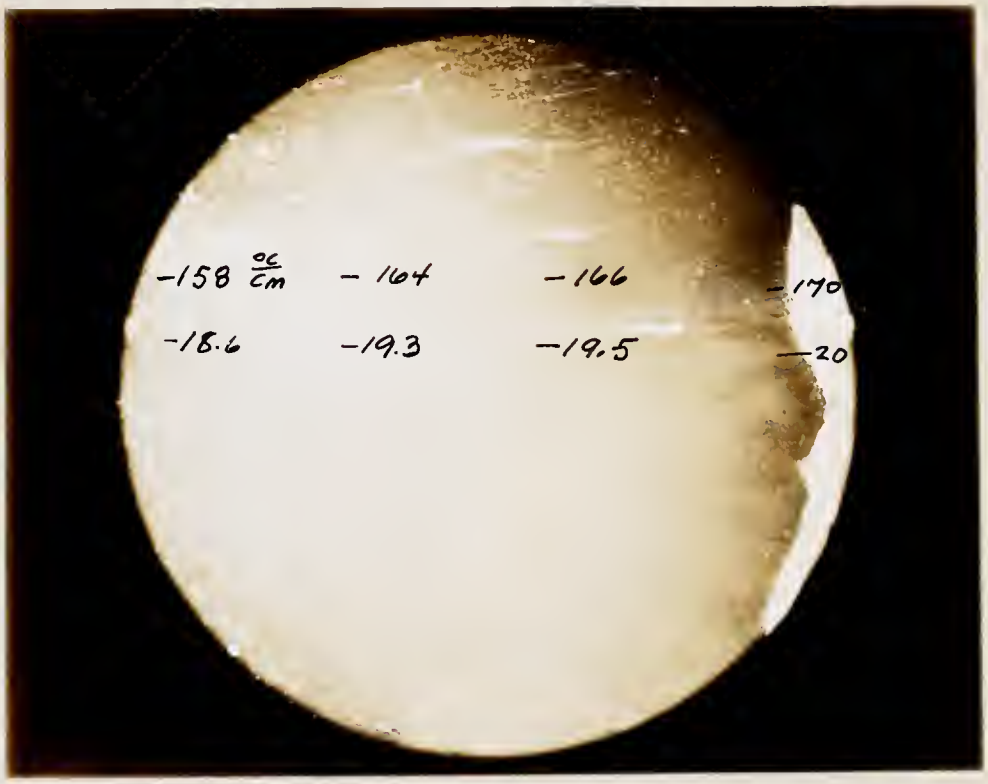

Figure 28 Photomicrograph of Boule #5, Giving Thermal Gradient and Quality Parameter Profiles

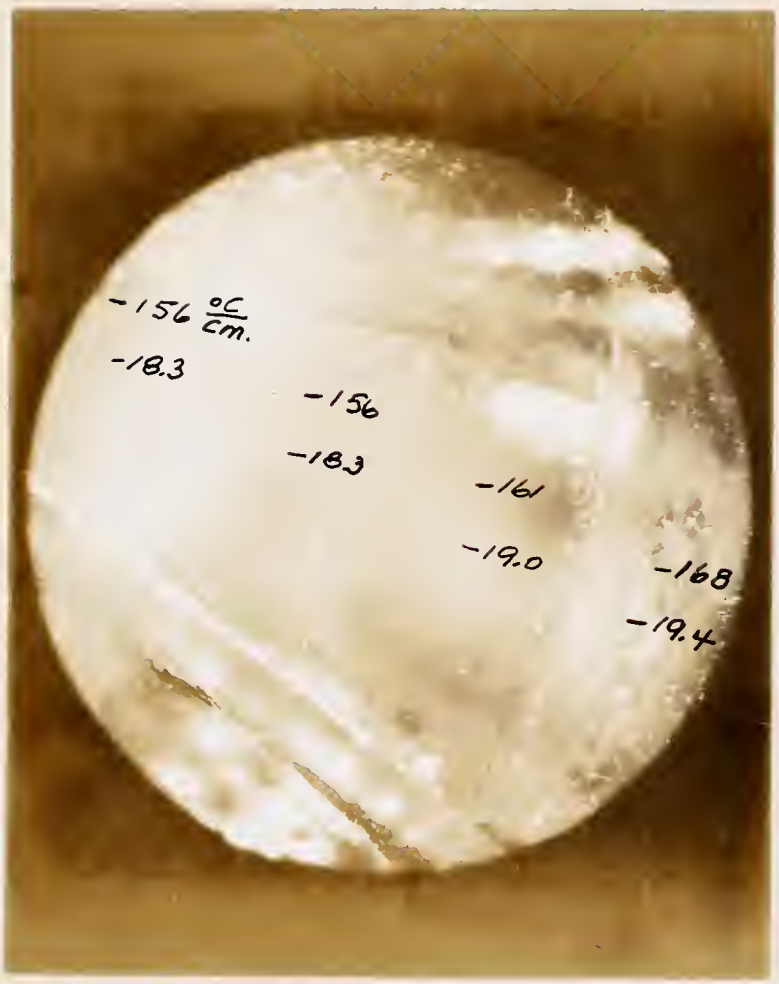

Figure 29 Photomicrograph of Boule #9, Giving Thermal Gradient and Quality Parameter Profiles

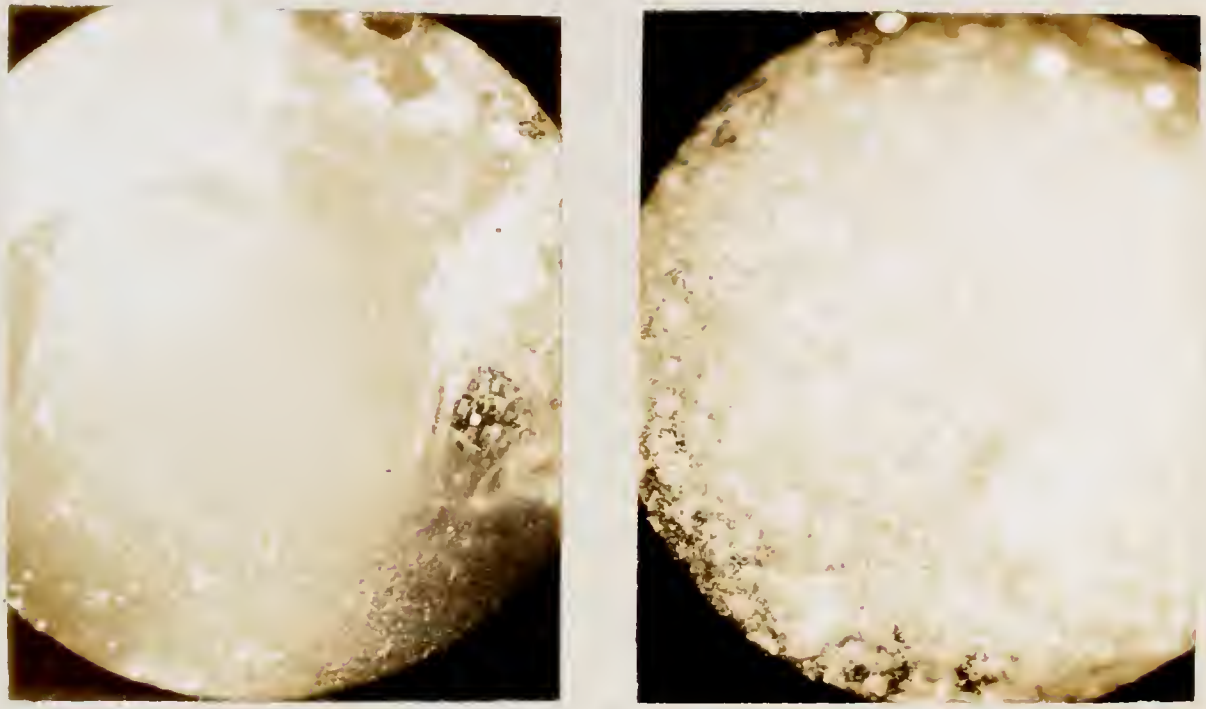

(a) (b)

Figure 30 Photomicrographs of Cross Sections of Boule #7. View (a) was taken at a cross section just above the seed. View (b) was taken at a cross section near the end of growth. Quality deterioration is attributed to completely inadequate growth environment.

the boules. The difference in observed quality is negligible. However, as was described in a previous experiment, the smaller powder grains have a tendency to cool the plasma more than do the larger grains. Such cooling can have an adverse effect of $\bar{T}_L$. It is believed that the 0.004" grains were at the threshold of causing this effect since a perceptible change in color of the plasma fireball was observed with their use. For the conditions utilized for the growing of the aluminum oxide boules it would appear that 0.004" diameter powder grains are the smallest that should be used.

K. Summary of the Factors Affecting Crystal Quality

Based on the results just presented, certain conclusions can be drawn as to the general requirements for growing high quality crystals. These are summarized as follows:

1. The environmental variables affecting crystal quality are the average temperature of the liquid cap ($\bar{T}_L$), the ratio $\nabla T/\dot{m}$ of thermal gradient to powder feed rate, and the rf power. It was found that there is an interdependence between the thermal gradient and rf power, such that as the rf power increases the thermal gradient decreases. Also, as the thermal gradient decreases, $\bar{T}_L$ tends to increase.

2. The maintenance of an adequately high average temperature of the liquid cap, $\bar{T}_L$, is of fundamental importance to crystal quality.

3. The cores of boules successfully grown from seeds are of higher quality than those grown unseeded. The quality of the periphery of boules grown both seeded and unseeded can be the same if they are grown sufficiently large in an adequate growth environment.

4. Crystal quality is generally worse at the core of a boule than at the periphery, and worse at the end that solidifies last than at the midpoint of the boule.

5. Since the maintenance of a high temperature of the molten cap is important, small powder grain sizes should be avoided due to their tendency to cause cooling of both the plasma and the boule.

Part 3. Growth of a Crystal Based on the Theory and the Experiments Just Concluded

The purpose of this research was to analyze the he heat transfer-crystallization mechanism taking place in a plasma fireball, in order to gain some understanding of the crystal growth capabilities of the plasma-Verneuil furnace. The analysis just presented included a heat transfer-crystallization theory, several experiments to determine the heat transfer capabilities of the plasma fireball, and experiments to determine the conditions for the growth of high quality crystals within the fireball. It now seems fitting to illustrate how the information just presented can be utilized to predict the proper growth environment for a boule of a different material than the aluminum oxide used in the previous analysis.

One criterion for the choice of a new material for this last experiment was that the melting point of the material must be less than 2000 C. The work done on aluminum oxide (melting point of 2015 C) indicates that the existing furnace has only marginal capability at temperatures over 2000 C. A better evaluation of the crystallization capability of the particular furnace used could be made by growing a crystal of a material that is more easily melted.

Another criterion was that there could be no solid-solid phase transformation within the crystal when it cooled to room temperature. With these criteria in mind, ferric oxide was chosen. This material has a melting point of 1565 C

and a stable (trigonal) lattice structure on cooling. Even if reduced slightly to ferrosoferric oxide, the resulting structure remains stable on cooling.

Two minor problems arose after the powder was obtained. The first was that the powder was very fine grained, approximately 40 microns (0.0016") diameter. The second was that the powder had adsorbed considerable moisture and would not flow freely. These problems were overcome by dehydrating the powder in a conventional oven for 48 hours at 220 F, and then reseiving it through a #65 mesh screen, to eliminate all lumps. The resulting powder was found to flow through a 0.0292" diameter hole in the shaker hopper at a steady rate of 12 gms/hour. This rate had been established, from the previous work, as being acceptable for the growth of high quality crystals.

The next point of consideration involved the location of the boule tip in the fireball. It was assumed that the average temperature of the liquid cap could be approximately 100 C above the melting point of the material, or about 1665 C. Referring to Table 1, which is based on an rf power of 4.7 kw, it is seen that the location D-0 (Figure 11) can provide this temperature with an ample margin for further adjustment by variations in the rf power and amount of diatomic gas. With the boule tip set at D-0, the powder probe tip was then set at a distance of 4 cm from it, based on the results expressed in Figure 12. A powder-gas flow rate of 2 SCFH was chosen, as per Figure 13.

The first boule grown had to be initiated without a seed, of necessity. Data on this boule (#12) are given in Appendix E. The boule was grown to a length of 1.5 cm and a radius of 0.5 cm. It was found to contain large single crystals (approximately 4 mm square) which could be sheared apart easily (by hand) due to the extreme brittleness of the

material. The individual crystals could not be sheared by hand, however. At one point during the growth the rf power was deliberately raised to a point (approximately 8.5 kw) where the molten cap became so large and limpid that it flowed over the sides of the boule. The remainder of the boule was then grown at powers below this level to assure stability. It should be noted that some reduction to ferrosoferric oxide did occur since the resulting crystals were found to have high magnetic susceptibility.

The second boule grown (#13) was initiated from a seed of boule #12. This boule, also, was grown to a length of 1.5 cm and a radius of 0.5 cm. During growth the power was held at 6.7 kw which was found sufficient to maintain a liquid cap of about 3 mm in depth at the axis. One interesting feature of the ferric oxide was that its liquid cap was slightly transparent in the highly luminous plasma, allowing one to see the liquid-solid interface (which was approximately flat) and also to see the powder grains entering the liquid, swirling around momentarily, and finally disappearing (melting). When the powder was shut off, and the rf power gradually lowered, one could also see the liquid-solid interface advancing upwards as the cap solidified. It was found that a drop of approximately 0.5 kw in rf power would cause the interface to advance approximately 1 mm. Clearly, use of the plasma-Verneuil furnace in this temperature range enables a very fine degree of control on the crystallization process.

The results were also very gratifying. Almost the entire core of the boule was single crystal, and only slightly cracked from cooling stresses. Figure 31 is presented showing a photomicrograph of a cross section of this boule. Except for a few small bubbles the quality is almost perfect. There was no apparent quality difference with length so that

Figure 31 is representative of the entire crystal. With further refinements in powder quality, and with the use of suitable fluxes, the quality could presumably be even better.

Figure 31 Photomicrograph of a Cross Section of a Ferric Oxide Single Crystal Grown in the Plasma-Verneuil Furnace

CHAPTER IV. SUMMARY AND CONCLUSIONS

In the research reported here, it is notable that the crystals grown were not particularly large or perfect; such was not the intent of the work. What was considered of primary interest was the nature of the thermal regime as affecting crystal growth and quality.

It appears that the large, radiant heat loss from the side of the boule dominates the thermal conditions during crystal growth. When the rf power is low, the boule is cool and the thermal gradients are large. As the boule increases in length, rf power must be boosted in order to maintain a molten cap. If the rf power were held constant during growth, a length would eventually be reached causing a thermal gradient that would be large enough to solidify the molten cap. At this point all growth would stop.

The large radiant heat losses from the side of the boule are not necessarily or always as important as was found in the growing of aluminum oxide crystals. If materials of a lower melting point are involved, radiation losses become less important. If materials of higher melting points are involved, clearly the importance of the radiation losses becomes much more critical.

The importance of a diatomic gas as a means of heat transfer to the boule is an interesting observation. The use of such gases for such purposes is not, of course, original with this work. On the other hand, the dramatic increase in the heat transfer rate from the plasma when

diatomic gases are used constitutes an important improvement in this application.

The effect of loss of heat due to the introduction of fine powder grains into the plasma is another observation not originally anticipated. The study here clarifies and rationalizes the observation.

Details of the experimental arrangements might be of some interest, although how general their applications may be is questionable. No information could be found in the literature, however, concerning such effects on boule heat transfer as the powder probe to boule distances and powder-gas flow rates.

It is concluded that the work reported here contributes to a more effective use of the plasma-Verneuil furnace in growing crystals of refractory materials.

CHAPTER V. SUGGESTIONS FOR FURTHER EXPERIMENTATION

It is believed that the use of fluxes in the powder being crystallized would greatly increase the crystal quality (by aiding in maintaining a limpid molten cap and by removing entrained gases). The plasma-Verneuil furnace appears to be a most convenient tool to use in the evaluation of fluxes. Powder charges can be changed rapidly, thus permitting the evaluation of many fluxes in a short period of time. Also, visual observation of the crystallization site is possible, unhampered by heavily insulated furnaces and crucibles. And, finally, only small quantities of powder and flux would be required, since the size of the boule grown need only be a few cubic centimeters.

A program of experimentation into the effects of flux on crystal quality would appear to be a worthwhile undertaking. This seems especially so in the case of refractory crystals, where research has been hampered by the difficulties of working with and containing very high temperatures. Use of the plasma-Verneuil furnace would overcome many of these difficulties.

APPENDIX A

CALIBRATION OF THE POWDER FEED MECHANISM

The powder feed mechanism described on page 7 of Chapter I was calibrated by weighing the amount of powder fed over constant intervals of time as a function of the powder grain size, hole size in the hopper, and vibrating frequency. The sizes of hopper hole used were .016", .018", .019", .020", .021", .0225", .024", .026", .028" and .0292".

During the calibration procedure it was noticed that one of the five possible frequencies of the shaker motor (setting #4) seemed to be close to one of the natural frequencies of the entire powder feed mechanism. This near-resonance resulted in a strong shaking response and produced the most constant feed rate. Consequently all further calibration was made at this frequency.

The ratio of the hole size to the grain size was found to be the key parameter in governing the rate of dry powder flow for a constant shaking frequency. The results of the calibration are presented in Figure A-1 for aluminum oxide powder mixed with 2% chromium, 40 micron size. Designations of the powder grain size are as follows:

Nominal Grain Size	Will Pass Sieve #	Will Not Pass Sieve #
(.007)	#65 (.008")	#100 (.0058")
(.005)	#100 (.0058")	#150 (.0041")
(.004)	#150 (.0041")	#170 (.0035")
(.003)	#170 (.0035")	#250 (.0024")
(.002)	#250 (.0024")	

The powder fell freely through the hole if the ratio of the hole to grain size was greater than about 5 for the large grains or 10 for the small grains. Clogging of the hole was encountered if the hole to grain size ratio was less than 3 for the large grains or 7 for the small grains.

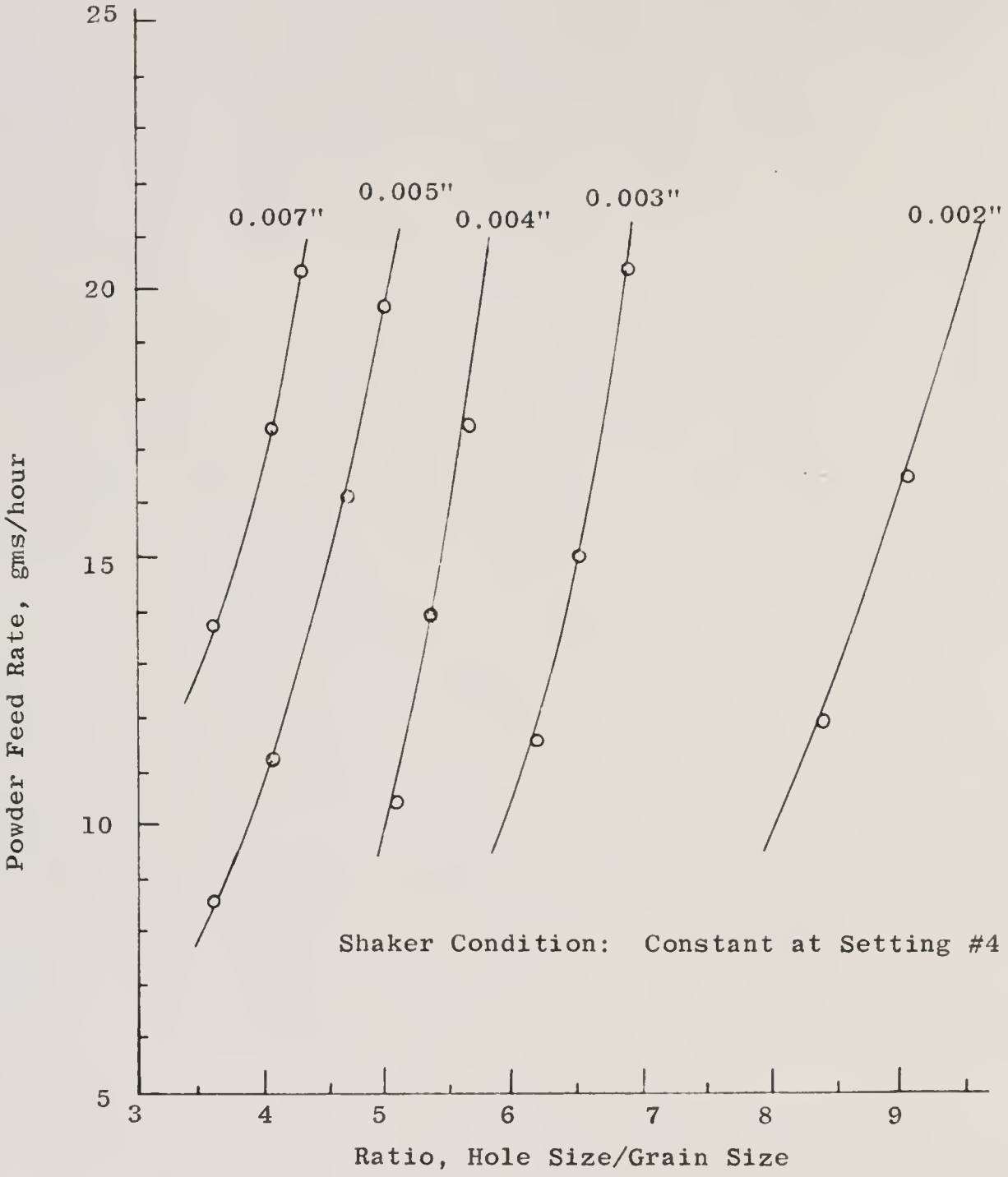

Figure A-1 Powder Feed Rate as a Function of the Hole to Grain Size Ratio, for Various Sizes of Powder Grains

APPENDIX B

CALCULATION OF THE THERMAL PROFILE IN THE BOULE

The geometry on which the mathematical model for the thermal profile in the boule is based is shown in Figure 5, page 24. The assumptions made in the solution are as follows:

1. steady state conditions exist
2. temperature is a function of x and r:

$$T = T_{(x,r)} \qquad \text{B-1}$$

3. thermal conductivity and emissivity are constant in the temperature range under consideration
4. the temperature at the liquid-solid interface is the melting temperature of the material being considered

$$T_{(0,r)} = T_{m.p.} \qquad \text{B-2}$$

5. the heat loss per unit area from the side of the boule can be expressed by the equation:

$$Q_{\text{side loss}} = h_s \left[T_{(x,r_o)} - T_{\text{Ambient}} \right] \qquad \text{B-3}$$

or

$$-k \left(\frac{\partial T}{\partial r} \right)_{r=1} = \sigma \epsilon \left[T^4_{(x,r_o)} - T^4_A \right] - h_p \left[T_p - T_{(x,r_o)} \right] \qquad \text{B-4}$$

6. the heat loss per unit area from the base can be expressed by the equation:

$$Q_{\text{base loss}} = h_b \left[T_{(1,r)} - T_A \right] = -k \left(\frac{\partial T}{\partial x} \right)_{x=L} \qquad \text{B-5}$$

Assumptions 5 and 6 are made to linearize the mathematical expressions at the boundaries of the boule, and thus make them more amenable to solution. The assumption 5 is valid if the side heat loss is dependent on the first power of temperature along the entire length of the boule. This condition, as is shown in Appendix D, is only approximated over short boule lengths.

Assumption 6 is valid if the heat loss from the base is proportional to both the temperature and the thermal gradient, for all L. It is more properly applicable to the case where the end of the boule is flat and entirely exposed to the ambient temperature. The actual geometry is not of this type but includes a support for the boule that tapers up from the pedestal (see Figure 5). Since the face at x = L is taken at the top of this taper (Figure 5), there is actually no exposure of the face to the ambient temperature.

However, the assumption 6 is approximately valid for either large values of L or for small changes in L, since, as will be shown, both the temperature and the thermal gradient have similar functional dependence on L:

$$T_L \propto A \cosh(\beta L) + B \sinh(\beta L) \qquad \text{B-6}$$

$$\left(\frac{dT}{dx}\right)_{x=L} \propto \beta B \cosh(\beta L) + \beta A \sinh(\beta L) \qquad \text{B-7}$$

For large L both the sinh and cosh tend toward infinity, and the effect of the constants is minimized. Thus the application of equation B-5 will show negligible changes in h_b with L, for large L. And even for small L, h_b remains almost constant provided the changes in L are also kept small. A quantitive check of this assumption is given in Appendix D.

The equation describing the steady state temperature profile in the boule of Figure 4 is the Laplace equation, expressed in cylindrical coordinates:

$$\frac{\partial^2 T}{\partial r^2} + \frac{1}{r}\frac{\partial T}{\partial r} + \frac{\partial^2 T}{\partial x^2} = 0 \qquad \text{B-8}$$

In order to obtain solutions applicable to all boules, the variables in B-8 will be expressed non-dimensionally.

Let

$$\Theta_{(x,r)} = \frac{T_{(x,r)} - T_A}{T_A} \qquad \text{B-9}$$

where $$x_1 = \frac{x}{L} \qquad \text{B-10}$$

and $$r_1 = \frac{r}{r_0} \qquad \text{B-11}$$

then $$\frac{\partial \Theta}{\partial r_1} = \frac{1}{T_A}\frac{\partial T}{\partial r}\frac{dr}{dr_1} = \frac{r_0}{T_A}\frac{\partial T}{\partial r} \qquad \text{B-12}$$

$$\frac{\partial^2 \Theta}{\partial r_1^2} = \frac{r_0^2}{T_A}\frac{\partial^2 T}{\partial r^2} \qquad \text{B-13}$$

$$\frac{\partial^2 \Theta}{\partial x_1^2} = \frac{L^2}{T_A}\frac{\partial^2 T}{\partial x^2} \qquad \text{B-14}$$

Substitute the above into B-8 and simplify:

$$\frac{\partial^2 \Theta}{\partial r_1^2} + \frac{1}{r_1}\frac{\partial \Theta}{\partial r} + \left(\frac{r_0}{L}\right)^2 \frac{\partial^2 \Theta}{\partial x_1^2} = 0 \qquad \text{B-15}$$

Separate variables:

let $$\Theta_{(x,r)} = X_{(x)} R_{(r)} \qquad \text{B-16}$$

Substitute B-16 into B-15

$$\frac{1}{R}\left[\frac{d^2R}{dr_1^2} + \frac{1}{r_1}\frac{dR}{dr_1}\right] = -\frac{1}{X}\left[\left(\frac{r_0}{L}\right)^2 \frac{d^2X}{dx_1^2}\right] = -\lambda^2 \qquad \text{B-17}$$

where λ is a constant.

The boundary conditions applying to the solution are:

1. (from assumption 5):

$$-k\left(\frac{\partial T}{\partial r}\right)_{r=r_0} = h_s\left[T_{(x,r_0)} - T_A\right] \qquad \text{B-18}$$

but

$$T_{(x,r_0)} = T_A\left[1 + \theta_{(x,r_0)}\right] \qquad \text{B-19}$$

Therefore, expressing B-18 non-dimensionally gives:

$$-k\left[\frac{T_A}{r_0}\frac{\partial \theta}{\partial r_1}\right]_{r_1=1} = h_s\left[T_A\,\theta_{(x_1,1)}\right] \qquad \text{B-20}$$

or

$$\left(\frac{\partial \theta}{\partial r_1}\right)_{r_1=1} = -h_1\,\theta_{(x_1,1)} \qquad \text{B-21}$$

where

$$h_1 = \frac{r_0 h_s}{k} \qquad \text{B-22}$$

2. (from assumption 6):

$$-k\left(\frac{\partial T}{\partial x}\right)_{x=L} = h_b\left[T_{(L,r)} - T_A\right] \qquad \text{B-23}$$

but

$$T_{(L,r)} = T_A\left[\theta_{(L,r)} + 1\right] \qquad \text{B-24}$$

Therefore, expressing B-23 non-dimensionally gives:

$$\left(\frac{\partial \theta}{\partial x_1}\right)_{x_1=1} = -h_2\,\theta_{(1,r_1)} \qquad \text{B-25}$$

where

$$h_2 = \frac{Lh_b}{k} \qquad \text{B-26}$$

3. (from assumption 4):

$$T_{(o,r)} = T_{m.p.} \qquad \text{B-2}$$

Expressing B-3 non-dimensionally gives:

$$\theta_{(o,r_1)} = \frac{T_{m.p.}-T_A}{T_A} \qquad \text{B-27}$$

where

$$T_{m.p.} = \text{melting temp. of material} \qquad \text{B-29}$$

In order to simplify the notation, let

$$x_1 \sim x \qquad \text{B-30}$$

and

$$r_1 \sim r \qquad \text{B-31}$$

If $\lambda = 0$, then solutions of B-17 are:

$$X_{(x)} = Cx+D \qquad \text{B-32}$$

$$R_{(r)} = E \ln r+F \qquad \text{B-33}$$

where C, D, E and F are constants of integration.

When $\lambda \neq 0$, then solutions of B-17 are:

$$X_{(x)} = A \cosh \propto \lambda x + B \sinh \propto \lambda x \qquad \text{B-34}$$

$$R_{(r)} = J_o(\lambda r), \text{ Bessel Function of Zeroth order} \qquad \text{B-35}$$

where $$\propto = \frac{L}{r_o} \qquad \text{B-36}$$

and A and B are constants of integration.

Since B-15 is linear and homogeneous, the sum of the above solutions also satisfies the basic equation:

$$\theta_{(x,r)} = \left[A \cosh \propto \lambda x + B \sinh \propto \lambda x\right] J_{o(\lambda r)} + \left[Cx+D\right]\left[E \ell nr + F\right] \quad \text{B-37}$$

which is valid for all values of $\lambda \geqq 0$.

The constants in B-37 must be chosen in order to satisfy all the boundary conditions.

Since $\theta_{(o,o)}$ is finite, and since

$$L_{r \to \infty} \ell nr = -\infty \quad \text{B-38}$$

then E must equal zero, and B-37 reduces to

$$\theta_{(x,r)} = \left[Gx+H\right] + \left[A \cosh \propto \lambda x + B \sinh \propto \lambda x\right] J_{o(\lambda r)} \quad \text{B-39}$$

where $G = CF$ and $H = DF$. B-40

Applying boundary condition (1), equation B-21:

$$\left[A \cosh \propto \lambda x + B \sinh \propto \lambda x\right]\left[-\lambda J_1(\lambda)\right] = -h_1\left\{\left[G_x+H\right] + \left[A \cosh \propto \lambda x + B \sinh \propto \lambda x\right] J_o(\lambda)\right\} \quad \text{B-41}$$

and if $\lambda = 0$ we get

$$0 = -h_1\left[G_x+H\right] \quad \text{B-42}$$

since the remaining terms on the right of B-41 hold only for $\lambda \neq 0$.

And since B-42 must hold for all values of x, we can conclude:

$$G = H = 0, \text{ for } h_1 > 0 \quad \text{B-43}$$

Thus B-37 reduces to

$$\theta_{(x,r)} = \left[A \cosh \propto \lambda x + B \sinh \propto \lambda x\right] J_o(\lambda r) \quad \text{B-44}$$

Again applying boundary condition (1), equation B-21, but this time for $\lambda > 0$:

$$\left[A \cosh \alpha\lambda x + B \sinh \alpha\lambda x\right]\left[-\lambda J_1(\lambda)\right] =$$

$$= -h_1\left[A \cosh \alpha\lambda x + B \sinh \alpha\lambda x\right] J_o(\lambda) \qquad \text{B-45}$$

which is satisfied whenever λ_i is a root of the equation

$$h_1 = \frac{\lambda_i J_1(\lambda_i)}{J_o(\lambda_i)} \quad , \; h_1 > 0 \qquad \text{B-46}$$

Applying boundary condition (2), equation B-25:

$$\left[A\alpha\lambda \sinh \alpha\lambda + B\alpha\lambda \cosh \alpha\lambda\right] J_o(\lambda r)$$

$$= -h_2\left[A \cosh \alpha\lambda + B \sinh \alpha\lambda\right] J_o(\lambda r) \qquad \text{B-47}$$

Solving for B in terms of A yields:

$$B = -A\left[\frac{\alpha\lambda \sinh \alpha\lambda + h_2 \cosh \alpha\lambda}{\alpha\lambda \cosh \alpha\lambda + h_2 \sinh \alpha\lambda}\right] \qquad \text{B-48}$$

And substituting B-48 into B-44 gives:

$$\theta(x,r) = \left[A \cosh \alpha\lambda x - A\left(\frac{\alpha\lambda \sinh \alpha\lambda + h_2 \cosh \alpha\lambda}{\alpha\lambda \cosh \alpha\lambda + h_2 \sinh \alpha\lambda}\right) \sinh \alpha\lambda x\right] J_o(\lambda r) \qquad \text{B-49}$$

By use of the double angle formulas

$$\cosh\left[\alpha\lambda(1-x)\right] = \cosh \alpha\lambda \cosh \alpha\lambda x - \sinh \alpha\lambda \sinh \alpha\lambda x \qquad \text{B-50}$$

$$\sinh\left[\alpha\lambda(1-x)\right] = \sinh \alpha\lambda \cosh \alpha\lambda x - \cosh \alpha\lambda \sinh \alpha\lambda x \qquad \text{B-51}$$

B-49 can be simplified to:

$$\theta(x,r) = A\,\frac{\alpha\lambda \cosh\left[\alpha\lambda(1-x)\right] + h_2 \sinh\left[\alpha\lambda(1-x)\right]}{\alpha\lambda \cosh \alpha\lambda + h_2 \sinh \alpha\lambda} J_o(\lambda r) \qquad \text{B-52}$$

For the third boundary condition, equation B-28, we utilize the property of linear, homogeneous equations that permit expressing the solution B-52 as:

$$\theta_{(x,r)} = \sum_{i=1}^{\infty} A_i \left[\frac{\alpha\lambda_i \cosh\alpha\lambda_i(1-x) + h_2 \sinh\alpha\lambda_i(1-x)}{\alpha\lambda_i \sinh\alpha\lambda_i + h_2 \cosh\alpha\lambda_i} \right] J_o(\lambda_i r) \qquad \text{B-53}$$

where we assume that $\theta_{(o,r)}$ is a function that can be expanded in a Fourier-Bessel series, so that B-28 reduces to:

$$\theta_{(o,r)} = \sum_{i=1}^{\infty} A_i J_o(\lambda_i r) \qquad \text{B-54}$$

Provided the above assumption holds, then we identify A_i as the Fourier-Bessel coefficients, given by (from Churchill):[31]

$$A_i = \frac{2\lambda_i^2}{(\lambda_i^2 + h_1^2) J_o^2(\lambda_i)} \int_0^1 r\, \theta_{(o,r)} J_o(\lambda r)\, dr \qquad \text{B-55}$$

The convergence of B-54 to $\theta_{(o,r)}$ is assured by the piecewise continuity of $\theta_{(o,r)}$ and its first derivative on the interval $0 < r < 1$.[31]

We thus note that at x = 0 and r = 0

$$\theta_{(o,o)} = \frac{T_{mp}}{T_A} - 1 = \sum_{i=1}^{\infty} A_i \qquad \text{B-56}$$

Differentiating B-53 with respect to x, and setting x = 0, we obtain the thermal gradient at the liquid-solid interface:

$$\left.\frac{\partial\theta}{\partial x}\right)_{x=0} = -\sum_{i=1}^{\infty} A_i \alpha\lambda_i \left[\frac{\alpha\lambda_i \sinh\alpha\lambda_i + h_2 \cosh\alpha\lambda_i}{\alpha\lambda_i \cosh\alpha\lambda_i + h_2 \sinh\alpha\lambda_i} \right] J_o(\lambda_i r) \qquad \text{B-57}$$

The above solution is similar to that given by Carslaw and Jaeger.[19] Numerical determination of the eigenvalues is facilitated by the use of curves given by Nancarrow,[32] one of which is reproduced in Figure B-1 to illustrate the method of solution.

The case where $\bar{h}_s = 0$ should also be considered. If, in equation B-4, the radiation loss from the sides equals the heat gain from the plasma, then both the temperature gradient, with respect to r, at r_o, and $\bar{h}_s$ are zero.

Assuming that the temperature at x = 0 is constant over the cross section, then there is no heat flow in the r-direction and equation B-8 simplifies to:

$$\frac{d^2T(x)}{dx^2} = 0 \qquad \text{B-58}$$

The general solution is:

$$T_{(x)} = ax + b \qquad \text{B-59}$$

where a and b are constants of integration.

Introducing the boundary conditions:

1. $$T_{(o)} = T_{m.p.} \qquad \text{B-60}$$

2. $$-k \left.\frac{dT}{dx}\right)_{x=L} = h_b(T_{(L)}-T_A) \qquad \text{B-61}$$

yields:

(from B-60) $$T_{(o)} = b = T_{(m.p.)} \qquad \text{B-62}$$

(from B-61) $$a = \frac{-h(T_{m.p.}-T_A)}{k+hL} \qquad \text{B-63}$$

Therefore, if there is no radial heat flow, the temperature gradient along the axis is constant for any given length of boule:

$$\frac{dT}{dx} = a = \frac{-h(T_{m.p.}-T_A)}{k + hL} \qquad \text{B-64}$$

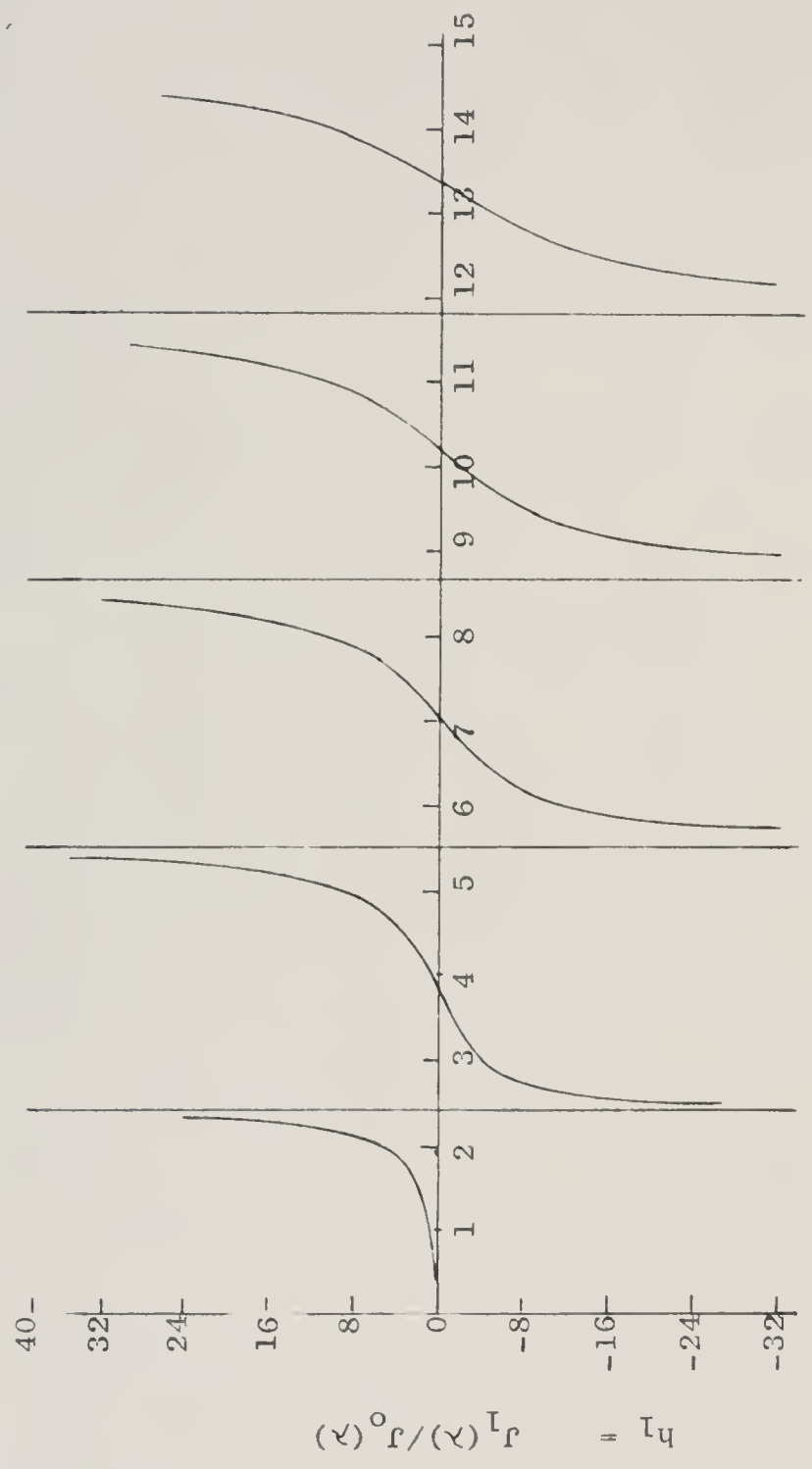

Figure B-1 Plot of Equation B-46 as a Function of λ for Use in Determining the Eigenvalues λ_i That Are the Roots of B-46; Reproduced from "Tables to Facilitate the Calculation of the Temperature Distribution in a Cylinder," H. A. Nancarrow, Physical Society Proceedings, Vol. 45, 1933, p. 463.

APPENDIX C

CALCULATION OF THERMAL GRADIENT AT THE LIQUID-SOLID INTERFACE AS A FUNCTION OF THE RADIUS AND LENGTH OF THE BOULE

This appendix is provided to give examples of the calculation method used to determine the thermal gradient profile in a growing boule. The first example illustrates the calculation method used to determine the points on the curves of Figures 5, 6, 7 and 8. The second example illustrates how the cross sectional thermal gradient profile is determined from use of both the theoretical curves of the above figures and also from the experimental data for the thermal gradient at the side of the growing boule.

Example 1

Determination of the thermal gradient at $x = 0$ and $r = 1$ for the assumed case where:

$h_S = (0.25)(10^{-3})$ cal/(sec cm^2C)
$r_o = 0.6$ cm
$L = 1.0$ cm
boule is aluminum oxide

This point is seen on Figure 7. Additional required data are as follows:

$k = 16.67(10^{-3})$ cal/(sec cm^2C/cm)[33]
$T_A = 1000$ K (data)
$T_{mp} = 2290$ K (data)
$dt/dx)_{x=L} = -140$ C/cm (data)
$T_L = 2190$ K (data)

Using the above data, h_1 is calculated from equation B-22:

$$h_1 = r_o h_S / k = 0.009$$

Using equation B-46

$$h_1 = 0.009 = \frac{\lambda_i J_1(\lambda_i)}{J_o(\lambda_i)}$$

and also using the curves given by Nancarrow,[32] the first four eigenvalues of λ_i are found to be:

$$\lambda_1 = 0.134$$
$$\lambda_2 = 3.83$$
$$\lambda_3 = 7.02$$
$$\lambda_4 = 10.17$$

From equation B-36:

$$\alpha = L/r_o = 1.667$$

From equation B-5:

$$h_b = \frac{-k \left(\frac{dT}{dx}\right)_{x=L}}{T_{(L,r)} - T_A} = 1.96\ (10^{-3})\ \text{cal/(sec cm}^2\text{C)}$$

From equation B-26:

$$h_2 = \frac{Lh_b}{k} = 0.118$$

From tables for the first term of the series:

$$J_o(.134) = 0.9960$$
$$J_1(.134) = 0.0668$$

From equation B-55:

$$A_1 = \frac{2\ \lambda_1^2}{(\lambda_1^2 + h_1^2) J_o^2(\lambda_1)} \int_0^1 r\ \theta_{(o,r)} J_o(\lambda, r)\, dr$$

But since

$$\theta_{(o,r)} = \frac{T_{m.p.}}{T_A} - 1 = \text{constant}$$

and since

$$\int_0^1 r\ J_o(\lambda r)\, dr = \frac{J_1(\lambda)}{\lambda} \quad [31]$$

then

$$A_1 = \Theta_{(o,r)}(.999)$$

From tables:

$$\sinh \alpha\lambda_1 = \sinh(.223) = 0.222$$
$$\cosh \alpha\lambda_1 = \cosh(.223) = 1.025$$

From equation B-57, the first term of the series is:

$$A_1 \alpha\lambda_1 \left[\frac{\alpha\lambda_1 \sinh \alpha\lambda_1 + h_2 \cosh \alpha\lambda_1}{\alpha\lambda_1 \cosh \alpha\lambda_1 + h_2 \sinh \alpha\lambda_1}\right] J_o(\lambda_1) = (.1521)\Theta_{(o,r)}$$

In a similar manner the following terms of the series are:

2nd term: $(0.0076)\Theta_{(o,r)}$

3rd term: $(0.0035)\Theta_{(o,r)}$

4th term: $(0.0030)\Theta_{(o,r)}$

and the sum of the first four terms are:

$$\frac{\partial \Theta}{\partial x}\Big)_{\substack{x=0 \\ r=1}} = -(.1662)\Theta_{(o,r)}$$

From equation B-9:

$$\Theta_{(x,r)} = \frac{T_{(x,r)}}{T_A} - 1$$

Therefore, and remembering that $x_1 \sim x$:

$$\frac{\partial \Theta}{\partial x_1} = \frac{L}{T_A} \frac{\partial T}{\partial x}$$

and

$$\frac{\partial T}{\partial x}\Big)_{\substack{x=0 \\ r=1}} = \frac{T_A}{L} \frac{\partial \Theta}{\partial x_1}\Big)_{\substack{x=0 \\ r=1}} = -\frac{T_A}{L}\left[.1662\,\Theta_{(o,r)}\right] = \frac{-.1662}{1.0}(T_{mp} - T_A)$$

and finally:

$$\frac{\partial T}{\partial x}\Big)_{\substack{x=0 \\ r=1}} = -215\ {}^{oC}/_{cm}$$

Example 2

Determination of the thermal gradient profile that existed at the time of growth in a cross sectional sample of an aluminum oxide boule.

The cross sectional sample to be considered is from boule #1 grown on 3/23/66. Data taken at the time of growth are as follows:

Powder feed rate:	16.1	gms/hour
Rf Power	: 11.5	kw
Diatomic Gas	: 1.3	SCFH oxygen
Powder-Gas	: 0.7	SCFH argon
Plasma-Gas	: 19.0	SCFH argon, outside quartz tube
	19.0	SCFH argon, inside quartz tube

The sample slice was cut from the boule at a point where:

$$r_o = 0.6 \text{ cm}$$

$$L = 1.5 \text{ cm}$$

$$dT/dx)_{0,1} = -162 \text{ C/cm}$$

From Figure 8, for the above point:

$$\bar{h}_s = (0.075)(10^{-3} \text{ cal}/(\text{sec cm}^2\text{C})$$

Calculation of the terms of the series, done in the manner described in example 1, yields:

Series term

(0,1)	at r+0	r=0.25	r=0.50	r=0.75	r=1.0
1	+.1820	+.1820	+.1820	+.1820	+.1820
2	-.0085	-.0066	-.0022	+.0018	+.0034
3	+.0070	+.0025	-.0027	-.0005	+.0021
4	-.0025	+.0002	+.0004	-.0006	+.0006
Summation	+.1780	+.1781	+.1775	+.1827	+.1881
$dT/dx)_{x=0}$	-153	-153	-150	-157	-162

The above gradients constitute the approximate thermal gradient profile existing in the cross section at the time the crystal was formed.

APPENDIX D

ANALYSIS OF THE VALIDITY OF THE SIMPLIFYING ASSUMPTIONS GIVEN BY EQUATIONS B-4 AND B-5

It will be shown that assumption (5), equation B-5, page 106, for the heat loss from the side of the boule, is reasonably approximated over short boule lengths. The actual heat transfer is somewhat unusual in that heat transfer both to and from the sides occurs simultaneously. One flow is a radiant loss proportional to the fourth power of the temperature at any given element of area. It is reasonably assumed that the surrounding plasma is transparent to this radiant loss. The second heat flow is a heat gain to the sides since the plasma is at a higher temperature than the side temperature. The combination of these flows is expressed in equations B-3 and B-4. Normally the radiant loss exceeds the gain from the plasma. However, it is conceivable that the plasma heat gain, especially near the boule tip, could at least equal the radiant loss, in which case there is no net heat flow from the sides and h_s is zero.

The actual calculation of h_s by equations B-3 and B-4 is not possible, however, because of insufficient data in the literature both on plasma heat transfer and on plasma temperature profiles, for this particular geometric orientation, power level and percentage of diatomic gas. For this reason Figures 5, 6, 7 and 8 are plotted for assumed values of an average h_s.

Mathematically, the $\bar{h}_s$ used in the plotting of the above figures is given by:

$$\bar{h}_s = \frac{\int_0^L h_s(x)dx}{L} = \bar{h}_s(L) \qquad \text{D-1}$$

Equation D-1 suggests that $h_s(x)$ could be determined empirically by a properly designed set of experiments. By measuring the temperature and temperature gradient at different locations along the side of a test cylinder, of a known material, and by determination of the $\bar{h}_s$ that fits the data, as was done in example 2, Appendix C, the relationship of $h_s(x)$ and x could be empirically determined. By expressing $h_s(x)$ as a power series, then the constants of the series can be determined by simultaneous solution of various equations resulting from the use of $h_s(x)$ and x from the experimental data.

Based on the data given in Appendix E, for the actual growing of boules, it appears that $\bar{h}_s$ is quite small and that the sides can be considered almost as adiabatic surfaces, at least near the boule tip. Since the side heat flow is small, any errors arising from the linearization of the heat flow must be small also. And, by using the method given in example 2, Appendix C, these small errors are even further minimized in the determination of the thermal gradient profile. Thus, as long as the boules are short (approximately 1.5 cm), the assumption (5) is reasonably approximated. As the boules get longer, the condition of the nearly adiabatic surface no longer holds, and the linearization errors will increase.

The assumption (6), equation B-5, for the heat flow at the base of the boule, holds approximately for the case of large L, or for small changes in L. Since the growth

of long boules is not the purpose of this research, the former case will not be considered.

Data available on the actual growth of boules to 1.5 cm in length show that the range of h_b is from $(1.8)(10^{-3})$ to $(2.2)(10^{-3})$cal/(sec cm^2C) for boule lengths of 1.5 and 0.5 cm respectively, with slight variations due to boule radius. These figures are obtained from the data on boule growth given in Appendix E. Thus if an average h_b is chosen of $(2.0)(10^{-3})$cal/(sec cm^2C), the maximum error at any time will be 10%. This appears to be a reasonable price to pay for the advantages of obtaining a linearized heat transfer equation.

The possible 10% error in h_b, however, does not produce a corresponding 10% error in the thermal gradient. For instance, the thermal gradient at x=0, r=1 for the case r_o=0.5 cm, L=0.5 cm, and $h_s=(0.15)(10^{-3})$cal/(sec cm^2C) is -177 C/cm when h_b is $(2.0)(10^{-3})$cal/(sec cm^2C) and -164 C/cm when h_b is $(1.8)(10^{-3})$cal/(sec cm^2C), or a difference of 7.35%. And even this amount of error is not carried over to the calculation of the thermal gradient profile. By the method of example 2, Appendix C, the actual, experimental gradient at x=0, r=1 is imposed on the solution, so that only minor errors are encountered in calculating the thermal gradient differences occurring within the interior of the sample.

APPENDIX E

DATA ON THE GROWTH OF VARIOUS BOULES

Boule #1

1. Powder Feed Conditions:

   a. 0.005" diameter aluminum oxide, 2% chromium
   b. 16.1 gms/hour feed rate

2. Final Size of Boule:

   a. $\bar{r}_o$ = 0.55 cm (average)
   b. L = 1.9 cm
   c. 1.86 gms

3. Average Growth Rate: 1.13 gms/hour

4. Data During Growth:

Time		Thermal Gradient	Boule Dimensions		Power Level	
hr	min	C/cm	r_o (cm)	L	kw	
0	0	-200	0.4	0.0	11.5	(seeded pedestal)
0	22	-140	0.5	0.5	11.5	
0	47	-162	0.6	1.0	11.5	
1	15	-167	0.6	1.5	11.5	
1	39	-178	0.6	1.9	11.5	

5. Notes on Growth:

   a. boule started from a preseeded pedestal
   b. boule cap ebullient at start
   c. boule cap apparently not molten at end
   d. boule expanding as it grows
   e. plasma stable during growth

6. Visual Observations on Boule:

   a. apparently polycrystalline

Boule #2

1. Powder Feed Conditions:
   a. 0.005" diameter aluminum oxide, 2% chromium
   b. 16.1 gms/hour feed rate
2. Final Size of Boule:
   a. r_o = 0.625 cm
   b. L = 1.5 cm
   c. 8.92 gms
3. Average Growth Rate: 7.75 gms/hour
4. Data During Growth:

Time		Thermal Gradient	Boule Dimensions		Power Level
hr	min	C/cm	r_o (cm)	L	kw
0	22	-105	0.6	0.5	13.2
0	42	-175	0.625	1.0	13.2
1	09	-197	0.75	1.5	13.2

5. Notes on Growth:
   a. boule started from unseeded pedestal
   b. boule cap ebullient throughout growth
   c. boule cap still molten at end of growth
   d. boule expanding as it grows
   e. plasma stable
6. Visual Observations of Boule:
   a. large (3mm) single crystals seen within the large boule
   b. best quality seems to be about .5 cm up from the base
   c. quality at the tip seems poor, apparently due to insufficient melting of the powder grains

Boule #3

1. Powder Feed Conditions:
   a. 0.005" diameter aluminum oxide, 2% chromium
   b. 8.5 gms/hour feed rate
2. Final Size of Boule:
   a. $\bar{r}_o$ = 0.55
   b. L = 1.0 cm
   c. 3.21 gms
3. Average Growth Rate: 2.75 gms/hour

4. Data During Growth:

Time		Thermal Gradient	Boule Dimensions		Power Level
hr	min	C/cm	r_o (cm)	L	kw
0	23	-214	0.5	0.5	11.5
1	0	-178	0.6	1.0	11.5
1	10	Shut off			

5. Notes on Growth:

   a. boule started from unseeded pedestal
   b. boule cap barely ebullient throughout growth
   c. boule cap not molten at end of growth
   d. boule expanded rapidly as it grew
   e. plasma unstable; had difficulty introducing sufficient oxygen; had to shut down prematurely

6. Visual Observations of the Boule:

   a. base looks of best quality
   b. cap is evidently polycrystalline

Boule #4

1. Powder Feed Conditions:

   a. 0.005" diameter aluminum oxide, 2% chromium
   b. 8.5 gms/hour

2. Final Size of Boule:

   a. r_o = 0.5 cm
   b. L + 0.5 cm
   c. 2.88 gms

3. Average Growth Rate: 2.46 gms/hour

4. Data During Growth:

Time		Thermal Gradient	Boule Dimensions		Power Level
hr	min	C/cm	r_o (cm)	L	kw
0	20	-180	0.4	0.25	11.5
1	10	-214	0.6	0.50	12.2

5. Notes on Growth:

   a. boule started from seeded pedestal
   b. boule cap maintained just ebullient by variation of power
   c. boule cap not molten at end of growth
   d. boule expanded as it grew
   e. plasma unstable at high power

6. Visual Observation of the Boule:
   a. does not look as if seed joined properly to rest of boule
   b. tip evidently polycrystalline

Boule #5

1. Powder Feed Conditions:
   a. 0.005" diameter aluminum oxide, 2% chromium
   b. 8.5 gms/hour feed rate
2. Final Size of Boule:
   a. $\bar{r}_o$ = 0.7 cm
   b. L = 2.0 cm
   c. 3.66 gms
3. Average Growth Rate: 1.22 gms/hour
4. Data During Growth:

Time		Thermal Gradient	Boule Dimensions		Power Level
hr	min	C/cm	r_o (cm)	L	kw
0	25	-158	0.5	0.5	9.5
0	55	-170	0.6	1.0	12.5
2	17	-150	0.7	1.5	13.2
3	02	-230	0.7	2.0	13.2

5. Notes on Growth:
   a. boule started from unseeded pedestal
   b. boule cap kept ebullient by increasing power as boule grew
   c. boule cap barely molten at end of growth
   d. boule grew in radius as it got longer
   e. plasma was stable
6. Visual Observations of the Boule:
   a. large (4mm) clear crystals can be seen within the large boule
   b. boule cracked on cooling

Boule #6

1. Powder Feed Conditions:
   a. 0.005" diameter aluminum oxide, 2% chromium
   b. 9.7 gms/hour

2. Final Size of Boule:

   a. $\bar{r}_o$ = 0.5 cm
   b. L = 1.5 cm
   c. 5.18 gms

3. Average Growth Rate: 3.65 gms/hour

4. Data During Growth:

Time		Thermal Gradient	Boule Dimensions		Power Level
hr	min	C/cm	r_o (cm)	L	kw
0	25	-240	.35	0.5	9.5
0	50	-210	.45	1.0	10.0
1	25	-145	.55	1.5	11.0

5. Notes on Growth:

   a. boule started from seeded pedestal
   b. boule kept slightly ebullient by varying the power
   c. boule cap barely molten at end of run
   d. boule grew in radius as it got longer
   e. plasma was unstable during most of run; had trouble applying high power

6. Visual Observations of the Boule:

   a. boule grew crooked, at about an angle of 10^o off the vertical
   b. part of boule, near end of growth, is clear and apparently single crystal

Boule #7

1. Powder Feed Conditions:

   a. 0.005" diameter aluminum oxide, 2% chromium
   b. 9.7 gms/hour

2. Final Size of Boule:

   a. r_o = .40 cm
   b. L = 1.20 cm
   c. 2.12 gms

3. Average Growth Rate: 1.62 gms/hour

4. Data During Growth:

Time		Thermal Gradient	Boule Dimensions		Power Level
hr	min	C/cm	r_o (cm)	L	kw
0	23	-246	.25	0.5	7.5
0	38	-246	.40	1.0	7.5
1	18	-243	.45	1.5	9.7

5. Notes on Growth:

   a. boule started from seeded pedestal
   b. boule kept slightly ebullient by varying the power
   c. boule cap barely molten at end of run
   d. boule grew slightly in radius as it got longer
   e. plasma unstable at high power levels

6. Visual Observations of Growth:

   a. does not appear that seed has joined properly with the body of the boule, apparently due to insufficient heating
   b. stem of boule appears of better quality than the tip, which is obviously polycrystalline

Boule #8

1. Powder Feed Conditions:

   a. 0.004" diameter aluminum oxide, 2% chromium
   b. 10.5 gms/hour

2. Final Size of Boule:

   a. r_o = .5 cm
   b. L = .8 cm
   c. 2.91 gms

3. Average Growth Rate: 4.31 gms/hour

4. Data During Growth:

Time		Thermal Gradient	Boule Dimensions		Power Level
hr	min	C/cm	r_o (cm)	L	kw
0	15	-256	.45	0.5	10.8
0	30	-215	.50	0.8	12.0
0	40	Shut off			

5. Notes on Growth:

   a. boule started from a seeded pedestal
   b. boule cap kept ebullient by increasing power as boule grew
   c. boule cap barely molten at end of run
   d. boule grew in radius as it got longer
   e. plasma reasonably stable to the 12.0 kw level

6. Visual Observations of the Boule:

   a. grew slightly off center and at an angle (about 5^{o} to the vertical)
   b. no indications of gross imperfections
   c. not optically clear, however

Boule #9

1. Powder Feed Conditions:

   a. 0.005" diameter aluminum oxide, 2% chromium
   b. 8.5 gms/hour

2. Final Size of Boule:

   a. r_o = 0.5 cm
   b. L^o = 1.5 cm
   c. 4.52 gms

3. Average Growth Rate: 2.88 gms/hour

4. Data During Growth:

Time		Thermal Gradient	Boule Dimensions		Power Level
hr	min	C/cm	r_o (cm)	L	kw
0	17	-195	.35	0.5	12.7
0	27	-168	.45	1.0	12.7
0	47	-168	.50	1.5	12.7
1	34	-135	.70	2.0	13.1

5. Notes on Growth:

   a. boule started from seeded pedestal
   b. boule cap kept vigorously ebullient during growth by maintaining maximum power throughout the run
   c. boule cap barely molten at end of run
   d. boule expanded as it grew
   e. plasma stable; made so by adjustment of plasma gas flow rates of inside and outside quartz tubes

6. Visual Observations of the Boule:

   a. large, clear crystals seen at the boule cap, where the maximum expansion in radius occurred (about 5 mm)
   b. entire cap may have been single crystal before cooling since there is no evidence of polycrystalline nature of the cap

Boule #10 (grown at position C-0)

1. Powder Feed Conditions:

   a. 0.005" diameter aluminum oxide, 2% chromium
   b. 8.5 gms/hour

2. Final Size of Boule:

   a. r_o = 0.65 cm
   b. L = 1.5 cm
   c. 5.0 gms

3. Average Growth Rate: 3.32 gms/hour

4. Data During Growth:

Time		Thermal Gradient	Boule Dimensions		Power Level
hr	min	C/cm	r_o (cm)	L	kw
0	20	-148	0.5	0.5	13.5
1	10	-132	0.7	1.0	13.5
1	38	-140	0.8	1.5	13.5
1	50	-140	0.8	1.7	13.5

5. Notes on Growth:

   a. boule started from unseeded pedestal
   b. ebullient boule cap throughout growth, although not as violently ebullient as at position B-0
   c. boule cap barely molten at end of run
   d. boule radius expanded as it grew
   e. plasma stable

6. Visual Observations of the Boule:

   a. one large single crystal seen near cap, on periphery; rest of boule polycrystalline

Boule #11 (grown at position C-0)

1. Powder Feed Conditions:
   a. 0.005" diameter aluminum oxide, 2% chromium
   b. 8.5 gms/hour

2. Final Size of Boule:
   a. r_o = 0.50 cm
   b. L = 1.0 cm
   c. 1.83 gms

3. Average Growth Rate: 2.44 gms/hour

4. Data During Growth:

Time		Thermal Gradient	Boule Dimensions		Power Level
hr	min	C/cm	r_o (cm)	L	kw
0	15	-178	0.5	0.5	10.8
0	35	-137	0.5	1.0	13.5
0	45	Turned off powder--plasma unstable			

5. Notes on Growth:
   a. boule started from seed
   b. boule cap ebullient during growth, but does not seem quite as ebullient as those grown at B-0
   c. boule expanded only slightly as it grew
   d. plasma not overly stable; blew out at end of run

6. Visual Observations of the Boule:
   a. large, clear single crystal formed at part of tip, at periphery; remainder of boule polycrystalline
   b. core quality seems to be diminishing as growth proceeds

Boule #12

1. Powder Feed Conditions:
   a. 0.007" diameter ferric oxide
   b. 12.0 gms/hour

2. Final Size of Boule:
   a. r_o = 0.5 cm
   b. L = 1.5 cm
   c. 8.5 gms

3. Average Growth Rate: 4.33 gms/hour

4. Data During Growth:

Time		Thermal Gradient	Boule Dimensions		Power Level
hr	min	C/cm	r_o (cm)	L	kw
0	30	-306	0.5	0.5	6.85
0	50	-314	0.5	1.0	7.40
1	20	-326	0.5	1.5	7.40
1	55	Shut off			

5. Notes on Growth:

   a. boule started from unseeded pedestal
   b. ebullient boule cap throughout growth
   c. constant radius with growth
   d. stable plasma

6. Visual Observations of the Boule:

   a. made up of large single crystals
   b. material very brittle; breaks apart easily

Boule #13

1. Powder Feed Conditions:

   a. 0.007" diameter ferric oxide
   b. 12.0 gms/hour

2. Final Size of Boule:

   a. r_o = 0.5 cm
   b. L = 1.5 cm
   c. 7.85 gms

3. Average Growth Rate: 5.65 gms/hour

4. Data During Growth:

Time		Thermal Gradient	Boule Dimensions		Power Level
hr	min	C/cm	r_o (cm)	L	kw
0	15	-314	0.5	0.5	6.7
0	40	-294	0.5	1.0	6.7
1	23	-326	0.5	1.5	7.4

5. Notes on Growth:

   a. boule started from seed
   b. ebullient cap throughout growth
   c. constant radius with growth

6. Visual Observations of Boule:

   a. almost entire core is single crystal
   b. molten cap may have solidified too quickly since part of it appears polycrystalline

LIST OF REFERENCES

1. G. I. Babat, Instn. Elect. Engrs. J. 94, part 3, 27 (1947).

2. T. B. Reed, J. Appl. Phys. 32, 821 (1961).

3. T. B. Reed, J. Appl. Phys. 32, 2534 (1961).

4. T. B. Reed, Int. Science & Tech. 6, 42 (1962).

5. A. Verneuil, Compt. Rend. 135, 791-794 (1902).

6. S. K. Popov, "Growth and Uses of Gen-grade Corundum Crystals," Growth of Crystals, eds. Shubnikov and Sheftal (Chapman and Hall, London, 1959), 2, 103.

7. H. R. Griem, Phys. Rev. 131 (3), 1170 (1963).

8. T. B. Reed, J. Appl. Phys. 34 (8), 2266 (1963).

9. M. Jacob, Heat Transfer (John Wiley & Sons, New York, 1949), 1, 469; reference cited taken from: E. Pohlhausen, Zeitschr. f. angew Math. u. Mech. 1, 115 (1921).

10. J. A. Fay and F. R. Riddell, J. Aeron. Sci. 25, 73 (1958).

11. J. P. Reilly, Phys. Fluids 7 (12), 1905 (1964).

12. W. J. Wohlenberg and D. G. Morrow, Transactions of the A. S. M. E. 47, 127 (1925).

13. H. E. Buckley, Crystal Growth (John Wiley & Sons, New York, 1951), 182-222, 345.

14. W. K. Burton and N. Cabrera, Discussions of the Faraday Society 5, 33 (1949).

15. F. C. Frank, Discussions of the Faraday Society 5, 48 (1949).

16. N. N. Sheftal, "Real Crystal Formation," Growth of Crystals, eds. Shubnikov and Sheftal (Chapman and Hall, London, 1959), 1, 7.

17. W. Moore, Physical Chemistry (Prentice Hall, Englewood Cliffs, N. J., 1962), 3rd Edition, 703.

18. O. M. Anshcles, "Some Problems of the Relation Between Form and Structure in Crystals," Growth of Crystals, eds. Shubnikov and Sheftal (Chapman and Hall, London, 1959), 1, 53.

19. H. S. Carslaw and J. C. Jaeger, Conduction of Heat in Solids (Oxford Press, London, 1959), 2nd Edition, 219.

20. N. V. Gliki and A. A. Urusovskaya, Soviet Physics Crystallography 10 (5), 551 (March-April 1966).

21. E. H. Kraus, W. F. Hunt and L. S. Ramsdell, Minerology (McGraw-Hill Book Company, New York, 1951), 4th Edition, 96-114.

22. C. Abbott, Minerals from the Earth and Sky, Smithsonian Institution Series 3 (1929).

23. B. D. Cullity, Elements of X-ray Diffraction (Addison-Wesley Press, Reading, Mass., 1956), 84.

24. E. W. Muller, "Direct Observations of Crystal Imperfections by Field Ion Microscopy," Direct Observations of Imperfections in Crystals (Interscience Press, New York, 1962), 18.

25. The Florida Alumnus, University of Florida, Gainesville, Florida, 3 (March, 1966).

26. J. W. Mitchell, "Direct Observations of Dislocations in Crystals by Optical and Electron Microscopy," Direct Observations of Imperfections in Crystals (Interscience Press, New York, 1962), 18.

27. K. M. Pell, Plasma Temperature Profiles (unpublished), University of Florida (June, 1966).

28. D. R. Keefer, Magnetic and Electric Field Effects in an RF Plasma (unpublished), University of Florida (June, 1966).

29. D. G. Samaras, Theory of Ion Flow Dynamics (Prentice Hall, Englewood Cliffs, N. J., 1962), 163.

30. K. M. Pell, Diagnostics of an RF Plasma Based on Heat Transfer Rates, Master's Degree Thesis, University of Florida, 38 (December, 1963).

31. R. V. Churchill, Fourier Series and Boundary Value Problems (McGraw-Hill Book Company, New York, 1963), 2nd Edition, 187.

32. H. A. Nancarrow, Physical Society Proceedings 45, 462 (1933).

33. W. D. Kingery, Introduction to Ceramics (John Wiley & Sons, New York, 1960), 487.

BIOGRAPHICAL SKETCH

William Austin Smith was born on May 1, 1927, at Newark, New Jersey. He attended the N. Y. State Maritime Academy from 1945 to 1947, graduating with a U. S. Coast Guard License as Third Engineer in the Maritime Service. He attended Stevens Institute of Technology, Hoboken, New Jersey, from 1947 to 1951 and graduated with the degree of Mechanical Engineer, with Honor. From 1951 to 1952 he was employed by the Permutit Company, New York City, manufacturers of industrial and municipal water treatment equipment. During 1953 and 1954 he served with the U. S. Navy as an Ordnance Inspection Officer, stationed at the Hamilton Watch Company, Lancaster, Pennsylvania. From 1955 to 1961 he was employed by Jenkins Brothers, New York City, manufacturers of industrial valves.

In 1961, Mr. Smith entered the graduate school of the University of Florida as an engineering fellow in Mechanical Engineering. He received the degree of Master of Science in 1962, and for the next two years was employed by the Department of Mechanical Engineering as an instructor and Assistant in Research. He was a project leader on a sponsored contract investigating solar heat gain through fenestration and published several articles on that subject. For the past two years he has been a NASA Fellow in the Department of Aerospace Engineering while pursuing the degree of Doctor of Philosophy.

William A. Smith is a member of Tau Beta Pi, Phi Kappa Phi, Pi Delta Epsilon and Gear and Triangle honor

societies. He is a member of the American Society of Heating, Refrigerating and Air Conditioning Engineers, is married, and is the father of three children.

This dissertation was prepared under the direction of the chairman of the candidate's supervisory committee and has been approved by all members of that committee. It was submitted to the Dean of the College of Engineering and to the Graduate Council, and was approved as partial fulfillment of the requirements for the degree of Doctor of Philosophy.

August, 1966

Dean, College of Engineering

Dean, Graduate School

Supervisory Committee:

Chairman